

Vol. 25, no. 2, 2025

eISSN 2687-1653

PEER-REVIEWED SCIENTIFIC AND PRACTICAL JOURNAL

Advanced Engineering Research (Rostov-on-Don)

Mechanics

Machine Building
and Machine Science

Information Technology,
Computer Science
and Management



www.vestnik-donstu.ru
DOI 10.23947/2687-1653



Advanced Engineering Research (Rostov-on-Don)

Peer-reviewed scientific and practical journal

eISSN 2687–1653

Published since 2000

Periodicity – 4 issues per year

DOI: 10.23947/2687–1653

Founder and Publisher — Don State Technical University (DSTU), Rostov-on-Don, Russian Federation

The journal is aimed at informing the readership about the latest achievements and prospects in the field of mechanics, mechanical engineering, computer science and computer technology. The publication is a forum for cooperation between Russian and foreign scientists, it contributes to the convergence of the Russian and world scientific and information space.

The journal is included in the List of the leading peer-reviewed scientific publications (Higher Attestation Commission under the Ministry of Science and Higher Education of the Russian Federation), where basic scientific results of dissertations for the degrees of Doctor and Candidate of Science in scientific specialties and their respective branches of science should be published.

The journal publishes articles in the following fields of science:

- Theoretical Mechanics, Dynamics of Machines (Engineering Sciences)
- Deformable Solid Mechanics (Engineering, Physical and Mathematical Sciences)
- Mechanics of Liquid, Gas and Plasma (Engineering Sciences)
- Mathematical Simulation, Numerical Methods and Program Systems (Engineering Sciences)
- System Analysis, Information Management and Processing, Statistics (Engineering Sciences)
- Automation and Control of Technological Processes and Productions (Engineering Sciences)
- Software and Mathematical Support of Machines, Complexes and Computer Networks (Engineering Sciences)
- Computer Modeling and Design Automation (Engineering, Physical and Mathematical Sciences)
- Computer Science and Information Processes (Engineering Sciences)
- Machine Science (Engineering Sciences)
- Machine Friction and Wear (Engineering Sciences)
- Technology and Equipment of Mechanical and Physicotechnical Processing (Engineering Sciences)
- Engineering Technology (Engineering Sciences)
- Welding, Allied Processes and Technologies (Engineering Sciences)
- Methods and Devices for Monitoring and Diagnostics of Materials, Products, Substances and the Natural Environment (Engineering Sciences)
- Hydraulic Machines, Vacuum, Compressor Equipment, Hydraulic and Pneumatic Systems (Engineering Sciences)

<i>Registration</i>	Extract from the Register of Registered Mass Media ЭЛ № ФС 77 – 78854 dated August 07, 2020, issued by the Federal Service for Supervision of Communications, Information Technology and Mass Media
<i>Indexing and Archiving</i>	Scopus, RISC (core), CyberLeninka, CrossRef, Dimensions, DOAJ, EBSCO, Index Copernicus, Internet Archive, Google Scholar
<i>Website</i>	http://vestnik-donstu.ru
<i>Address of the Editorial Office</i>	1, Gagarin sq., Rostov-on-Don, 344003, Russian Federation
<i>E-mail</i>	vestnik@donstu.ru
<i>Telephone</i>	+7 (863) 2–738–372
<i>Date of Publication No.2,2025</i>	30.06.2025





ДОНСКОЙ ГОСУДАРСТВЕННЫЙ
ТЕХНИЧЕСКИЙ УНИВЕРСИТЕТ

Advanced Engineering Research (Rostov-on-Don)

Рецензируемый научно-практический журнал

eISSN 2687–1653

Издается с 2000 года

Периодичность – 4 выпуска в год

DOI: 10.23947/2687–1653

Учредитель и издатель — Федеральное государственное бюджетное образовательное учреждение высшего образования «Донской государственный технический университет» (ДГТУ), г. Ростов-на-Дону

Создан в целях информирования читательской аудитории о новейших достижениях и перспективах в области механики, машиностроения, информатики и вычислительной техники. Издание является форумом для сотрудничества российских и иностранных ученых, способствует сближению российского и мирового научно-информационного пространства.

Журнал включен в перечень рецензируемых научных изданий (К2), в котором должны быть опубликованы основные научные результаты диссертаций на соискание ученой степени кандидата наук, на соискание ученой степени доктора наук (Перечень ВАК) по следующим научным специальностям:

- 1.1.7 – Теоретическая механика, динамика машин (технические науки)
- 1.1.8 – Механика деформируемого твердого тела (технические, физико-математические науки)
- 1.1.9 – Механика жидкости, газа и плазмы (технические науки)
- 1.2.2 – Математическое моделирование, численные методы и комплексы программ (технические науки)
- 2.3.1 – Системный анализ, управление и обработка информации, статистика (технические науки)
- 2.3.3 – Автоматизация и управление технологическими процессами и производствами (технические науки)
- 2.3.5 – Математическое и программное обеспечение вычислительных систем, комплексов и компьютерных сетей (технические науки)
- 2.3.7 – Компьютерное моделирование и автоматизация проектирования (технические, физико-математические науки)
- 2.3.8 – Информатика и информационные процессы (технические науки)
- 2.5.2 – Машиноведение (технические науки)
- 2.5.3 – Трение и износ в машинах (технические науки)
- 2.5.5 – Технология и оборудование механической и физико-технической обработки (технические науки)
- 2.5.6 – Технология машиностроения (технические науки)
- 2.5.8 – Сварка, родственные процессы и технологии (технические науки)
- 2.5.9 – Методы и приборы контроля и диагностики материалов, изделий, веществ и природной среды (технические науки)
- 2.5.10 – Гидравлические машины, вакуумная, компрессорная техника, гидро- и пневмосистемы (технические науки)

Регистрация	Выписка из реестра зарегистрированных средств массовой информации ЭЛ № ФС 77 – 78854 от 07 августа 2020 г., выдано Федеральной службой по надзору в сфере связи, информационных технологий и массовых коммуникаций
Индексация и архивация	Scopus, РИНЦ (ядро), CyberLeninka, CrossRef, Dimensions, DOAJ, EBSCO, Index Copernicus, Internet Archive, Google Scholar
Сайт	http://vestnik-donstu.ru
Адрес редакции	344003, Российская Федерация, г. Ростов-на-Дону, пл. Гагарина, 1
E-mail	vestnik@donstu.ru
Телефон	+7 (863) 2–738–372
Дата выхода №2, 2025 в свет	30.06.2025



Editorial Board

Editor-in-Chief

Alexey N. Beskopylny, Dr.Sci. (Eng.), Professor, Don State Technical University (Rostov-on-Don, Russian Federation)

Deputy Chief Editor

Alexandr I. Sukhinov, Corresponding Member, Russian Academy of Sciences, Dr.Sci. (Phys.-Math.), Professor, Don State Technical University (Rostov-on-Don, Russian Federation)

Executive Editor

Manana G. Komakhidze, Cand.Sci. (Chemistry), Don State Technical University (Rostov-on-Don, Russian Federation)

Executive Secretary

Nadezhda A. Shevchenko, Don State Technical University (Rostov-on-Don, Russian Federation)

Ahilan Appathurai, National Junior Research Fellow, Anna University Chennai (India)

Ahmet Uyumaz, PhD (Eng.), Professor, Burdur Mehmet Akif Ersoy University (Turkey)

Alexander T. Rybak, Dr.Sci. (Eng.), Professor, Don State Technical University (Rostov-on-Don, Russian Federation)

Ali M. Hasan, PhD (Computer Engineering), Al Nahrain University (Baghdad, Iraq)

Andrey V. Nasedkin, Dr.Sci. (Phys.-Math.), Professor, Southern Federal University (Rostov-on-Don, Russian Federation)

Arestak A. Sarukhanyan, Dr.Sci. (Eng.), Professor, National University of Architecture and Construction of Armenia (Armenia)

Arkady N. Solovyev, Dr.Sci. (Phys.-Math.), Professor, Crimean Engineering and Pedagogical University the name of Fevzi Yakubov (Simferopol, Republic of Crimea)

Batyr M. Yazyev, Dr.Sci. (Eng.), Professor, Don State Technical University (Rostov-on-Don, Russian Federation)

Bertram Torsten, Dr.Sci. (Eng.), Professor, TU Dortmund University (Germany)

Evgenii A. Demekhin, Dr.Sci. (Phys.-Math.), Professor, Financial University under the RF Government, Krasnodar branch (Krasnodar, Russian Federation)

Geny V. Kuznetsov, Dr.Sci. (Phys.-Math.), Professor, Tomsk Polytechnic University (Tomsk, Russian Federation)

Gultekin Basmaci, PhD (Eng.), Professor, Burdur Mehmet Akif Ersoy University (Turkey)

Hamid A. Jalab, PhD (Computer Science & IT), University of Malaya (Malaysia)

Hubert Anysz, PhD (Eng.), Assistant Professor, Warsaw University of Technology (Republic of Poland)

Huchang Liao, Professor, IAAM Fellow, IEEE Business School Senior Fellow, Sichuan University (China)

Igor M. Verner, PhD (Eng.), Professor, Technion — Israel Institute of Technology (Israel)

Ilya I. Kudish, PhD (Phys.-Math.), Kettering University (USA)

Imad R. Antipas, Cand.Sci. (Eng.), Don State Technical University (Rostov-on-Don, Russian Federation)

Janusz Witalis Kozubal, Dr.Sci. (Eng.), Wroclaw Polytechnic University (Republic of Poland)

José Carlos Quadrado, PhD (Electrical Engineering and Computers), DSc Habil, Polytechnic Institute of Porto (Portugal)

Kamil S. Akhverdiev, Dr.Sci. (Eng.), Professor, Rostov State Transport University (Rostov-on-Don, Russian Federation)

Karen O. Egiazaryan, Dr.Sci. (Eng.), Professor, Tampere University of Technology (Finland)

Konstantin V. Podmaster'ev, Dr.Sci. (Eng.), Professor, Orel State University named after I.S. Turgenev (Orel, Russian Federation)

LaRoux K. Gillespie, Dr.Sci. (Eng.), Professor, President-Elect of the Society of Manufacturing Engineers (USA)

Mezhlum A. Sumbatyan, Dr.Sci. (Phys.-Math.), Professor, Southern Federal University (Rostov-on-Don, Russian Federation)

Mikhail A. Tamarkin, Dr.Sci. (Eng.), Professor, Don State Technical University (Rostov-on-Don, Russian Federation)

Murat Tezer, Professor, Near East University (Turkey)

Murman A. Mukutadze, Dr.Sci. (Eng.), Professor, Rostov State Transport University (Rostov-on-Don, Russian Federation)

Muzafer H. Saračević, Full Professor, Novi Pazar International University (Serbia)

Nguyen Dong Ahn, Dr.Sci. (Phys.-Math.), Professor, Academy of Sciences and Technologies of Vietnam (Vietnam)

Nguyen Xuan Chiem, Dr.Sci. (Eng.), Le Quy Don Technical University (Vietnam)

Nikolay E. Galushkin, Dr.Sci. (Eng.), Professor, Institute of Service and Business, DSTU branch (Shakhty, Russian Federation)

Nikolay N. Prokopenko, Dr.Sci. (Eng.), Professor, Don State Technical University (Rostov-on-Don, Russian Federation)

Oleg V. Dvornikov, Dr.Sci. (Eng.), Professor, Belarusian State University (Belarus)

Revaz Z. Kavtaradze, Dr.Sci. (Eng.), Professor, Raphael Dvali Institute of Machine Mechanics (Georgia)

Roman N. Polyakov, Dr.Sci. (Eng.), Associate Professor, Orel State University named after I.S. Turgenev (Orel, Russian Federation)

Sergei A. Voronov, Dr.Sci. (Eng.), Associate Professor, Russian Foundation of Fundamental Research (Moscow, Russian Federation)

Sergey G. Parshin, Dr.Sci. (Eng.), Associate Professor, St. Petersburg Polytechnic University (St. Petersburg, Russian Federation)

Sergey M. Aizikovich, Dr.Sci. (Phys.-Math.), Professor, Don State Technical University (Rostov-on-Don, Russian Federation)

Tamaz M. Natriashvili, Academician, Raphael Dvali Institute of Machine Mechanics (Georgia)

Umid M. Turdaliev, Dr.Sci. (Eng.), Professor, Andijan Machine-Building Institute (Uzbekistan)

Valentin L. Popov, Dr.Sci. (Phys.-Math.), Professor, Berlin University of Technology (Germany)

Valery N. Varavka, Dr.Sci. (Eng.), Professor, Don State Technical University (Rostov-on-Don, Russian Federation)

Victor A. Ereemev, Dr.Sci. (Phys.-Math.), Professor, Southern Scientific Center of RAS (Rostov-on-Don, Russian Federation)

Victor M. Kureychik, Dr.Sci. (Eng.), Professor, Southern Federal University (Rostov-on-Don, Russian Federation)

Vilor L. Zakovorotny, Dr.Sci. (Eng.), Professor, Don State Technical University (Rostov-on-Don, Russian Federation)

Vladimir I. Lysak, Dr.Sci. (Eng.), Professor, Volgograd State Technical University (Volgograd, Russian Federation)

Vladimir I. Marchuk, Dr.Sci. (Eng.), Professor, Institute of Service and Business, DSTU branch (Shakhty, Russian Federation)

Vladimir M. Mladenovic, Dr.Sci. (Eng.), Professor, University of Kragujevac (Serbia)

Vladimir N. Sidorov, Dr.Sci. (Eng.), Russian University of Transport (Moscow, Russian Federation)

Vyacheslav G. Tsybulin, Dr.Sci. (Phys.-Math.), Associate Professor, Southern Federal University (Rostov-on-Don, Russian Federation)

Yuri O. Chernyshev, Dr.Sci. (Eng.), Professor, Don State Technical University (Rostov-on-Don, Russian Federation)

Редакционная коллегия

Главный редактор

Бескопыйный Алексей Николаевич, доктор технических наук, профессор, Донской государственный технический университет (Ростов-на-Дону, Российская Федерация)

Заместитель главного редактора

Сухинов Александр Иванович, член-корреспондент РАН, доктор физико-математических наук, профессор, Донской государственный технический университет (Ростов-на-Дону, Российская Федерация)

Ответственный редактор

Комахидзе Манана Гивиевна, кандидат химических наук, Донской государственный технический университет (Ростов-на-Дону, Российская Федерация)

Ответственный секретарь

Шевченко Надежда Анатольевна, Донской государственный технический университет (Ростов-на-Дону, Российская Федерация)

Айзикович Сергей Михайлович, доктор физико-математических наук, профессор, Донской государственный технический университет (Ростов-на-Дону, Российская Федерация)

Антибас Имад Ризакалла, кандидат технических наук, Донской государственный технический университет (Ростов-на-Дону, Российская Федерация)

Ахилан Аппатурай, младший научный сотрудник, Инженерно-технологический колледж PSN, Университет Анны Ченнаи (Индия)

Ахвердиев Камил Самед Оглы, доктор технических наук, профессор, Ростовский государственный университет путей сообщения (Ростов-на-Дону, Российская Федерация)

Варавка Валерий Николаевич, доктор технических наук, профессор, Донской государственный технический университет (Ростов-на-Дону, Российская Федерация)

Вернер Игорь Михайлович, доктор технических наук, профессор, Технологический институт в Израиле (Израиль)

Воронов Сергей Александрович, доктор технических наук, доцент, Российский фонд фундаментальных исследований (Москва, Российская Федерация)

Галушкин Николай Ефимович, доктор технических наук, профессор, Институт сферы обслуживания и предпринимательства, филиал ДГТУ (Шахты, Российская Федерация)

Лару Гиллесси, доктор технических наук, профессор, Президент Общества машиностроителей (США)

Аныш Губерт, доктор наук, доцент, Варшавский технологический университет (Польша)

Басмачи Гюльтекин, доктор наук, профессор, Университет Бурдура Мехмета Акифа Эрсея (Турция)

Дворников Олег Владимирович, доктор технических наук, профессор, Белорусский государственный университет (Беларусь)

Демехин Евгений Афанасьевич, доктор физико-математических наук, профессор, Краснодарский филиал Финансового университета при Правительстве РФ (Краснодар, Российская Федерация)

Хамид Абдулла Джалаб, доктор наук (информатика и ИТ), университет Малайя (Малайзия)

Егназарян Карен Оникович, доктор технических наук, профессор, Технологический университет Тампере (Финляндия)

Еремеев Виктор Анатольевич, доктор физико-математических наук, профессор, Южный научный центр РАН (Ростов-на-Дону, Российская Федерация)

Заковоротный Вилор Лаврентьевич, доктор технических наук, профессор, Донской государственный технический университет (Ростов-на-Дону, Российская Федерация)

Кавтарадзе Реваз Зурабович, доктор технических наук, профессор, Институт механики машин им. Р. Двали (Грузия)

Козубал Януш Виталис, доктор технических наук, профессор, Вроцлавский технический университет (Польша)

Хосе Карлос Куадрадо, доктор наук (электротехника и компьютеры), Политехнический институт Порту (Португалия)

Кудиш Илья Исидорович, доктор физико-математических наук, Университет Кеттеринга (США)

Кузнецов Гений Владимирович, доктор физико-математических наук, профессор, Томский политехнический университет (Томск, Российская Федерация)

Курейчик Виктор Михайлович, доктор технических наук, профессор, Южный федеральный университет (Ростов-на-Дону, Российская Федерация)

Лысак Владимир Ильич, доктор технических наук, профессор, Волгоградский государственный технический университет (Волгоград, Российская Федерация)

Марчук Владимир Иванович, доктор технических наук, профессор, Институт сферы обслуживания и предпринимательства, филиал ДГТУ (Шахты, Российская Федерация)

Владимир Младенович, доктор технических наук, профессор, Крагуевацкий университет (Сербия)

Мукутадзе Мурман Александрович, доктор технических наук, доцент, Ростовский государственный университет путей сообщения (Ростов-на-Дону, Российская Федерация)

Наседкин Андрей Викторович, доктор физико-математических наук, профессор, Южный федеральный университет (Ростов-на-Дону, Российская Федерация)

Натришвили Тамаз Мамиевич, академик, Институт механики машин им. Р. Двали (Грузия)

Нгуен Донг Ань, доктор физико-математических наук, профессор, Институт механики Академии наук и технологий Вьетнама (Вьетнам)

Нгуен Суан Тьем, доктор технических наук, Вьетнамский государственный технический университет им. Ле Куй Дона (Вьетнам)

Паршин Сергей Георгиевич, доктор технических наук, доцент, Санкт-Петербургский политехнический университет (Санкт-Петербург, Российская Федерация)

Подмастерьев Константин Валентинович, доктор технических наук, профессор, Орловский государственный университет им. И.С. Тургенева (Орел, Российская Федерация)

Поляков Роман Николаевич, доктор технических наук, доцент, Орловский государственный университет им. И.С. Тургенева (Орел, Российская Федерация)

Попов Валентин Леонидович, доктор физико-математических наук, профессор, Институт механики Берлинского технического университета (Германия)

Прокопенко Николай Николаевич, доктор технических наук, профессор, Донской государственный технический университет (Ростов-на-Дону, Российская Федерация)

Рыбак Александр Тимофеевич, доктор технических наук, профессор, Донской государственный технический университет (Ростов-на-Дону, Российская Федерация)

Музафер Сарачевич, доктор наук, профессор, Университет Нови-Пазара (Сербия)

Саруханиян Арестак Арамаисович, доктор технических наук, профессор, Национальный университет архитектуры и строительства Армении (Армения)

Сидоров Владимир Николаевич, доктор технических наук, Российский университет транспорта (Москва, Российская Федерация)

Соловьёв Аркадий Николаевич, доктор физико-математических наук, профессор, Крымский инженерно-педагогический университет имени Февзи Якубова (Симферополь, Республика Крым)

Сумбатян Межлум Альбертович, доктор физико-математических наук, профессор, Южный федеральный университет (Ростов-на-Дону, Российская Федерация)

Тамаркин Михаил Аркадьевич, доктор технических наук, профессор, Донской государственный технический университет (Ростов-на-Дону, Российская Федерация)

Мурат Тезер, профессор, Ближневосточный университет (Турция)

Бертрам Торстен, доктор технических наук, профессор, Технический университет Дортмунда (Германия)

Турдалиев Умид Мухтаралиевич, доктор технических наук, профессор, Андижанский машиностроительный институт (Узбекистан)

Ахмет Уюмаз, доктор технических наук, профессор, университет Бурдура Мехмета Акифа Эрсея (Турция)

Али Маджид Хасан Алвазли, доктор наук (компьютерная инженерия), доцент, Университет Аль-Нахрейн (Ирак)

Цибулин Вячеслав Георгиевич, доктор физико-математических наук, доцент, Южный федеральный университет (Ростов-на-Дону, Российская Федерация)

Чернышев Юрий Олегович, доктор технических наук, профессор, Донской государственный технический университет (Ростов-на-Дону, Российская Федерация)

Хухан Ляо, профессор, научный сотрудник ИААМ Старший член Школы бизнеса IEEE, Университет Сычуань (Китай)

Языев Батыр Меретович, доктор технических наук, профессор, Донской государственный технический университет (Ростов-на-Дону, Российская Федерация)

Contents

MACHINE BUILDING AND MACHINE SCIENCE

Analytical Modeling of a Heat Source under Welding of a Steel Sleeve by the Centrifugal Method Using an Axisymmetric Electric Arc	83
<i>Sergey P. Glushko</i>	
Study of Operating Modes of a Biofuel Diesel Engine	91
<i>Vitaly A. Likhanov, Oleg P. Lopatin</i>	
Analysis of Temperature Characteristics of Electrolytic-Plasma Discharge in Jet Processing of a Metal Anode	99
<i>Alexander I. Popov, Vitaly I. Novikov, Dmitry N. Ivanov, Igor A. Kozyrskiy</i>	
A Method for Monitoring the Reliability of Technical Systems by Identifying the Entropy of the Causes of their Failures	112
<i>Svetlana V. Teplyakova, Alexander T. Rybak, Anastasiya V. Olshevskaya, Alexey S. Prutskov</i>	

INFORMATION TECHNOLOGY, COMPUTER SCIENCE AND MANAGEMENT

Forecasting Delivery Time of Goods in Supply Chains Using Machine Learning Methods	120
<i>Vladislav K. Reznov, Oksana M. Romakina, Ekaterina V. Zaytseva</i>	
Ab initio Calculations of the Electronic-Energy Structure and Optical Properties of Lanthanum and Neodymium Pyrozirconates	129
<i>Anatoliy A. Lavrentyev, Boris V. Gabrelian, Vu Van Tuan, Ksenia F. Kalmykova</i>	
Integration of Sensor Data and Mathematical Modeling of Underwater Robot Behavior Using a Digital Twin	142
<i>Mikhail D. Gladyshev, Alexey V. Rybakov</i>	
Approximate Synthesis of H_∞ – Controllers in Nonlinear Dynamic Systems over a Semi-Infinite Time Period.....	152
<i>Andrei V. Pantelev, Aleksandra A. Yakovleva</i>	

Содержание

МАШИНОСТРОЕНИЕ И МАШИНОВЕДЕНИЕ

- Аналитическое моделирование теплового источника при наплавке стальной втулки центробежным методом с использованием осесимметричной электрической дуги 83
С.П. Глушко
- Исследование рабочих режимов дизельного двигателя на биотопливе 91
В.А. Лиханов, О.П. Лопатин
- Анализ температурных характеристик электролитно-плазменного разряда при струйной обработке металлического анода 99
А.И. Попов, В.И. Новиков, Д.Н. Иванов, И.А. Козырский
- Метод контроля надежности технических систем путем выявления энтропии причин их отказов 112
А.Т. Рыбак, С.В. Теплякова, А.В. Ольшевская, А.С. Пруцков

ИНФОРМАТИКА, ВЫЧИСЛИТЕЛЬНАЯ ТЕХНИКА И УПРАВЛЕНИЕ

- Прогнозирование сроков доставки товаров в цепях поставок с использованием методов машинного обучения 120
В.К. Резванов, О.М. Ромакина, Е.В. Зайцева
- Ab initio расчеты электронно-энергетической структуры и оптических свойств пироцирконатов лантана и неодима 129
А.А. Лаврентьев, Б.В. Габрельян, Ву Ван Туан, К.Ф. Калмыкова
- Интеграция сенсорных данных и математическое моделирование поведения подводного робота с использованием цифрового двойника 142
М.Д. Гладышев, А.В. Рыбаков
- Приближенный синтез H_∞ –регуляторов в нелинейных динамических системах на полубесконечном промежутке времени 152
А.В. Пантелеев, А.А. Яковлева

MACHINE BUILDING AND MACHINE SCIENCE МАШИНОСТРОЕНИЕ И МАШИНОВЕДЕНИЕ



UDC 621.793.182

Original Theoretical Research

<https://doi.org/10.23947/2687-1653-2025-25-2-83-90>

Analytical Modeling of a Heat Source under Welding of a Steel Sleeve by the Centrifugal Method Using an Axisymmetric Electric Arc

Sergey P. Glushko

Kuban State Technological University, Krasnodar, Russian Federation

✉ sputnik_s7@mail.ru

EDN: PZSKEU

Abstract

Introduction. The technology of centrifugal bimetalization using an independent axisymmetric electric arc is becoming increasingly important due to the high need to improve the quality of bimetallic compositions used in the manufacture of plain bearings, cylinder barrels for hydraulic units, and friction pair elements in internal combustion engines. The existing research in this area emphasizes the need for a more in-depth study of the features of thermal processes associated with this technology. In modern scientific literature, issues related to temperature control at the interface of materials are not fully disclosed, and the existing gap in the concept of the behavior of bimetallic compounds under heating conditions hinders the implementation of this technology in industrial production. The objective of this study is to conduct analytical modeling of a heat source in the form of an axisymmetric electric arc to determine the heat concentration coefficient and reduce the proportion of experimental data in the thermal process model, which will increase its versatility. The tasks arising from the stated goal are comparison of the results of calculating the effective heat flux density from two different expressions (using trigonometric and exponential functions), as well as evaluation of the distribution of the heat flux of an axisymmetric arc along the inner surface of the sleeves (this is required to establish the relationship between the temperature of the outer surface of the welded sleeve and the temperature at the interface between the materials).

Materials and Methods. Direct control of the temperature at the interface between the base material and the deposited layer is difficult, but it is possible to carry out indirect control using the temperature of the outer surface. To determine the relationship between the temperature of the outer surface of the deposited sleeve (billet) and the temperature on its inner surface, i.e., at the interface between the base material and the deposited layer, a heat source was modeled, the heat flux distribution of an axisymmetric electric arc along the inner surface of the sleeve was estimated, and an analytical expression was obtained to determine the heat concentration coefficient.

Results. In the course of the work, an analytical expression was obtained for determining the coefficient of heat concentration, $k = 0.945 / R_1^2$. It was required for calculating the electric arc parameters considering the distribution of the effective thermal power in the hot spot according to an exponential dependence. To simulate the heat source of the facing process (bimetalization) of the inner surface of steel sleeves with heating by an independent axisymmetric electric arc, the results of calculating the effective heat flux density were compared using two expressions: $q = q_0 \cdot \cos^3 \varphi$ and $q = q_0 \cdot e^{-k \cdot r_n^2}$. This comparison showed that for calculating temperature fields during facing of the inner surface of steel sleeves (billets) with metal alloys under heating by an independent axisymmetric arc, it was possible to use the analytical exponential form of representation of the heat source.

Discussion and Conclusion. Modeling thermal processes of the centrifugal bimetalization using simplified schemes of uniform distribution of heat flow $q = \text{const}$ on the entire free surface of the deposited layer, which simulates the spread of heat of an electric arc, requires the introduction of correction factors and a series of experiments to determine them. In this case, the description of the thermal process in the thermal process model contains a high proportion of experimental data and correction factors. Therefore, in order to exclude most of the experimental components when modeling the heat source and heat flow distribution of the facing process (bimetalization) of the inner surface of steel sleeves under heating by an independent axisymmetric electric arc, the author in this paper proposes an analytical solution for calculating the effective heat flow density in the form of an exponential function. This function allows determining the heat concentration coefficient of an independent axisymmetric electric arc during the facing process, which is required to increase the accuracy of calculating the temperature field of the bimetalized sleeve and improve the temperature control of the thermal parameters of the technological process.

Keywords: bimetals, surfacing, electric arc, centrifugal bimetalization, machine parts, wear-resistant coating, antifriction coating, restoration of parts, heat source, temperature calculation, heat concentration coefficient, electric arc modeling

Acknowledgements. The author would like to thank the Editorial board of the journal and the reviewers for their professional analysis and assistance in correcting the article.

For Citation. Glushko SP. Analytical Modeling of a Heat Source under Welding of a Steel Sleeve by the Centrifugal Method Using an Axisymmetric Electric Arc. *Advanced Engineering Research (Rostov-on-Don)*. 2025;25(2):83–90. <https://doi.org/10.23947/2687-1653-2025-2-83-90>

Оригинальное теоретическое исследование

Аналитическое моделирование теплового источника при наплавке стальной втулки центробежным методом с использованием осесимметричной электрической дуги

С.П. Глушко 

Кубанский государственный технологический университет, г. Краснодар, Российская Федерация

✉ sputnik_s7@mail.ru

Аннотация

Введение. Технология центробежной биметаллизации с применением независимой осесимметричной электрической дуги становится всё более значимой ввиду высокой потребности в улучшении качества биметаллических композиций, используемых в производстве подшипников скольжения, гильз для цилиндров гидромашин и элементов пар трения в двигателях внутреннего сгорания. Имеющиеся исследования в этой области подчеркивают необходимость более глубокого изучения особенностей тепловых процессов, связанных с этой технологией. В современной научной литературе недостаточно полно раскрыты вопросы, касающиеся контроля температуры на границе раздела материалов, и имеющийся пробел в представлении о поведении биметаллических соединений в условиях нагрева тормозит внедрение этой технологии в промышленное производство. Цель данного исследования — проведение аналитического моделирования теплового источника в виде осесимметричной электрической дуги для определения коэффициента сосредоточенности тепла и снижения доли экспериментальных данных в модели теплового процесса, что позволит повысить ее универсальность. Задачи, вытекающие из поставленной цели, заключаются в сравнении результатов расчета эффективной плотности теплового потока по двум различным выражениям (с использованием тригонометрической и экспоненциальной функций), а также в оценке распределения теплового потока осесимметричной дуги по внутренней поверхности втулок (это необходимо для установления зависимости между температурой наружной поверхности наплавляемой втулки и температурой на границе раздела материалов).

Материалы и методы. Прямой контроль температуры на границе раздела материала основы и наплавляемого слоя является затруднительным, однако возможно осуществить косвенный контроль с помощью температуры наружной поверхности. Для определения зависимости между температурой наружной поверхности наплавляемой втулки (заготовки) и температурой на её внутренней поверхности, то есть на границе раздела материала основы и наплавляемого слоя, были проведены моделирование теплового источника и оценка распределения теплового потока осесимметричной электрической дуги по внутренней поверхности втулки.

Результаты исследования. В ходе работы получено аналитическое выражение для определения коэффициента сосредоточенности тепла, $k = 0,945 / R_1^2$, который необходим для расчёта параметров электрической дуги с учётом распределения эффективной тепловой мощности в пятне нагрева по экспоненциальной зависимости. Для моделирования теплового источника процесса наплавки (биметаллизации) внутренней поверхности стальных втулок с нагревом независимой осесимметричной электрической дугой были сравнены результаты расчета эффективной плотности теплового потока по двум выражениям: $q = q_0 \cdot \cos^3 \varphi$ и $q = q_0 \cdot e^{-k \cdot r_n^2}$. Это сравнение показало, что для расчетов температурных полей при наплавке внутренней поверхности стальных втулок (заготовок) металлическими сплавами с нагревом независимой осесимметричной дугой можно использовать аналитическую экспоненциальную форму представления теплового источника.

Обсуждение и заключение. Моделирование тепловых процессов центробежной биметаллизации с применением упрощенных схем равномерного распределения теплового потока $q = const$ на всей свободной поверхности наплавляемого слоя, что имитирует распространение тепла электрической дуги, требует введения корректирующих коэффициентов и проведения серии экспериментов для их определения. В этом случае в описании теплового процесса

в модели тепловых процессов высока доля экспериментальных данных и корректирующих коэффициентов. Поэтому для исключения большей части экспериментальных составляющих при моделировании теплового источника и распределения теплового потока процесса наплавки (биметаллизации) внутренней поверхности стальных втулок с нагревом независимой осесимметричной электрической дугой автором в данной работе предложено аналитическое решение для расчета эффективной плотности теплового потока в виде экспоненциальной функции, которая позволяет определить коэффициент сосредоточенности тепла независимой осесимметричной электрической дуги в процессе наплавки, который необходим для повышения точности расчета температурного поля биметаллизируемой втулки и улучшения контроля температуры тепловых параметров технологического процесса.

Ключевые слова: биметаллы, наплавка, электрическая дуга, центробежная биметаллизация, детали машин, износостойкое покрытие, антифрикционное покрытие, восстановление деталей, тепловой источник, расчет температуры, коэффициент сосредоточенности тепла, моделирование электрической дуги

Благодарности. Автор выражает благодарность редакционной коллегии журнала и рецензенту за профессиональный анализ статьи и рекомендации для ее корректировки.

Для цитирования. Глушко С.П. Аналитическое моделирование теплового источника при наплавке стальной втулки центробежным методом с использованием осесимметричной электрической дуги. *Advanced Engineering Research (Rostov-on-Don)*. 2025;25(2):83–90. <https://doi.org/10.23947/2687-1653-2025-25-2-83-90>

Introduction. In units and mechanisms of various processing equipment, plain bearings are used, for the manufacture of which expensive antifriction and wear-resistant alloys from various metals are used [1]. Mechanical engineering also needs parts for friction pairs of internal combustion engine sleeves, screw-nut sliding gears [2], sleeves for hydraulic machine cylinders operating under high pressure conditions in the range of 50–60 MPa [3]. To improve performance characteristics and reduce the consumption of expensive materials, it is advisable to manufacture these parts from bimetal, in particular, from a steel-bronze composition. For example, laser [4] or thermal spraying [5] can be used to obtain bimetallic compositions. However, with these spraying technologies, it is very difficult to obtain layers 2–4 mm thick with an allowance for roughing and finishing. To deposit layers of sufficient thickness for subsequent processing, it is possible to use powder surfacing according to additive technology with the energy of an electron or laser beam [6], and to obtain coatings from wear-resistant alloys, it is possible to use laser cladding [7]. In the production of metal composites with a metal matrix, laser additive technologies are used [8]. In addition, selective laser melting (SLM) and electron beam melting (EBM) are applied. These are new technologies of rapid additive manufacturing [9], which provide for the production of complex monoliths from metals or alloys by selective melting of powder layers directed according to a CAD model. However, when facing the internal surfaces of sleeves with diameters of 80–250 mm, it is either difficult or impossible to place energy source units inside them.

Due to the complexity of the technical implementation of the listed technologies, the use of centrifugal bimetalization technology with an independent axisymmetric electric arc is becoming increasingly important. In [10], the modeling of the thermal process of centrifugal bimetalization of the inner surface of sleeves is described. There, a simplified scheme of uniform distribution of heat $q = \text{const}$ over the entire free surface of the deposited layer was adopted to calculate the temperature field of the bimetalized sleeve, which simulated the spread of heat of an electric arc that moved from end to end of the deposited sleeve at a speed of $v = 0.086$ m/s (the value of the Peclet number for this case allowed for such imitation). The disadvantage of this scheme is that its use requires the introduction of correction factors and the performance of a series of experiments to determine them. In this case, the model loses its universality, and the proportion of experimental data and correction factors in the description of the thermal process increases.

Analytical modeling of the heat flux density of an electric arc, calculation of the material temperature in the arc hot spot, and description of the temperature field of a bimetalized sleeve (billet) will allow solving the problem that faces the author — to reduce the proportion of experimentally obtained data in the model, increase the accuracy of calculating the temperature field of a bimetalized sleeve, and strengthen control over the temperature of the process.

To evaluate the heat flow distribution of the bimetalization process of sleeves and exclude most of the experimentally obtained data, the following steps must be taken:

- compare the results of calculating the effective heat flux density to a trigonometric function and an exponential function;
- identify the possibility of representing a heat source during facing of the internal surfaces of steel sleeves using the proposed technology with an exponential form to determine the heat concentration coefficient of an independent axisymmetric electric arc during the facing process.

Materials and Methods. This paper studies the technology of centrifugal bimetallization using an independent axisymmetric electric arc, whose diagram is shown in Figure 1.

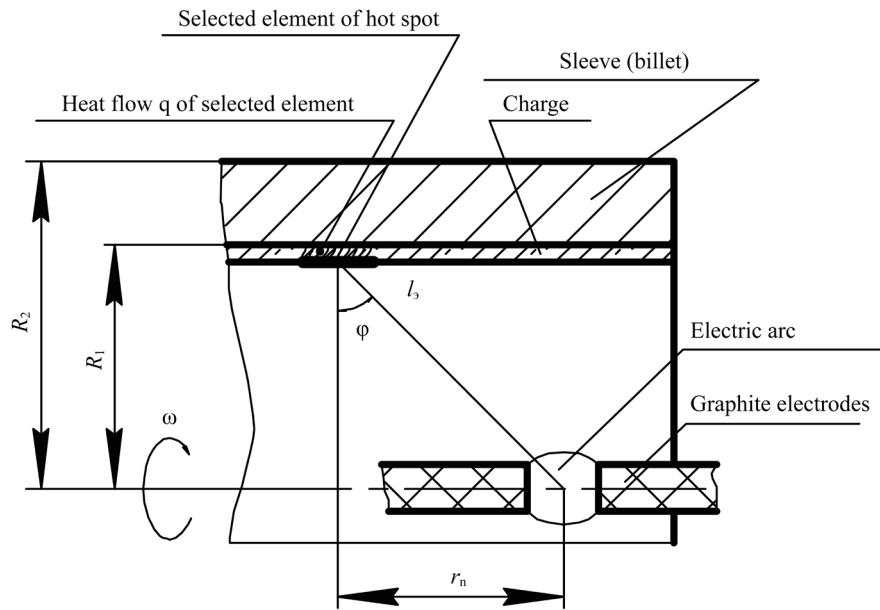


Fig. 1. Scheme of facing the inner surface of a steel sleeve (billet) using centrifugal method through heating by an independent axially symmetrical electric arc

The production of bimetallic sleeves (billets) with heating by an independent electric arc provides high quality of the deposited layer and bimetallic composition if correct temperature control is established at the interface between the deposited layer and the steel base — on the inner diameter of the sleeve R_1 . In production, direct control of temperature in the diffusion zone is difficult to implement, but indirect control is possible. It is based on the temperature of the outer surface of the steel base at diameter R_2 if there is a mathematical model that links the temperature of the outer surface of the welded billet (sleeve) at diameter R_2 and the temperature of its inner surface at diameter R_1 [10]. To solve this problem, it is necessary to use the heat transport theory [11]. In addition, initial data are needed, including a correct representation of the heat source [12] when calculating the temperature conditions of electric arc processes [10], e.g., bimetalized sleeves with heating by an independent axisymmetric electric arc.

Mathematical models of an electric arc can be divided into two groups according to the method of their construction [13]: theoretical models obtained on the basis of the laws of physics, and experimental models obtained as a result of approximating experimental data using various methods [14].

The use of models in which the heat source is presented as uniformly distributed along the length will not give accurate results for calculating the temperature fields of bimetalized sleeves, since it does not correspond to the real process.

To build a heating model for a bimetalized sleeve, it is proposed to estimate the distribution of the heat flow of an axisymmetric electric arc along the inner surface of the sleeve (billet) [10]. This is easier than modeling thermal processes for nonlinear asymmetric circuits [15].

We represent the problem as a linear one. To simplify the model, let us assume that the length of the billet is large enough to neglect heat losses at the ends. We replace the action of the arc with a point source of constant intensity (Fig. 1). The thermal power of the arc reaches the inner surface of the steel sleeve through the layer of charge practically without losses [1].

For such a scheme, the effective heat flux density on the inner surface of the steel sleeve at diameter R_1 is equal to:

$$q = \frac{0.9P_{\pi}}{4\pi} \cdot \frac{\cos \varphi}{l_3^2}, \text{ W/m}^2, \quad (1)$$

where P_{π} — electric arc power, W; l_3 — distance from the center of the arc to the center of the selected element on the inner surface of the steel sleeve, m; φ — angle between the direction of the flow radius vector and the normal to the element of the steel billet irradiated through the charge layer, deg.

At $\varphi = 0$, $l_3 = R_1$, the heat flux density is maximum:

$$q_0 = \frac{0.9P_n}{4\pi R_1^2}, \text{ W/m}^2,$$

here, R_1 — radius of the inner surface of the steel sleeve, m.

Considering that

$$l_3 = \frac{R_1}{\cos \varphi},$$

expression (1) can be represented as:

$$q = \frac{0.9P_n \cdot \cos \varphi}{4\pi R_1^2} = q_0 \cdot \cos^3 \varphi. \quad (2)$$

We introduce ratio $q/q_0 = 0.05$ into equality (2) and obtain $\varphi = 68^\circ 23'$, which corresponds to $\rho = r_n/R = 2.52$, where r_n — radius of the hot spot, i.e., at a distance close to 2.5–3.0 radii of the billet, the influence of the source is reduced to a minimum.

The distribution of the heat flux density of a point source can be described by the exponential dependence:

$$q = q_0 \cdot e^{-k \cdot r_n^2}, \quad (3)$$

where k — heat concentration coefficient, $1/\text{m}^2$.

Heat concentration coefficient k is required for calculating the parameters of an electric arc taking into account the distribution of effective thermal power in the hot spot. Determining the value of the heat concentration coefficient is needed for calculating the temperature of the material in the arc hot spot, since the pattern of the heat distribution has a significant effect on the temperature field in the area of the hot spot.

When the arc axis is directed perpendicular to the heating surface, the hot spot is obtained in the form of a circle with a specific flux normally distributed over the area. In this case, the source is called a normally-circular one.

In welding calculation schemes with vertical electrode placement relative to the heating surface, the values of heat concentration coefficients are in the range from 1.5 to 6.0. These schemes, which take into account the distribution of heat sources, are very complex and are rarely used in practice.

For specific cases, the values of parameters q_0 , q , and k , characterizing the heat flows of an electric arc, are most often determined experimentally.

To determine the preferability of using equalities (2) and (3) to calculate the specific heat flow (using these expressions), it is necessary to obtain an expression by which the heat concentration coefficient k can be calculated. For this purpose, the system of equations (2) and (3) should be solved.

Taking into account that

$$\cos \varphi = \frac{R_1}{\sqrt{R_1^2 + r_n^2}},$$

we determine the value of the heat concentration coefficient:

$$k = \frac{1}{2.52} \cdot \int_0^{2.52} \left(-\frac{3}{r_n^2} \right) \cdot \ln \left[\frac{R_1}{\sqrt{R_1^2 + r_n^2}} \right] \cdot dr.$$

Since $\cos \varphi$ can be represented as

$$\cos \varphi = \frac{1}{\sqrt{1 + \rho^2}},$$

then the heat concentration coefficient will be equal to:

$$k = \frac{1}{5.04 R_1^2} \cdot \int_0^{2.52} \frac{\ln(1 + \rho^2)}{\rho^2} \cdot dr. \quad (4)$$

We use a variable substitution in the form

$$g = \ln(1 + \rho^2),$$

and integrate equation (4) by parts:

$$k = \frac{3}{5.04 R_1^2} \cdot \left[-\frac{\ln(1 + \rho^2)}{\rho} + \int \frac{1}{\rho} \cdot \frac{2\rho}{1 + \rho^2} d\rho \right] \Bigg|_0^{2.52} = \frac{3}{5.04 R_1^2} \cdot \left[2 \arctg \rho - \frac{\ln(1 + \rho^2)}{\rho} \right] \Bigg|_0^{2.52}.$$

At $r = 0$, expression $\ln(1 + \rho^2) / \rho$ is not defined, therefore we use the limit transition:

$$\lim_{\rho \rightarrow 0} \frac{\ln(1 + \rho)^2}{\rho} = \lim_{\rho \rightarrow 0} \frac{\ln(1 + \rho^2) \cdot \rho}{\rho^2} = \lim_{\rho \rightarrow 0} \frac{\ln(1 + \rho^2)}{\rho^2} \cdot \lim_{\rho \rightarrow 0} \rho = 1 \cdot 0 = 0,$$

where $\lim_{\rho \rightarrow 0} \frac{\ln(1 + \rho)^2}{\rho} = 1$.

Since $k|_{r_n=0} = 0$, then the heat concentration coefficient will be equal to:

$$k = k|_{r_n=R_1} = k|_{r_n=R_1} - k|_{r_n=0} = \frac{3}{5.04 R_1^2} \cdot \left[2 \cdot \arctg 2.52 - \frac{\ln(1 + 2.52)^2}{2.52} \right] = \frac{0.945}{R_1^2}. \quad (5)$$

Research Results. We use obtained expression (5) to calculate the heat flux density through equation (3), in order to compare the results of calculations using equations (2) and (3) later on.

We compare values $Z_1 = \cos^3 \varphi$ and $Z_2 = e^{-k \cdot r_n^2}$ in equalities (2) and (3), setting $k = 0.945/R_1^2$.

The calculation results are presented in the form of a nomogram (Fig. 2).

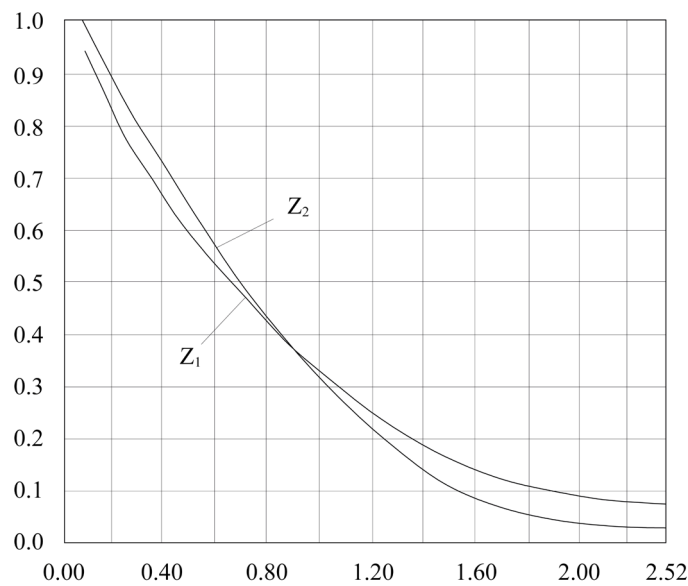


Fig. 2. Nomogram for comparing values $Z_1 = \cos^3 \varphi$ and $Z_2 = e^{-k \cdot r_n^2}$ in equalities (2) and (3)

The comparison of the calculated values of $Z_1 = \cos^3 \varphi$ and $Z_2 = e^{-k \cdot r_n^2}$ at $\rho = 0 \div 2.52$ have shown that they differ by no more than 10%. This provides using the exponential form of the heat source representation for calculating temperature fields under facing of the inner surface of steel sleeves (billets) with metal alloys heated by an independent axisymmetric arc.

Discussion and Conclusion. To calculate the temperature field of the bimetalized sleeve, a simplified scheme of uniform distribution of the heat flow $q = \text{const}$ over the entire free surface of the deposited layer of the electric arc, which reciprocate at a speed of $v = 0.086$ m/s (the value of the Peclet number for this case allows such imitation), is adopted. The disadvantage of this heat source model is that the heat flux density is determined from the condition of uniform heat distribution, i.e., it is necessary to apply correction factors and conduct a series of experiments to determine them. Thus, the description of the thermal process will contain a high proportion of experimental data and correction factors. Therefore, in order to exclude most of these data when modeling the heat source and heat flow distribution of the facing process (bimetalization) in the method under study, a comparison was made of the results of calculating the effective heat flow density using two expressions: with a trigonometric function and an exponential function. It is found that the exponential form of the heat source representation under facing the inner surfaces of steel sleeves (billets) through the centrifugal method with heating by an independent axisymmetric electric arc can be used to determine the heat concentration coefficient in the facing process. This coefficient is used to determine the density of the heat flow of an electric arc, the temperature at the heating point, and to describe the temperature field of a bimetalized sleeve in analytical form, which increases the accuracy of calculating its temperature field and the ability to control the temperature of a given production process.

References

1. Denisenko SG, Glushko SP. Optimization of Production Technology of Plain Bearings from Steel-Bronze Bimetal. In: *Abstracts of the IV Ukrainian Republican Scientific and Technical Conference “Modern Methods of Surfacing, Hardening Coatings and Materials Used”*. Kharkov: Kharkov Automobile and Highway Institute; 1990. P. 70–71. (In Russ.)
2. Glushko SP, Denisenko SG. Synthesis of Quality Criterion for Bimetallic Plain Bearings. In: *Abstracts of the All-Union Scientific Conference “Structural Strength, Durability, Hardening of Materials and Machine Parts”*. Volgograd: Center of Science and Technology; 1990. P. 202–204. (In Russ.)
3. Klevetov DV, Starostin DA. An Approach to Increasing the Durability of Hydraulic Machines by Reducing the Intensity of Wear during Technological Running. In: *Proc. All-Russian Sci.-Tech. and Research-Methodological Conference “Modern Problems of Reliability and Technosphere Safety: Education, Science, Practice”*, dedicated to the 20th Anniversary of the Department of Life Safety, Ecology and Chemistry, Kovrov State Technological Academy named after V.A. Degtyarev. Kovrov: Degtyarev State Technological Academy; 2019. P.41–46. (In Russ.)
4. Arias-González F, del Val J, Comesaña R, Penide J, Lusquiños F, Quintero F, et al. Production of Phosphor Bronze Coatings by Laser Cladding. *Procedia Manufacturing*. 2017;13:177–182. <https://doi.org/10.1016/j.promfg.2017.09.031>
5. Kumar RK, Kamaraj M, Seetharamu S, Pramod T, Sampathkumaran P. Effect of Spray Particle Velocity on Cavitation Erosion Resistance Characteristics of HVOF and HVOF Processed 86WC–10Co4Cr Hydro Turbine Coatings. *Journal of Thermal Spray Technology*. 2016;25(6):1217–1230. <https://doi.org/10.1007/s11666-016-0427-3>
6. Frazier WE. Metal Additive Manufacturing: A Review. *Journal of Materials Engineering and Performance*. 2014;23(6):1917–1928. <https://doi.org/10.1007/s11665-014-0958-z>
7. Zhenglei Yu, Lunxiang Li, Deqiang Zhang, Guangfeng Shi, Guang Yang, Zezhou Xu, et al. Study of Cracking Mechanism and Wear Resistance in Laser Cladding Coating of Ni-Based Alloy. *Chinese Journal of Mechanical Engineering*. 2021;34(92):1–14. <https://doi.org/10.1186/s10033-021-00599-8>
8. Neng Li, Wei Liu, Yan Wang, Zijun Zhao, Taiqi Yan, Guohui Zhang, et al. Laser Additive Manufacturing on Metal Matrix Composites: A Review. *Chinese Journal of Mechanical Engineering*. 2021;34(38):1–16. <https://doi.org/10.1186/s10033-021-00554-7>
9. Murr LE, Gaytan SM, Ramirez DA, Martinez E, Hernandez J, Amato KN, et al. Metal Fabrication by Additive Manufacturing Using Laser and Electron Beam Melting Technologies. *Journal of Materials Science & Technology*. 2012;28(1):1–14. [https://doi.org/10.1016/S1005-0302\(12\)60016-4](https://doi.org/10.1016/S1005-0302(12)60016-4)
10. Lawrence AR, Michaleris P. Effects of Thermal Transport in Computation of Welding Residual Stress and Distortion. *Science and Technology of Welding and Joining*. 2011;16(3):215–220. <https://doi.org/10.1179/1362171810Y.0000000027>
11. Glushko SP, Popravka DL, Abramov NS. Modeling the Thermal Process of Centrifugal Bimetalization of the Inner Surface of Bushings. *Welding Production*. 2009;(6):30–35. (In Russ.)
12. Sudnik VA, Erofeev VA, Maslennikov AV, Tsvelev RV. Methodology of Determining the Equivalent Heat Source Parameters for the Subsequent Calculations of the Structure Distortions. *Izvestiya Tula State University*. 2015;(6-2):32–43. URL: https://tidings.tsu.tula.ru/tidings/pdf/web/file/tsu_izv_technical_sciences_2015_06_part_2.pdf (accessed: 20.03.2025).
13. Polishchuk V. Mathematical Modeling of Welding Processes. *Scientific and Methodological Electronic Journal “Concept”*. 2014;20:356–360. URL: <http://e-koncept.ru/2014/54332.htm> (accessed: 20.03.2025).
14. Vershinin VP, Dmitriev IK. Experimental Research of Temperature Distribution in Tee Joints during Welding. *Engineering Journal of Don*. 2023;(4):1–9. URL: <http://www.ivdon.ru/ru/magazine/archive/n4y2023/8330> (accessed: 20.03.2025).
15. Ivanov SYu, Karhin VA, Michaylov VG. Modelling Welding Processes with Curvilinear Seams. *Izvestiya Tula State University*. 2015;(6-2):62–66. URL: https://tidings.tsu.tula.ru/tidings/pdf/web/file/tsu_izv_technical_sciences_2015_06_part_2.pdf (accessed: 20.03.2025).

About the Author:

Sergey P. Glushko, Cand.Sci. (Eng.), Associate Professor of the Department of Engineering of Control Systems, Materials and Technologies in Mechanical Engineering, Kuban State Technological University (2, Moskovskaya Str., Krasnodar, 350000, Russian Federation), [SPIN-code](#), [ORCID](#), sputnik_s7@mail.ru

Conflict of Interest Statement: the author declares no conflict of interest.

The author has read and approved the final version of manuscript.

Об авторе:

Сергей Петрович Глушко, кандидат технических наук, доцент, кафедра «Инженерии систем управления, материалов и технологий в машиностроении» Кубанского государственного технологического университета (350072, Российская Федерация, г. Краснодар, ул. Московская, 2), [SPIN-код](#), [ORCID](#), sputnik_s7@mail.ru

Конфликт интересов: автор заявляет об отсутствии конфликта интересов.

Автор прочитал и одобрил окончательный вариант рукописи.

Received / Поступила в редакцию 23.03.2025

Reviewed / Поступила после рецензирования 18.04.2025

Accepted / Принята к публикации 22.04.2025

MACHINE BUILDING AND MACHINE SCIENCE МАШИНОСТРОЕНИЕ И МАШИНОВЕДЕНИЕ



UDC 621.43

Original Empirical Research

<https://doi.org/10.23947/2687-1653-2025-25-2-91-98>

Study of Operating Modes of a Biofuel Diesel Engine

Vitaly A. Likhanov , Oleg P. Lopatin

Vyatka State Agrotechnological University, Kirov, Russian Federation

✉ nirs_vsaa@mail.ru

EDN: OUWFGB

Abstract

Introduction. Modern research aimed at reducing emissions of harmful substances resulting from the operation of diesel engines using alternative fuels emphasizes their importance and relevance. This topic is becoming increasingly significant in the context of global environmental changes. The development and implementation of alternative energy sources not only contribute to improving air quality, but also help reduce dependence on fossil fuels. Therefore, it is important to continue investing in research and new technologies that will provide for cleaner and more efficient use of resources. There are numerous such studies, specifically, theoretical ones, conducted in European and Asian countries. However, there are practically no experimental works devoted to hemispherical combustion chambers of Russian diesel engines, whose rotation speed, compression ratio and other design parameters differ significantly from similar characteristics described in known studies. In addition, there are practically no experiments devoted to the combustion process of Russian diesel engines with an undivided hemispherical combustion chamber in the piston, which determines the complexity of the volumetric-film mixing process. The research objective is an experimental study of the power and economic indicators, parameters of the combustion process of a diesel engine with an undivided hemispherical combustion chamber in the piston, running on ethanol and rapeseed oil (RO). The study is aimed at establishing dependences showing the effect of various engine operating modes on the specified indicators in order to determine their numerical characteristics.

Materials and Methods. The diesel engine was started using rapeseed oil, after which the ethanol supply was switched on, replacing the rapeseed oil until the set optimum value was reached. The increase in the operating load mode was provided through regulating the ethanol supply. An additional high-pressure fuel pump (HPFP) 2UTNM was installed to supply rapeseed oil, and ethanol was supplied through the standard fuel supply system.

Results. The indicators of the combustion process of a diesel engine running on ethanol and rapeseed oil differ from its regular diesel engine. When working with ethanol and rapeseed oil, an increase in the ignition delay period is noted, which affects the “rigidity” of the combustion process and results in a growth of P_z value. These factors are most likely the main limitations for the use of ethanol by direct injection. One of the solutions to this problem, proposed in this paper, is the use of ignition (pilot) rapeseed oil, which makes it possible to adjust parameters of the combustion process through controlling the amount of ignition fuel supply.

Discussion and Conclusion. The results of the conducted experimental study confirm the possibility of complete replacement of petroleum motor fuel in a diesel engine with an undivided hemispherical combustion chamber in the piston with an alternative (renewable) fuel. This undoubtedly solves important issues of environmental safety of diesel engines. The research results may be useful both to scientists working on this topic, and to engineers and technicians in the machine-building industry.

Keywords: diesel engine, ethanol, rapeseed oil, cylinder, combustion process, pressure, temperature, crankshaft speed

Acknowledgements. The authors would like to thank Vladimir Anatolyevich Markov, Dr.Sci. (Engineering), Professor, Head of the E-2 Department of Combined Engines and Alternative Power Plants, Bauman Moscow State Technical University; Andrey Mikhailovich Saikin, Dr.Sci. (Engineering), Senior Researcher, Chief Specialist of the Center of Information and Intelligent Systems, RF State Research Center “NAMI”; Lev Alekseevich Zholobov, Cand.Sci. (Engineering), Professor of the Department of Operation of Mobile Power Equipment and Agricultural Machinery, Nizhny Novgorod State Technical University named after L.Ya. Florentyev, for consultations and assistance provided in writing this paper.

For Citation. Likhanov VA, Lopatin OP. Study on Operating Modes of a Biofuel Diesel Engine. *Advanced Engineering Research (Rostov-on-Don)*. 2025;25(2):91–98. <https://doi.org/10.23947/2687-1653-2025-25-2-91-98>

Оригинальное эмпирическое исследование

Исследование рабочих режимов дизельного двигателя на биотопливе

В.А. Лиханов , О.П. Лопатин  

Вятский государственный агротехнологический университет, г. Киров, Российская Федерация

 nirs_vsaa@mail.ru

Аннотация

Введение. Современные исследования, направленные на снижение выбросов вредных веществ, образующихся в результате работы дизельных двигателей с использованием альтернативного топлива, подчеркивают их значимость и актуальность. Эта тема приобретает всё большую важность в контексте глобальных экологических изменений. Разработка и внедрение альтернативных источников энергии не только способствуют улучшению качества воздуха, но и помогают уменьшить зависимость от ископаемых топлив. Поэтому важно продолжать инвестировать в научные исследования и новые технологии, которые позволят добиться более чистого и эффективного использования ресурсов. На сегодняшний день известно множество таких исследований, особенно теоретических, проведённых в европейских и азиатских странах. Однако практически отсутствуют экспериментальные работы, посвящённые полусферическим камерам сгорания российских дизельных двигателей, у которых частота вращения, степень сжатия и другие конструктивные параметры существенно отличаются от аналогичных характеристик, описанных в известных исследованиях. Кроме того, нет практически никаких экспериментов, посвящённых процессу сгорания российских дизельных двигателей с неразделённой полусферической камерой сгорания в поршне, что обуславливает сложность процесса объемно-плёночного смесеобразования.

Целью работы является экспериментальное исследование мощностных и экономических показателей, параметров процесса сгорания дизельного двигателя с неразделённой полусферической камерой сгорания в поршне, работающего на этаноле и рапсовом масле (РМ). Исследование направлено на установление зависимостей, показывающих влияние различных режимов работы двигателя на указанные показатели, с целью определения их числовых характеристик.

Материалы и методы. Запуск дизельного двигателя осуществлялся на рапсовом масле, после чего включалась подача этанола, который заменял рапсовое масло до достижения установленного оптимального значения. Увеличение рабочего нагрузочного режима обеспечивалось регулированием подачи этанола. Для подачи рапсового масла был установлен дополнительный топливный насос высокого давления (ТНВД) 2УТНМ, а подача этанола производилась через стандартную систему топливоподачи.

Результаты исследования. Показатели процесса сгорания дизельного двигателя, работающего на этаноле и рапсовом масле, заметно отличаются от таковых у двигателя, функционирующего на дизельном топливе. При работе на этаноле и рапсовом масле наблюдается увеличение периода задержки воспламенения, что влияет на «жесткость» процесса сгорания и приводит к повышению значений величины P_z . Эти факторы, скорее всего, являются основными ограничениями для использования этанола посредством непосредственного впрыска. Одним из решений данной проблемы, предложенным в настоящей работе, является использование запального (пилотного) рапсового масла, которое позволяет корректировать параметры процесса сгорания, регулируя величину подачи запального топлива.

Обсуждение и заключение. Результаты проведенного экспериментального исследования подтверждают возможность полного замещения нефтяного моторного топлива в дизельном двигателе с неразделённой полусферической камерой сгорания в поршне альтернативным (возобновляемым) топливом, что, несомненно, решает важные вопросы экологической безопасности дизельных двигателей. Результаты исследования могут быть полезны как ученым, занимающимся данной темой, так и инженерно-техническим работникам машиностроительной отрасли.

Ключевые слова: дизельный двигатель, этанол, рапсовое масло, цилиндр, процесс сгорания, давление, температура, частота вращения коленчатого вала

Благодарности. Авторы выражают благодарность Маркову Владимиру Анатольевичу, доктору технических наук, профессору, заведующему кафедрой Э-2 «Комбинированные двигатели и альтернативные энергоустановки» МГТУ им. Н.Э. Баумана; Сайкину Андрею Михайловичу, доктору технических наук, старшему научному сотруднику, главному специалисту Центра интеллектуальных систем ГНЦ РФ ФГУП «НАМИ»; Жолобову Льву Алексеевичу, кандидату технических наук, профессору, профессору кафедры эксплуатации мобильных энергетических средств и сельскохозяйственных машин ФГБОУ ВО Нижегородский ГАТУ им. Л.Я. Флорентьева за консультации и помощь, оказанную при написании данной работы.

Для цитирования. Лиханов В.А., Лопатин О.П. Исследование рабочих режимов дизельного двигателя на биотопливе. *Advanced Engineering Research (Rostov-on-Don)*. 2025;25(2):91–98. <https://doi.org/10.23947/2687-1653-2025-25-2-91-98>

Introduction. In the short and long terms, sustainability and environmental safety issues in the mechanical engineering industry will remain crucial [1]. For example, within the framework of the program package, the European Council has set itself the goal of reducing carbon dioxide emissions by at least 55% by 2030 compared to 1990, and achieving zero CO₂ emissions by 2050. According to the latest forecasts, by 2040, about 75% of the 1.6 billion passenger cars on the road will be either internal combustion engine (ICE) vehicles or ICE hybrid vehicles [2]. Hybrid powertrains, both with high and low electrification, combined with modern internal combustion engines, can indeed provide significant benefits in various markets, including the environmental sphere [3]. However, today, the electrification of vehicles remains a challenging task due to numerous real and perceived factors. These factors include limited range, irregular charging infrastructure, regional availability of fully renewable energy sources, demand constraints, and challenges related to the mining and processing of rare earth and precious metals [4]. For light-duty freight applications, electrification may be considered an acceptable alternative to ICE, but it still has a carbon footprint [5].

The approaches to environmental safety in the mechanical engineering industry discussed above fit organically only in the long-term perspective. As a result, a transition to the use of low-carbon or carbon-free fuel is planned [6]. As for the near future and the internal combustion engines currently operating on traditional petroleum motor fuel [7], it is important to discuss the possibility of using alternative fuels both from the point of view of environmental safety and in the context of replacing petroleum-based fuels [8]. We believe that the mechanical engineering industry, being one of the main sources of atmospheric pollution, requires fundamental changes in approaches to fuel use [9]. In order to implement structural changes aimed at improving environmental parameters in mechanical engineering, original equipment manufacturers and their partners should consider the possibility of technological breakthroughs in the modernization of existing ICE [10] and the creation of low-emission vehicles [11, 12].

Given the high relevance of using alternative fuels in diesel power units, this circumstance forces the leading machine builders to consider the development of technologies that facilitate the use of various alternative fuels in diesel engines (DE) [13]. The search for new methods and promising technologies aimed at improving the environmental and energy performance of diesel power units, as well as the study on the competition of various types of fuel (diesel fuel, biofuel, natural gas, alcohols, emulsions, etc.) in terms of environmental efficiency can be a significant step towards activating the development and use of alternative motor fuels [14]. The transition to alternative fuels that are not petroleum products will be the most promising direction in the fight to improve the environmental performance for both diesel engines and vehicles in the engineering industry [16].

The most promising in terms of improving the environmental safety of DE are alcohols and vegetable oils [17]. Specifically, when considering alcohols, preference is given to ethanol, which meets the criteria of availability, ease of production and, most importantly, environmental friendliness during combustion [18]. From the authors' point of view, vegetable oils are of the greatest interest, among which rapeseed oil (RO) is the leader, having excellent technical characteristics, such as high energy density and good fluidity at low temperatures [19].

To date, numerous relevant scientific works have been conducted aimed at improving the environmental safety of diesel engines using alcohols and vegetable oils as motor fuel [20]. However, it should be noted that the analysis of the scientific research results demonstrates the lack of sufficient experimental tests of diesel power units with a working volume of up to 5 liters, running on ethanol and vegetable oils, performed taking into account the relationship between NO_x, CH_x, CO, CO₂ and soot content (SC) in exhaust gases [21]. Although these issues have been widely covered in the literature in terms of theory using various modern forms of modeling, the investigation of this problem only from a theoretical point of view does not help to reveal some critical aspects that are important for organizing the workflow of DE when using ethanol and vegetable oils [22].

This work is aimed at an experimental study of the power and economic indicators, as well as the parameters of the combustion process of a diesel engine with an undivided hemispherical combustion chamber in the piston, operating on ethanol and rapeseed oil, with the establishment of dependences of the impact of its operating modes on the specified indicators and the determination of their numerical characteristics.

Materials and Methods. To achieve the set goal, experimental studies of the DE 2Ch 10.5/12.0 were conducted when operating on ethanol and RO. The DE was started on RO, then the ethanol supply was turned on and replaced RO to the set optimal value (cyclic supply was at the level of 13 mg/cycle, which corresponded to an hourly RO consumption of 1.4 kg/h). An increase in the operating load mode was provided by increasing (regulating) the ethanol supply. An additional fuel injection pump was installed to supply RO, and ethanol was delivered through the standard fuel supply system.

To indicate the working process of the DE, the PS-01 pressure sensor was used, the signal from the sensor was sent to the AQ05-A.1.001 signal amplifier, the amplified signal was sent to the PC via the LA-2 USB analog-to-digital converter (ADC). The pressure sensor was installed in a sleeve mounted in the cylinder head, according to the instruction. The signal from the M50 crankshaft position sensor was fed to the ADC without amplification. The obtained data were processed using a special array superposition algorithm, then the combustion process indicators were determined using the obtained averaged indicator diagram by the methods of Central Research Diesel Institute and Central Research Institute of Materials based on the Wiebe theory [23].

Research Results. Figure 1 shows the results of determining the average indicator diagram for optimal installation angles of fuel injection advance for ethanol and RO, equal to 34° before top dead center (TDC) [15].

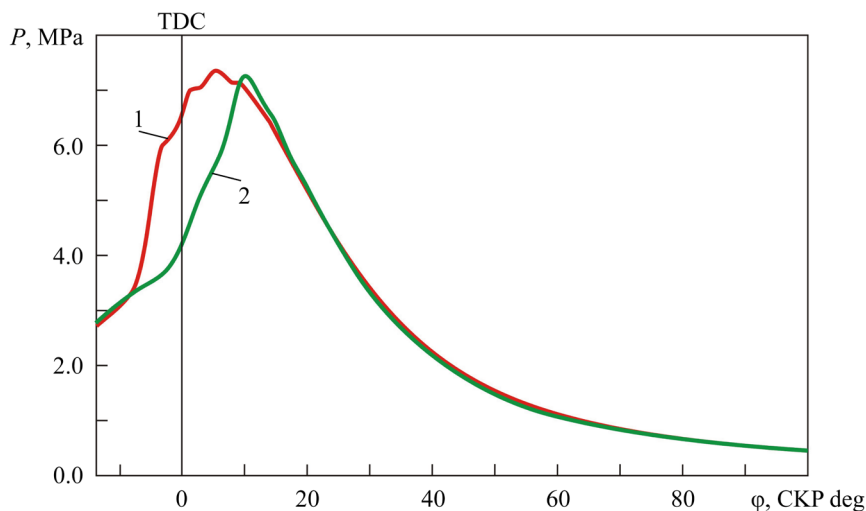


Fig. 1. Effect of DE crankshaft angle on the indicator pressure: 1 — DF; 2 — ethanol and RO [22]

From scientific literature, researchers are well aware of the valuable qualities of the indicator diagram. This direct recording of the actual (indicator) pressure depending on the crankshaft angle clearly demonstrates the value of the physical quantity without the need to perform any calculations. Using the indicator diagram, one can easily understand the dynamics of the working process and obtain valuable information on the amount of the maximum combustion pressure P_z of the ignition delay period (IDP). In addition, the indicator diagram is a visual representation of the dynamics of autoignition in a diesel engine [22]. Thus, the analysis of the indicator diagrams presented in Figure 2 shows that when operating on ethanol and RO, an increase in the IDP is observed, while no significant change in the maximum pressure in the cycle is noted. Since the calorific value of ethanol is lower than that of diesel fuel, it is required to compensate for this difference by increasing the cyclic fuel supply (Fig. 2).

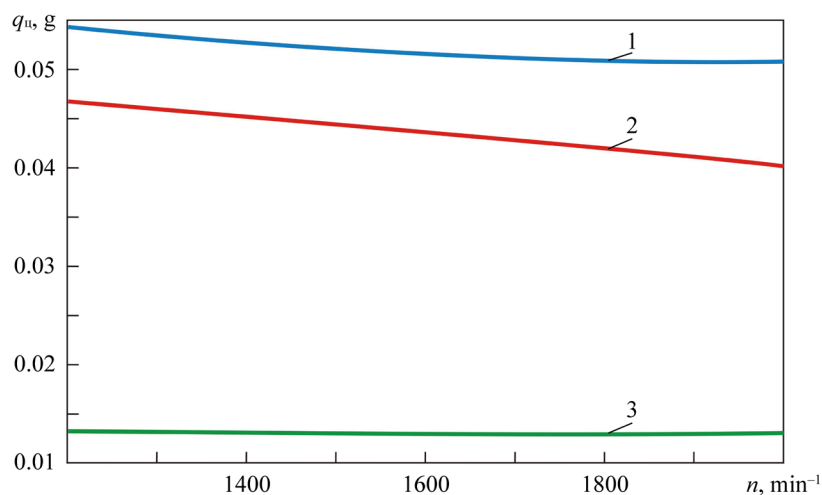


Fig. 2. Cyclic fuel supply: 1 — DF; 2 — ethanol; 3 — RO [11]

Considering the nominal speed mode ($n = 1,800 \text{ min}^{-1}$), we note that the RO supply was 13 mg/cycle, while the ethanol supply reached 52 mg/cycle (Fig. 2). In the diesel mode, the cyclic supply was 43 mg/cycle.

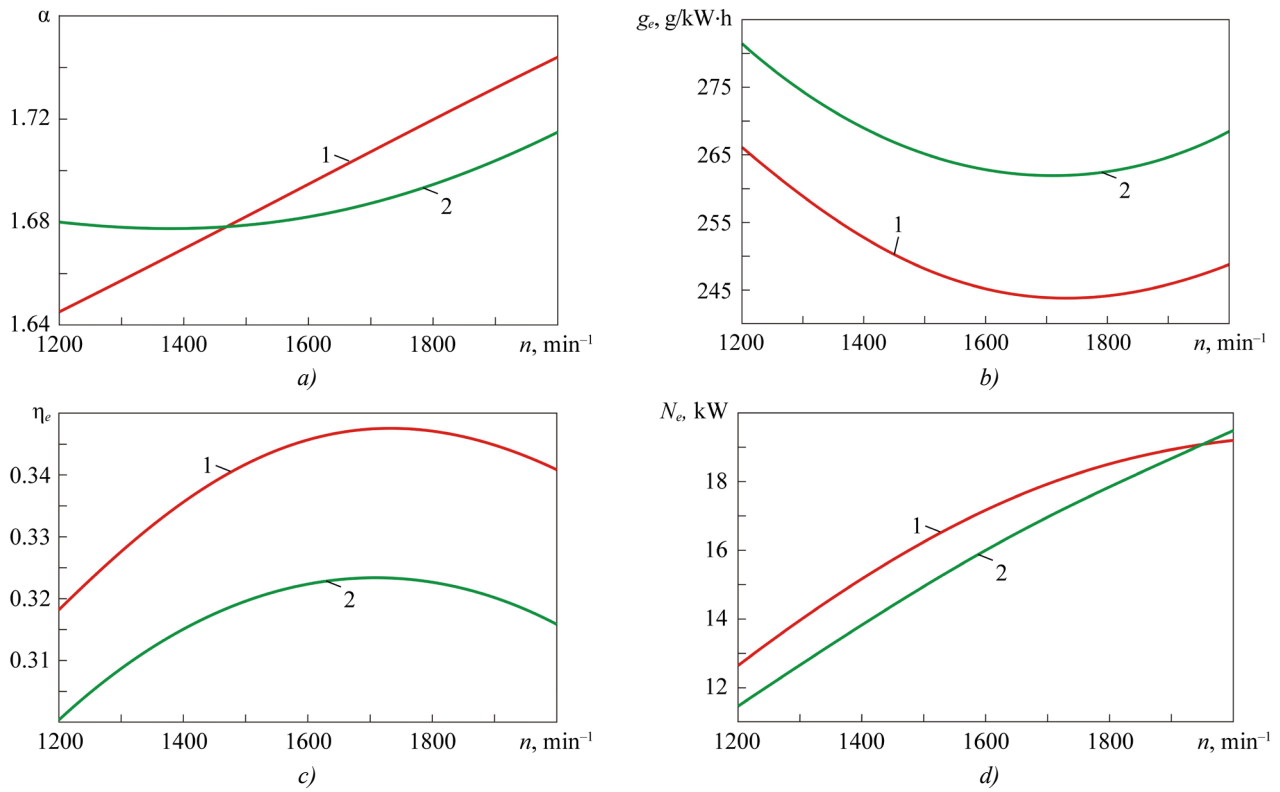


Fig. 3. DE performance:
 a — excess air factor; b — specific effective fuel consumption; c — effective efficiency;
 d — effective power; 1 — DF; 2 — ethanol and RO [11]

When operating on ethanol and RO, an increase in fuel consumption reduces the effective efficiency, specifically at low rotation speeds, which cannot but affect the effective power and leads to some reduction (Fig. 3 d). And at peak values, when the DE operates on ethanol and RO, the power indicators and characteristics of the combustion process (Fig. 4 a) already exceed the DF values.

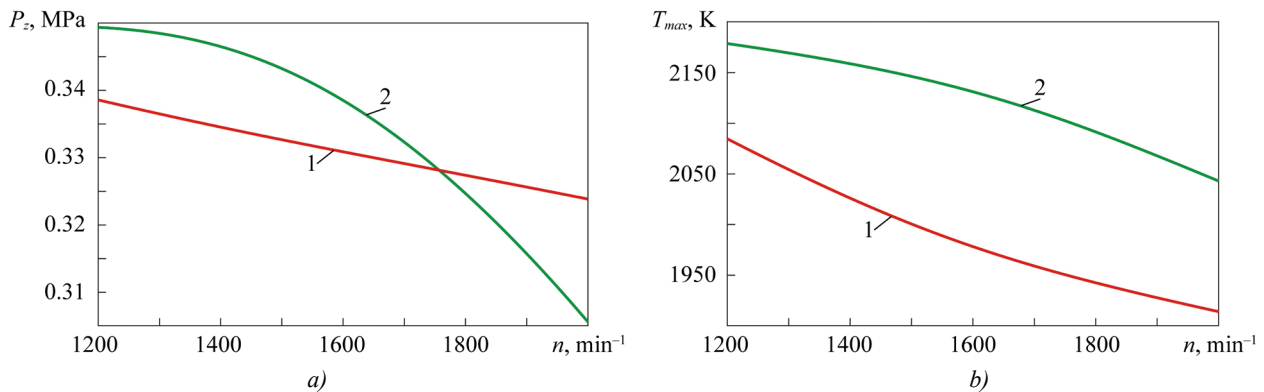


Fig. 4 Indicators of DE combustion process:
 a — maximum combustion pressure; b — maximum average temperature;
 1 — DF; 2 — ethanol and RO [15]

Analyzing the graphical dependences shown in Figure 4, it should be noted that at low rotational speeds of the DE operation on ethanol and RO, P_z is equal to 8.2 MPa, and at a lower rotation speed, it is 6.5 MPa. Value T_{max} also decreases, but remains higher than the values of the DE operation on DF. Apparently, this growth is due to the higher IDP of the DE when operating on ethanol and RO, since over a longer period of time, a larger amount of fuel evaporates when mixing with air. This, in turn, results in an increase in the intensity of heat release processes in the kinetic phase of combustion and an increase in T_{max} with the achievement of its maximum values at later angles. Thus, when DE operates on ethanol and RO, combustion starts later by approximately 4–7 degrees compared to operation on DF [15].

Figure 5 shows the toxicity characteristics of the exhaust gases (EG) of the DE at the nominal speed.

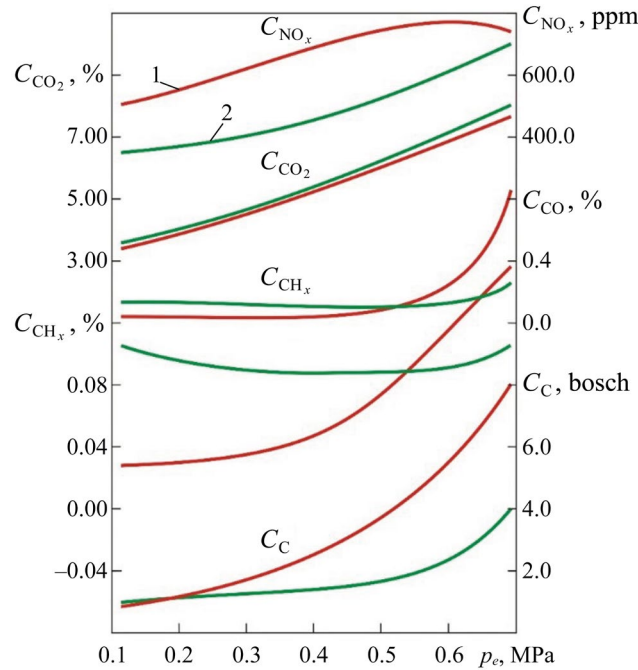


Fig. 5. DE EG toxicity indices ($n = 1800 \text{ min}^{-1}$):
1 — DF; 2 — ethanol and RO

The results of experimental studies on the toxicity of DE show that the use of ethanol and RO causes a decrease in the concentration of nitrogen oxides (NO_x), carbon dioxide (CO_2) and soot (S) in the studied modes. At loads above average, there is a decrease in the concentration of carbon monoxide (CO) and hydrocarbons (CH_x).

The numerical values of the results of experimental studies on the toxicity of DE at the nominal operating mode are summarized in Table 1.

Table 1

Results of Studies on Toxicity and Smoke Indicators of DE EG 2Ch 10.5/12.0
When Running on Ethanol and RO ($n = 1800 \text{ min}^{-1}$, $p_e = 0.588 \text{ MPa}$)

Fuel	Indicators			
	NO_x , ppm	S, ea on Bosch scale	CH_x , %	CO, %
Diesel fuel	790	5.3	0.11	0.22
Ethanol +RO	590 (decrease by 25.3%)	2.2 (2.4 times decrease)	0.09 (decrease by 18.2%)	0.14 (decrease by 36.4%)

Discussion and Conclusion. Analyzing the obtained results of the considered experimental studies, it should be noted that the combustion process indicators of the DE, working on ethanol and RO, differ from its standard one, working on DF. Especially when using ethanol and RO, an increase in the area of influence zone (IZA) is observed, which cannot but have a significant effect on the “rigidity” of the combustion process and will result in an increase in value P_z . These arguments are likely to be the main restraining factors for the use of ethanol by direct injection. One of the possible solutions to the problem, proposed in this paper, is the use of pilot RO, which allows the combustion process parameters to be adjusted through controlling the amount of pilot fuel supplied. It should be explained that the pilot RO value was changed to a certain value (indicated above in the paper), at which the required combustion parameter characteristics were obtained. After that, the RO value was fixed, and the change in the DE load modes was provided by the required ethanol supply. It is clear to experts that this solves the problem only in a particular case. In further research, it will be necessary to implement dynamic adjustment of both the RO ignition portion value and the fuel injection advance angle. This will facilitate further optimization of the fuel supply system, and the organization of the combustion process as a whole. Nevertheless, to sum up, we note that this work has solved the issues of improving the operational characteristics of DE by using biofuel with the establishment of characteristic dependences of the impact of operating modes on efficiency and the determination of their numerical values. Moreover, the effectiveness of the proposed solution is confirmed by the complete replacement of petroleum motor fuel with alternative (renewable) one.

References

1. Kavtaradze RZ, Onischenko DO, Golosov AS, Zelentsov AA, Chen Zh, Sakhvadze GZh. The Influence of the “Piston Heat Belt–Sleeve” Gap on Heat Exchange in the Combustion Chamber of an Engine Depending on the Fuel Utilized. *Journal of Machinery Manufacture and Reliability*. 2022;51(2):112–120. <https://doi.org/10.3103/S1052618822010046>
2. Kulagin V, Grushevenko D, Galkina A. Global and Russian Energy Outlook Up to 2050. *Contemporary World Economy*. 2024;2(1):6–22. <https://doi.org/10.17323/2949-5776-2024-2-1-6-22>
3. Sens M. Hybrid Powertrains with Dedicated Internal Combustion Engines are the Perfect Basis for Future Global Mobility Demands. *Transportation Engineering*. 2023;13:100146. <https://doi.org/10.1016/j.treng.2022.100146>
4. Beltrami D, Iora P, Uberti S, Tribioli L. Electrification of Compact Off-Highway Vehicles – Overview of the Current State of the Art and Trends. *Energies*. 2021;14(17):5565. <https://doi.org/10.3390/en14175565>
5. Vokhmin DM, Kozin ES. Basics of Monitoring the Carbon Footprint of Traffic Flows in Large Cities. *Transport: Science, Equipment, Management. Scientific Information Collection*. 2024;(6):11–17.
6. Fangyuan Zheng, Haeng Muk Cho. The Effect of Different Mixing Proportions and Different Operating Conditions of Biodiesel Blended Fuel on Emissions and Performance of Compression Ignition Engines. *Energies*. 2024;17(2):344. <https://doi.org/10.3390/en17020344>
7. Mateichyk V, Kryshchyna S, Kryshchyna L, Smieszek M, Kostian N, Mosciszewski J, et al. Research of Energy Efficiency and Environmental Performance of Vehicle Power Plant Converted to Work on Alternative Fuels. *Machines*. 2024;12(5):285. <https://doi.org/10.3390/machines12050285>
8. Markov VA, Devyanin SN, Bowen Sa, Normurodov AA. Investigation of the Operation of a Diesel Engine on Blended and Emulsified Biofuels with Rapeseed Oil Additives. *Dvigatelistroyeniye (Engines Construction)*. 2023;291(1):70–90. <https://doi.org/10.18698/jec.2023.1.70-90>
9. Keunsang Lee, Haeng Muk Cho. Effects of Castor and Corn Biodiesel on Engine Performance and Emissions under Low-Load Conditions. *Energies*. 2024;17(13):3349. <https://doi.org/10.3390/en17133349>
10. Kavtaradze RZ, Kondratyev AM, Rongrong Ch, Citian Ch, Baigang S, Sakhvadze GZh. Local Heat Exchange in the Combustion Chamber of a Hydrogen Engine Running on a Lean Fuel Mixture. *Journal of Machinery Manufacture and Reliability*. 2021;50(1):79–87. <https://doi.org/10.3103/S105261882101012X>
11. Likhanov VA, Lopatin OP. High-Speed Operation Modes of a Biofuel Diesel Engine. *Dvigatelistroyeniye (Engines Construction)*. 2024;296(2):75–83.
12. Rathinavelu V, Kulandaivel A, Pandey AK, Bhatt R, De Pours MV, Hossain I, et al. Production of Green Hydrogen from Sewage Sludge/Algae in Agriculture Diesel Engine: Performance Evaluation. *Heliyon*. 2024;10(1):e23988. <https://doi.org/10.1016/j.heliyon.2024.e23988>
13. Zheliezna T, Drahnev S. Comparative Analysis of Biodiesel and Renewable Diesel as Motor Fuels. *Journal of Science. Lyon*. 2024;57:34–39. <https://doi.org/10.5281/zenodo.13694682>
14. Kovbasenko S. Possibilities of Enhancing the Environmental Safety of Diesel Vehicles Using Alternative Fuels. *Journal of Mechanical Engineering and Transport*. 2023;16(2):51–57. <https://doi.org/10.31649/2413-4503-2022-16-2-51-57>
15. Likhanov VA, Lopatin OP. Research of the Combustion Process in a Tractor Diesel Engine When Operating on Alcohol and Vegetable Oil. *Tractors and Agricultural Machinery*. 2023;90(3):191–200. <https://doi.org/10.17816/0321-4443-320931>
16. Jurj S, Werner T, Grundt D, Hagemann W, Möhlmann E. Towards Safe and Sustainable Autonomous Vehicles Using Environmentally-Friendly Criticality Metrics. *Sustainability*. 2022;14(12):6988. <https://doi.org/10.3390/su14126988>
17. Lindemberg De Jesus Nogueira Duarte, Gilson Medeiros, Humberto Neves Maia De Oliveira, Eduardo Lins De Barros Neto, Rayandson Raimundo Da Silva, Jessyca Bezerra. Evaluation of the Effect of Ethyl Alcohol Content in a Ternary Ethanol/Biodiesel/Diesel System. *International Journal of Thermodynamics*. 2024;27(2):19–26. <https://doi.org/10.5541/ijot.1372558>
18. Krakowski R, Witkowski K. Investigating the Effects of Environmentally Friendly Additives on the Exhaust Gas Composition and Fuel Consumption of an Internal Combustion Engine. *Applied Sciences*. 2024;14(7):2956. <https://doi.org/10.3390/app14072956>
19. Doluda VYu, Laskina NV, Brovko RV, Sulman MG. Investigation of Optimal Physico-Chemical Parameters of the Catalytic Transformation of Ethanol and Isopropanol into Aromatic Hydrocarbons. *Herald of TvSU. Series: Chemistry*. 2024; 57(3):76–85. <https://doi.org/10.26456/vtchem2024.3.7>
20. Krivenko DA, Logvinov AY, Ishkov AV. Investigation of Operating Process of Automotive Diesel Engines of the Minsk Motor Plant in Maximum Power Mode Using Alternative Biofuel. *Bulletin of Altai State Agricultural University*. 2024;233(3):75–84. <https://doi.org/10.53083/1996-4277-2024-233-3-75-84>
21. Tsapenkov KD, Kuraeva YuG, Sidorova EI, Shtyrlov AE, Zubrilin IA. Effect of Fuel Composition on Soot Formation in Engines and Power Plants. *Combustion, Explosion and Shock Waves*. 2024;60(4):63–75. <https://doi.org/10.15372/FGV2023.9430>

22. Likhanov VA, Lopatin OP. Investigation of Carbon-Black Emissions of a Tractor Biofuel Diesel. *Tractors and Agricultural Machinery*. 2024;91(4):375–385. <https://doi.org/10.17816/0321-4443-625783>

23. Likhanov VA, Kozlov AN, Araslanov MI. Investigation of the Portion Size of Rapeseed Oil for Ethanol Ignition in a Diesel Engine. *IOP Conference Series: Earth and Environmental Science*. 2020;548:62053. <https://doi.org/10.1088/1755-1315/548/6/062053>

About the Authors:

Vitaly A. Likhanov, Dr.Sci. (Eng.), Professor, Head of the Department of Thermal Engines of Automobiles and Tractors, Vyatka State Agrotechnological University (133, Oktyabrsky Ave., Kirov, 610017, Russian Federation), [SPIN-code](#), [ORCID](#), [ScopusID](#), nirs_vsaa@mail.ru

Oleg P. Lopatin, Dr.Sci. (Eng.), Associate Professor, Professor of the Department of Thermal Engines of Automobiles and Tractors, Vyatka State Agrotechnological University (133, Oktyabrsky Ave., Kirov, 610017, Russian Federation), [SPIN-code](#), [ORCID](#), [ScopusID](#), nirs_vsaa@mail.ru

Claimed Contributorship:

VA Likhanov: conceptualization, supervision.

OP Lopatin: writing – original draft preparation, visualization.

Conflict of Interest Statement: the authors declare no conflict of interest.

All authors have read and approved the final manuscript.

Об авторах:

Виталий Анатольевич Лиханов, доктор технических наук, профессор, заведующий, кафедра «Тепловые двигатели автомобилей и тракторы» Вятского государственного агротехнологического университета (610017, Российская Федерация, г. Киров, Октябрьский пр., 133), [SPIN-код](#), [ORCID](#), [ScopusID](#), likhanov.va@mail.ru

Олег Петрович Лопатин, доктор технических наук, доцент, профессор, кафедра «Тепловые двигатели автомобилей и тракторы» Вятского государственного агротехнологического университета (610017, Российская Федерация, г. Киров, Октябрьский пр., 133), [SPIN-код](#), [ORCID](#), [ScopusID](#), nirs_vsaa@mail.ru

Заявленный вклад авторов:

В.А. Лиханов: разработка концепции, научное руководство.

О.П. Лопатин: написание черновика рукописи, визуализация.

Конфликт интересов: авторы заявляют об отсутствии конфликта интересов.

Все авторы прочитали и одобрили окончательный вариант рукописи.

Received / Поступила в редакцию 20.03.2025

Reviewed / Поступила после рецензирования 18.04.2025

Accepted / Принята к публикации 24.04.2025

MACHINE BUILDING AND MACHINE SCIENCE МАШИНОСТРОЕНИЕ И МАШИНОВЕДЕНИЕ



UDC 621.03

Original Empirical Research

<https://doi.org/10.23947/2687-1653-2025-25-2-99-111>

Analysis of Temperature Characteristics of Electrolytic-Plasma Discharge in Jet Processing of a Metal Anode

Alexander I. Popov¹ , Vitaly I. Novikov^{1,2} , Dmitry N. Ivanov¹ ,Igor A. Kozyrskiy¹ ¹ Peter the Great St. Petersburg Polytechnic University, St. Petersburg, Russian Federation² St. Petersburg State University of Architecture and Civil Engineering, St. Petersburg, Russian Federation✉ kigor1846@gmail.com

EDN: DGHAFFZ

Abstract

Introduction. Electrolytic plasma technologies used for dimensional and finishing processing of metal surfaces attract attention due to their high efficiency and precision. The key factor that determines the quality of processing is the temperature of the electrolytic-plasma discharge (EPD), which affects the ionization of the electrolyte and the properties of the surface. The lack of comprehensive studies of the temperature characteristics of jet EPD limits the optimization of processes. The research objective is to determine the distribution of temperatures and heat flows in the system “jet electrolytic cathode — metal anode” under various processing conditions.

Materials and Methods. The study was conducted using an electrolyte jet with a diameter of 3 mm and a mass flow rate of 0.25–3.75 g/s at a voltage of 20–500 V. KhVG and 08Kh18N9T steels were used as anodes, and the electrolytes were aqueous solutions of NaCl, (NH₄)₂SO₄, C₆H₈O₇, with a concentration of 4–50 g/l. The temperature was measured with a chromel-alumel thermocouple, an infrared pyrometer, and a thermal imager.

Results. A heat balance equation was developed, describing heat distribution among the metallic anode (MA), jet cathode, electrolyte, vapor, and radiation. The analysis of the volt-ampere characteristics (VAC) showed an increase in current at low electrolyte flow rates (0.75–1.2 g/s) followed by a decrease at 300–500 V, and a parabolic dependence with a maximum of 2.6 A at a flow rate of 2.37 g/s. The maximum MA temperature reached 100°C (NaCl, 4–35 g/L), decreasing to 82°C at 150 g/L, while the hollow cathode reached 158°C at an initial electrolyte temperature of 90°C. Vapor temperatures ranged from 67.3°C (high flow rates) to 87.5°C (low flow rates). Electrolyte loss due to evaporation reached 5.8 g at 300–340 V. The temperature at the periphery of the anode was 15–20% higher than in the center.

Discussion and Conclusion. The main source of heat was the Joule-Lenz law, with the contribution of exothermic reactions of carbon oxidation up to 260 V. The maximum heat release was observed in the EPD zone, forming an ellipsoid. The data obtained and the heat balance equation create the basis for optimizing jet electrolytic-plasma polishing in mechanical engineering, medicine, and microelectronics.

Keywords: electrolytic-plasma discharge, jet cathode, metallic anode, temperature distribution, heat balance, jet processing, volt-ampere characteristics, electrolyte

Acknowledgements. The authors would like to thank graphic designer Diana Popova for preparing the illustrations. In addition, we would like to thank the editorial team of the Journal and the reviewer for their competent expertise and valuable recommendations for improving the article.

For Citation. Popov AI, Novikov VI, Ivanov DN, Kozyrskiy IA. Analysis of Temperature Characteristics of Electrolytic-Plasma Discharge in Jet Processing of a Metal Anode. *Advanced Engineering Research (Rostov-on-Don)*. 2025;25(2):99–111. <https://doi.org/10.23947/2687-1653-2025-25-2-99-111>

Анализ температурных характеристик электролитно-плазменного разряда при струйной обработке металлического анода

А.И. Попов¹ , В.И. Новиков^{1,2} , Д.Н. Иванов¹ , И.А. Козырский¹  

¹ Санкт-Петербургский политехнический университет Петра Великого, г. Санкт-Петербург, Российская Федерация

² Санкт-Петербургский государственный архитектурно-строительный университет, г. Санкт-Петербург, Российская Федерация

 kigor1846@gmail.com

Аннотация

Введение. Электролитно-плазменные технологии, применяемые для размерной и финишной обработки металлических поверхностей, привлекают внимание благодаря их высокой эффективности и точности. Ключевым фактором, определяющим качество обработки, является температура электролитно-плазменного разряда (ЭПР), влияющая на ионизацию электролита и свойства поверхности. Недостаток комплексных исследований температурных характеристик струйного ЭПР ограничивает оптимизацию процессов. Цель данного исследования — определить распределение температур и тепловых потоков в системе «струйный электролитический катод — металлический анод» при различных условиях обработки.

Материалы и методы. Исследования проводились с использованием струи электролита диаметром 3 мм с массовой скоростью потока 0,25–3,75 г/с при напряжении 20–500 В. В качестве анода применялись стали ХВГ и 08Х18Н9Т, электролиты — водные растворы NaCl, (NH₄)₂SO₄, C₆H₈O₇ с концентрацией 4–50 г/л. Температура измерялась хромель-алюмелевой термопарой, инфракрасным пирометром и тепловизором.

Результаты исследования. Разработано уравнение теплового баланса, описывающее распределение тепла между металлическим анодом (МА), струйным катодом, электролитом, паром и излучением. Анализ вольт-амперных характеристик (ВАХ) показал рост тока при низких расходах электролита (0,75–1,2 г/с) с последующим снижением при 300–500 В и параболическую зависимость с максимумом 2,6 А при расходе 2,37 г/с. Максимальная температура МА достигала 100 °С (NaCl, 4–35 г/л) и снижалась до 82 °С при 150 г/л, а полого катода — 158 °С при начальной температуре электролита 90 °С. Температура пара варьировалась от 67,3 (высокие расходы) до 87,5 °С (низкие расходы). Убыль электролита на испарение достигала 5,8 г при 300–340 В. Температура на периферии анода была на 15–20 % выше, чем в центре.

Обсуждение и заключение. Основной источник тепла — закон Джоуля–Ленца, с вкладом экзотермических реакций окисления углерода до 260 В. Максимальное тепловыделение наблюдается в зоне ЭПР, формирующей эллипсоид. Полученные данные и уравнение теплового баланса создают основу для оптимизации струйного электролитно-плазменного полирования в машиностроении, медицине и микроэлектронике.

Ключевые слова: электролитно-плазменный разряд, струйный катод, металлический анод, распределение температуры, тепловой баланс, струйная обработка, вольт-амперные характеристики, электролит

Благодарности. Авторы выражают благодарность графическому дизайнеру Диане Поповой за подготовку иллюстраций. Кроме того, авторы благодарят рецензента и редакцию журнала за компетентную экспертизу и ценные рекомендации по улучшению статьи

Для цитирования. Попов А.И., Новиков В.И., Иванов Д.Н., Козырский И.А. Анализ температурных характеристик электролитно-плазменного разряда при струйной обработке металлического анода. *Advanced Engineering Research (Rostov-on-Don)*. 2025;25(2):99–111. <https://doi.org/10.23947/2687-1653-2025-25-2-99-111>

Introduction. Currently, electrolytic plasma technologies are increasingly used in various industries. One of the most promising areas of their application is local processing of conductive metal surfaces [1]. This method is characterized by a number of technology abilities. Depending on the conditions of plasma formation, an electric discharge (ED) can occur both at atmospheric pressure [2] and in low vacuum conditions [3]. According to the method of plasma supply to the surface of the product, the treatment of ER in air [4] and in an electrolytic bath [5] is distinguished. It is possible to supply a stream of electrolyte from a metal [6] or plastic tube [7], as well as applying buried current leads of various designs [8]. The composition of the operating environment in which aqueous solutions of electrolytes are used can have a concentration from fractions of a percent [9] to their complete saturation [10]. There are known cases of additional introduction of inert gases (Ar, Kr) into the electrolytic plasma as an operating environment [11]. According to spatial orientation, there are different directions of the electrolyte flow (current lead) relative to the product: from above [12],

from below [13], and at an angle [14]. The product itself, in turn, can be located vertically [14], horizontally, or at an angle to the axis of the stream (current lead) [10].

The formation of a limited ED volume involves moving it relative to the surface of the workpiece manually or according to a CNC (industrial robot) machine program. In this case, depending on the input parameters, the ED is formed in the electrolysis mode [15], electrolytic plasma [16] or a combination of these processes. The movement of the ED relative to the surface of the metal anode at a given feed rate provides the achievement of the required values for dimensionless (dimensional) processing, the accuracy of the size being performed, and the required parameters: Ra — average arithmetic deviation of the profile, and R_{max} — greatest height of the material profile.

In [17], the technologies of jet focused electrolytic plasma treatment are studied. The specific feature of the processes of jet electrolytic-plasma treatment, in comparison to processing in an electrolytic bath [18], can be a significantly higher processing speed, dimensional and dimensionless treatment, local processing zone, lower equipment cost, higher processing accuracy [19], and incomparably lower roughness parameters [20]. This opens up prospects for even more active use of jet processing methods.

However, the widespread application of jet technologies with an electrolytic electrode and a metal anode is hindered by the lack of information on the operating temperatures of the process in the treatment zone and on the surface of the metal anode. This fact is important, since numerous studies on plasma heating of products in flowing and stationary electrolytes show the presence of high temperatures, up to the melting point [21]. In addition, studies on the plasma discharges themselves demonstrate plasma temperatures from 1,400 to 4,000°K [22].

The interaction of the ED with the metal anode, when the temperature of phase transformations in alloys is exceeded, reduces the performance of manufactured products. There are a limited number of studies in the field of integrated temperature and heat flow distribution in the “hollow current lead – electrolytic cathode – MA – environment” system. These studies, as a rule, describe only the local part of the system.

The research objective was to analyze temperatures in the system obtained by an electric discharge between a metal cathode and a metal anode at atmospheric pressure. To achieve this, the authors solved the following problems: the volt-ampere characteristics of the discharge were studied; the temperature of the steam, anode, hollow cathode (current lead), electrolyte in the receiving bath was measured; and the distribution of heat flows was analyzed.

Materials and Methods. An electric discharge formed in the voltage range ($U = 20\text{--}500\text{ V}$) at low electrolyte flow rates ($0.25\text{--}3.75\text{ g/s}$) and small interelectrode gaps ($2\text{--}8\text{ mm}$) was investigated for a free-falling electrolyte jet of $\varnothing 3\text{ mm}$ on the surface of a metal anode with the application of a constant bias voltage between the metal anode and the hollow cathode tube.

The diagram of local temperature measurement locations is shown in Figure 1.

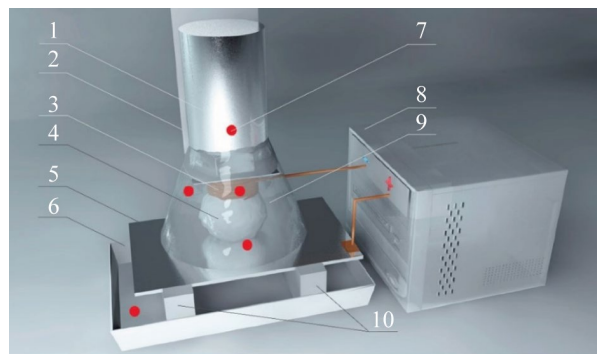


Fig. 1. Layout of temperature measurement points: 1 — electrolyte feeder; 2 — copper tube (hollow cathode) fastener; 3 — copper tube; 4 — foamed electrolytic stream; 5 — metal anode; 6 — electrolyte receiving bath; 7 — temperature measurement points; 8 — power source; 9 — heat-insulating screen; 10 — supports on insulators

The studies were conducted at room temperature ($T = 20.0^\circ\text{C}$) in the pressure range $(9.9\text{--}10.1) \times 10^4\text{ Pa}$. For MA, 25 marked samples with a diameter of $45 \times 1\text{ mm}$ were made. The sample material was KhVG tool steel. Samples made of 08Kh18N9T stainless steel with dimensions of $100 \times 200 \times 1\text{ mm}$ were also used. Samples made of KhVG steel were treated with a NaCl solution in tap water at a concentration of $3\text{--}160\text{ g/l}$. Samples made of 08Kh18N9T steel were treated with $(\text{NH}_4)_2\text{SO}_4$ at a concentration of $2\text{--}55\text{ g/l}$ and $\text{C}_6\text{H}_8\text{O}_7$ at a concentration of $10\text{--}35\text{ g/l}$ in tap water. The discharge voltage varied from 20 to 500 V with a step of 20 volts. The interelectrode gap L was varied in the range from 2 to 8 mm. The voltage and current were measured with a UT61B millivoltmeter with an accuracy of $\pm (0.5\% + 1)$ for voltage and $\pm (1.5\% + 3)$ for current. The unit of mass flow rate of electrolyte G was equal to $0.2\text{--}3.8\text{ g/s}$. A mass of 100 g was taken as a fixed mass of

electrolyte for passing through the hollow cathode tube. The mass loss Δ , was determined on a scale with an accuracy of 5×10^{-5} kg. The mass loss was calculated as the difference between the initial mass of electrolyte poured into the electrolyte feeder and the final mass collected in the electrolyte receiving bath after the electric discharge. The hollow cathode temperature was measured by an insulated junction of a chromel-alumel thermocouple installed 2 mm above the lower end of the current lead tube.

The temperature of the MA was measured by a thermocouple installed at a distance of 0.3 mm from its surface, built into a protective stainless housing. The temperature was measured by contact with a chromel-alumel thermocouple and by contactless means with a TA601C infrared pyrometer and a Testo 875 thermal imager. The height of the electrolyte feeder above the sample surface was 300 mm. The samples were given an angle of inclination of $3-5^\circ$ for electrolyte flow. The distance between the MA and the bottom of the electrolyte receiving bath was 40 mm for KhVG steel and 200 mm for 08Kh18N9T steel. 3D models were simulated in the Cinema4D program.

Research Results. Initial Heat Flow in ED. Numerous studies have shown that the range of operating voltages U from 0 to 500 V can be conditionally attributed to two main processes. The first corresponds to the process of anodic dissolution during electrolysis and is widely used in industry in the range of 12–60 V. It is accompanied by intensive heating of the anode and in some cases is used for the process heating of workpieces. The second process conditionally corresponds to the range of operating voltages from 60 to 500 V and to the electrolytic-plasma mechanism [15]. This process is used for heating anode materials, chemical-thermal treatment, coating, microarc oxidation, cleaning, and polishing. Electrolytic plasma treatment is characterized by a wide temperature range. It depends on the ratio of the sizes of the current leads used. For example, when two current leads are immersed in an electrolytic bath, the smaller of them starts to actively generate heat. Thus, a loop of 0.8 mm thick nichrome wire placed around the MA plate is locally heated and burns out in less than 60 s, forming a ball at the end closest to the anode.

When the ratio of the sizes of the active electrode to the larger one is $\leq 3-5$, an effervescence occurs on the surface of the first one, and with increasing voltage, a “thin luminous plasma shell” appears [16], which turns (for anodic processes) into an anode shell of significantly larger dimensions [8].

The interaction zone of the MA and the plasma (gas-vapor) shell is characterized by the size, intensity, resistance, ionization of the components. The size of the electrolyte-plasma (anodic) shell for different cases can be 10–500 μm above the MA surface. This layer corresponds to high resistance (specific electrical conductivity of the layer is $1.1 \cdot 10^5 \text{ Ohm} \cdot \text{cm}^{-1}$) [16].

In this case, the high electric field strength of 10^4-10^6 V/m (in the case of an electrolytic bath) provides ionization of the components of air, steam, and electrolyte. With an increase in voltage, the process is accompanied by visible glow and the presence of microdischarges that occur mainly at the tops of microroughnesses, and when leveling the surface — on blocks, dislocations, or individual atoms. The shell, depending on the composition of the electrolyte, has a characteristic glow up to white with an electron gas temperature from 1,400 to 4,000°K [22]. Depending on the conditions, the material of the MA, the shape of the negative current lead, the concentration and type of electrolyte, the capacity and number of capacitors of the power source, the ED can take the character of a discharge similar to a glow, spark or arc discharge.

The discharge zone during electrolysis and the occurrence of an electrolyte-plasma discharge in the case under consideration is a local area. This determines the heat flows propagating from this area. Heat release in the ED occurs on the MA surface in the electrolyte-plasma layer zone and is directed into the MA, electrolyte, steam, hollow cathode, and into the environment in the form of radiation.

The relationship linking the release and consumption of heat in the system “hollow cathode – electrolytic electrode – MA” per unit of time can be written in general form by the heat balance equation:

$$\frac{dQ_1}{dt} + \frac{dQ_2}{dt} = \frac{dQ_4}{dt} + \frac{dQ_5}{dt} + \frac{dQ_6}{dt} + \frac{dQ_3}{dt} + \frac{dQ_7}{dt}. \quad (1)$$

The left side of the equation defines the initial amount of heat released in the electrolyte-plasma layer. It consists of $\frac{dQ_1}{dt}$ — amount of heat released according to the Joule-Lenz law, and $\frac{dQ_2}{dt}$ — amount of heat released by the oxidation of carbon in steel [13].

The right side of the equation shows the heat flows from the ED zone.

Expressions $\frac{dQ_5}{dt}, \frac{dQ_6}{dt}, \frac{dQ_4}{dt}, \frac{dQ_3}{dt}, \frac{dQ_7}{dt}$ are heat flows directed into the hollow cathode, into the flowing electrolyte, into the MA, into the environment in the form of steam.

When determining parameters I and U for calculating the initial heat flux arising in the ED, the volt-ampere characteristics were obtained for a NaCl solution at different electrolyte flow rates — from 0.75 to 2.37 g/s. It was shown that in the voltage range from 20 to 500 V, at a low electrolyte flow rate, $G = 0.75$ g/s and $G = 1.20$ g/s, an increase in the electric discharge current was observed with a characteristic decrease in the range of 300–500 V. With an increase in the electrolyte flow rate to $G = 2.37$ g/s in the range of 20–500 V, the curve had the form of a flat parabola branch and a maximum current value 2.6 A. In this case, the current density per MA could reach $3.2\text{--}5.2 \times 10^4$ A/m².

Study on Volt-Ampere Characteristic. Up to $U = 240$ V, the difference in discharge current between the three curves is in the range of 0.2–0.4 A (Fig. 2). After $U = 240$ V, the differences between curves 1 and 2 become more significant. For curves 2 and 3, in the range of $U = 180\text{--}400$ V, there is almost complete coincidence of values. The most significant differences between them start at point $U = 400$ V and range from 0.4 to 1.4 A for the highest $G = 2.37$ g/s and the lowest $G = 0.75$ g/s of electrolyte consumption.

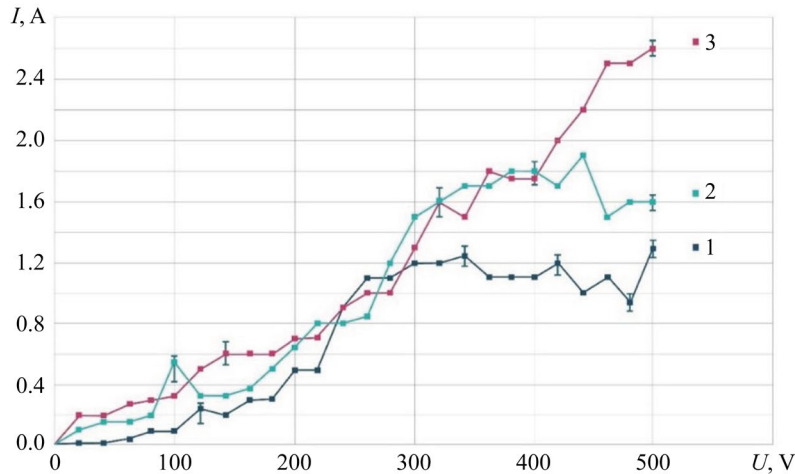


Fig. 2. Dependence of VAC of electric discharge between electrolytic cathode and MA on electrolyte consumption; MA — KhVG steel; NaCl — 4 g/l; 1 — $G = 0.75$ g/s; 2 — $G = 1.20$ g/s; 3 — $G = 2.36$ g/s

Study on MA Temperature. Study on the heat flow in the MA from the ED was performed on a sample made of KhVG steel. A thermocouple in a protective housing made of stainless steel was tightly fixed on the back side of the MA at a distance of 0.3 mm from the surface.

The MA temperature was measured at different values of the concentration of the electrolyte based on NaCl. The temperature values were taken after the steady-state heat flow (Fig. 3).

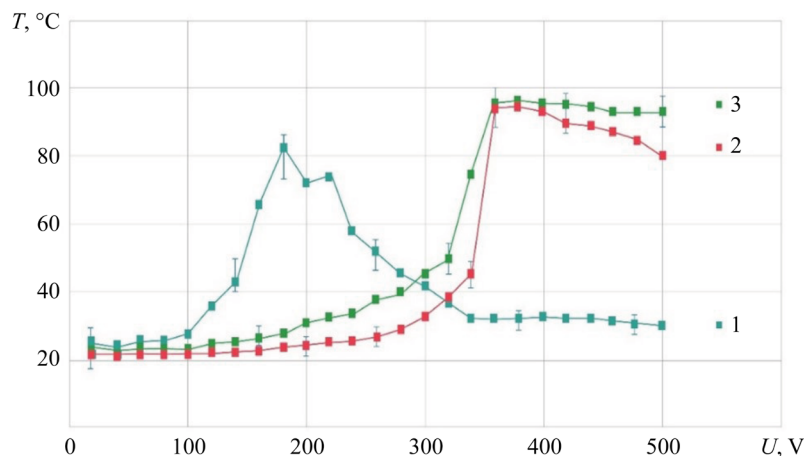


Fig. 3. Dependence of MA temperature on ED voltage; MA — KhVG steel; $G = 1.14$ g/s; electrolyte with NaCl concentration: 1 — 4 g/l; 2 — 35 g/l; 3 — 150 g/l

It is shown that at the electrolyte concentrations of NaCl 4 and 35 g/l up to the range of $U = 320\text{--}340$ V, the curves have a flat character, which may indicate stable electrolysis processes in this range and at these concentrations of the electrolyte. In the range of $U = 320\text{--}360$ V, a sharp increase in the anode temperature is recorded on these curves. Obviously, this region is a transitional one, characterized by an increase in the double layer and a change in the mechanism of transfer of MA atoms.

The increase in the double layer insulating the MA surface occurs simultaneously with the growth of the electric field strength. When the breakdown voltage is exceeded, a microdischarge occurs, destroying the nonconductive film formed on the surface. Both the peaks of the surface profile microroughness and the areas between the depressions are the zone of microdischarge occurrence with developed surface roughness. The occurrence of a microdischarge at the top and in the area of the depressions is caused by the high intensity of the electric field. In the first case, the cause is the shape of the protrusion itself, and in the second case — the presence of a high charge on the surface between the depressions. It can be caused by a high negative charge of nonconductive films (contamination, anode layer, spray products).

The mechanism of material transfer from the surface of the metal anode is changed in two stages. First, the chemical weakening of atomic bonds occurs under the action of electrolyte components, which facilitates the detachment of electrons and atoms. Then, when microdischarges are formed, the thermal mechanism of destruction of these bonds becomes predominant. This causes additional emission of electrons and promotes further interaction of the anode with the electrolyte, leading to the removal of its atoms into the solution.

In the range of $U = 360\text{--}500$ V, a smooth decrease in temperature is recorded for curves 1 and 2, which may indicate an increase in the locking effect. It is characterized by an increase in the nonconductive film, a decrease in the discharge current, an increase in the power of individual microdischarges, but a decrease in the number, and consequently, the amount of heat released in the electrolyte-plasma layer.

With an increase in the salt (NaCl) concentration to 150 g/l (curve 3) in the electrolyte, the region of maximum temperatures shifts to the region of lower voltages, from 360 to 180 V. Obviously, this also reduces the ignition threshold of the electrolyte-plasma discharge. In this case, the crimson glow characteristic of the formation of the electrolyte-plasma layer was already recorded for NaCl at $U = 140$ V. In addition, it is noted that with an increase in the concentration of the electrolyte, a decrease in the maximum temperature to 82°C is observed. For a saturated NaCl solution, an ED is formed in the shape of an ellipsoid truncated on both sides at $U = 160$ V and $U = 200$ V. This corresponds to the region of maximum temperatures.

In general, it can be noted that the temperature near the contact surface with the electrolyte plasma on the metal anode does not exceed 100°C . The difference in the voltage range $U = 320\text{--}340$ V is characteristic for curves 1 and 2. This determines the transition to ED in the form of an ellipsoid truncated on both sides with a maximum temperature [9].

Study on Hollow Cathode Temperature. The hollow cathode temperature was measured by fixing the thermocouple junction, insulated from the surface of the current lead. The thermocouple junction was installed on the outer side of the current lead above 2 mm from the lower end of the tube. It was recorded that for all experiments (Fig. 4, curves 1, 2, 3), having different initial electrolyte temperatures at the input of the hollow cathode, areas with a virtually constant temperature were characteristic. These areas included the voltage range of $U = 20\text{--}260$ V.

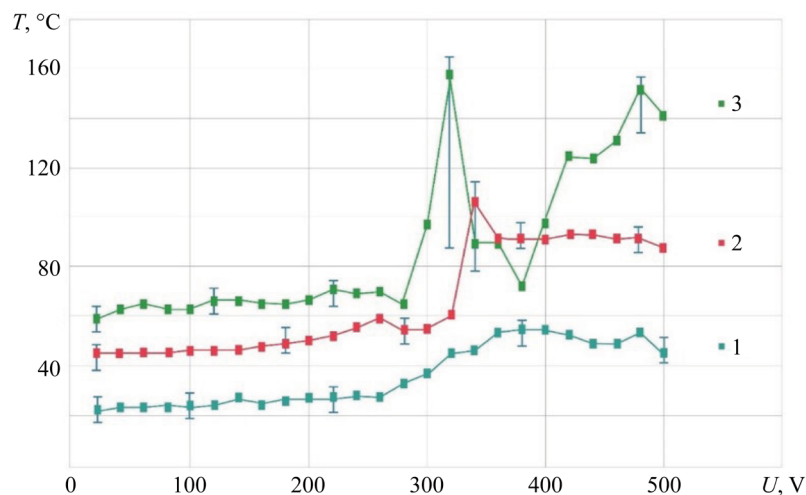


Fig. 4. Dependence of the hollow cathode temperature on voltage when using NaCl electrolyte — 4 g/l; MA — KhVG steel; $G = 1.06$ g/s; 1 — $T = 21^\circ\text{C}$; 2 — $T = 50^\circ\text{C}$; 3 — $T = 90^\circ\text{C}$

It was noted that at the initial temperature of the electrolyte ($T = 21^\circ\text{C}$), supplied to the hollow cathode, the surface temperature of the current lead tube at the measurement location did not exceed 60°C (curve 1). This is generally consistent with the data obtained by the authors of paper [2].

Increasing the initial temperature of the electrolyte to $T = 50^\circ\text{C}$ showed that in the range of $U = 20\text{--}340$ V, the temperature of the hollow cathode remained virtually unchanged (curve 2). However, from value $U = 340$ V, a sharp increase in temperature to 105°C was recorded. After which the temperature dropped to an average of 90°C .

For the initial temperature of the electrolyte $T = 90^\circ\text{C}$ in the range of $U = 20\text{--}280\text{ V}$ (curve 3), a drop in temperature was observed taking into account losses in the pipeline to $T = 60\text{--}70^\circ\text{C}$. However, the energy reserve in the form of additional heat of the electrolyte placed in the ED zone shifted the total peak temperature increase to the region of lower voltage. At $U = 320\text{ V}$, the temperature reached a short-term peak value — 158°C . After that, there was a sharp decrease in temperature and a repeated increase to 151°C at $U = 480\text{ V}$.

Study on Electrolyte Temperature after ED. The heat flow from the electrolyte-plasma layer to the electrolyte was estimated taking into account the difference in temperatures obtained at the inlet to the hollow cathode and at the outlet from the ED in the electrolyte collection bath. Temperature measurements were made in the flow of electrolyte running down into the bath. Depending on the flow rate, the runoff occurred in drops or a stream. When filling the receiving bath with electrolyte that had passed through the ED, its temperature was measured. The time for the temperature drop by 1°C for 0.1 kg of electrolyte that had entered the receiving bath was about 60 s . Cooling of the drop or jet during the fall was neglected. The measurement results are shown in Figure 5. With an increase in the voltage of the ED formed by the electrolytic cathode and MA, a smooth increase in the temperature of the spent electrolyte is observed. Up to $U = 220\text{ V}$, a characteristic feature is that the entire family of curves lies in the range of $\leq 10^\circ\text{C}$. The electrolyte flow rate has an ambiguous effect on the temperature of the electrolyte in the receiving bath. With an increase in the electrolyte flow rate to $G = 1.2\text{ g/s}$, an increase in temperature with a shift to a smaller voltage range is observed. This can be explained by the growth of the number of charged particles under increasing the electrolyte flow rate. With an increase in the electrolyte flow rate to $G = 2.37\text{ g/s}$ in the range of $U = 200\text{--}500\text{ V}$, a lower temperature is observed, which may indicate a faster passage of electrolyte through the ED, and a lower specific power per unit volume for heating the electrolyte. At the same time, the maximum temperature of the electrolyte collected in the receiving bath for all three electrolyte flow rates does not exceed 55°C .

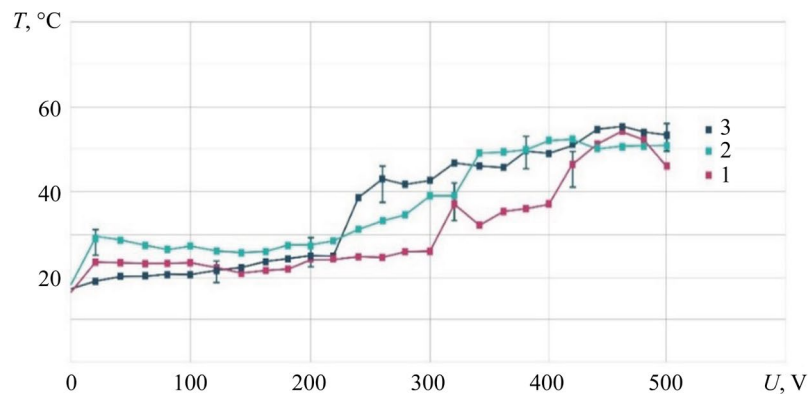


Fig. 5. Dependence of hollow cathode temperature on voltage when using NaCl electrolyte — 4 g/l ; MA — KhVG steel; 1 — $G = 2.36\text{ g/s}$; 2 — $G = 1.20\text{ g/s}$, 3 — $G = 0.75\text{ g/s}$

Study on Steam Temperature. To investigate the steam temperature of the ED, the device presented in [13], consisting of a cone made of heat-insulating material, was used. A chromel-alumel thermocouple was installed at the top of the cone. This allowed localizing the evaporated and sprayed electrolyte in a limited volume and measuring its average temperature. The obtained experimental data are presented in Figure 6.

The research has shown that at an electrolyte flow rate of $G = 1.2\text{--}2.36\text{ g/s}$ up to $U = 200\text{ V}$, the ED vapor temperature differs slightly from room temperature and has a slight increase in the range of $220\text{--}300\text{ V}$. At voltage $U = 260\text{--}420\text{ V}$, a sharp increase in the vapor temperature to 67.3°C is observed, proportional to the discharge power between the electrolytic cathode and MA. Then, a slight decrease in the vapor temperature to 56.3°C is seen. After $U = 420\text{ V}$, a drop in the vapor temperature is recorded due to a change in the geometric shape of the electrolyte-plasma discharge.

For low electrolyte flow rates ($G = 0.75\text{ g/s}$ and $G = 1.2\text{ g/s}$), a sharp increase in steam temperature to 87.5°C is observed in the range of $U = 180\text{--}300\text{ V}$ for curves 2 and 3, which have the form of an exponential function. Such a difference in steam temperature may indicate that at $G = 2.36\text{ g/s}$ and practically equal discharge power, the volumetric flow rate of electrolyte localized by the electromagnetic field in the ED is 2–3 times greater. Therefore, with an increase in the volumetric flow rate of electrolyte, the power of the electric discharge generated in the electrolyte-plasma layer is not enough to convert part of the liquid into steam.

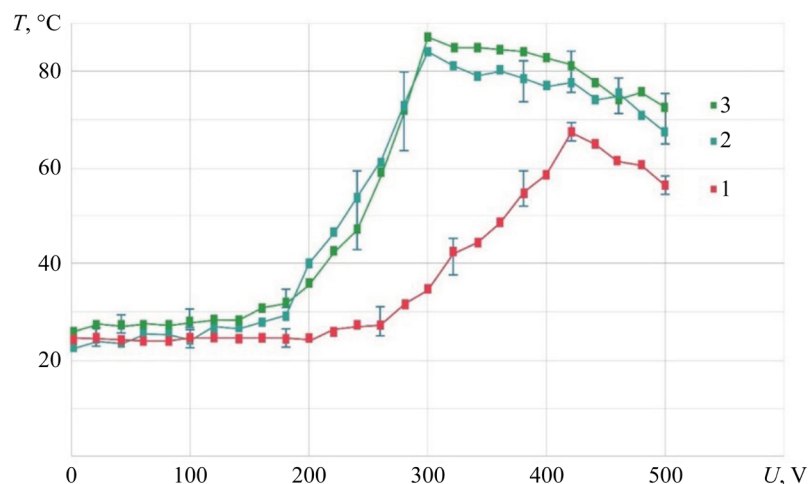


Fig. 6. Dependence of temperature of steam generated by ED on voltage; MA — KhVG steel; NaCl — 4 g/l; 1 — $G = 2.36$ g/s; 2 — $G = 0.75$ g/s; 3 — $G = 1.20$ g/s

Loss of Electrolyte Consumed for Evaporation. The change in the electrolyte volume was recorded after passing 0.1 kg of electrolyte through the hollow cathode during the formation of the ED. The spent electrolyte was collected in the receiving bath and re-weighed. The increase in the ED temperature at $G = 2.37$ g/s started with $U = 220$ V and led to an increase in the transfer of electrolyte in the form of vapor into the environment for all the studied flow rates (Fig. 7). At voltage $U = 300$ V, an increase in the electrolyte consumption for evaporation was recorded only for its small flow rates when passing through the hollow cathode: $G = 0.75$ g/s and $G = 1.20$ g/s up to 5.50–5.80 g.

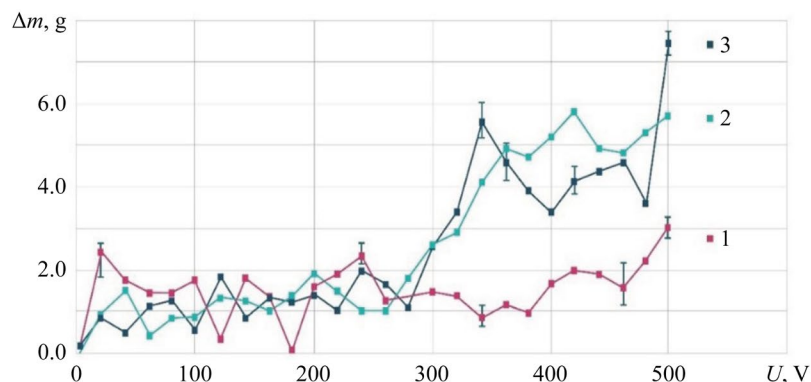


Fig. 7. Dependence of electrolyte mass loss on discharge voltage; NaCl — 4 g/l; MA — KhVG steel; 1 — $G = 2.36$ g/s; 2 — $G = 0.75$ g/s; 3 — $G = 1.20$ g/s

A characteristic increase in the loss of electrolyte mass for $G = 0.75$ g/s at the point $U = 340$ V is the zone of formation of an ellipsoid truncated on both sides [9]. After $U = 400$ V, a decrease in the mass of electrolyte entering the receiving bath is observed for all three curves, which results in an increase in temperature and in electrolyte consumption due to intensive evaporation.

In general, this can be explained by an increase in the heat flow from the electrolyte-plasma layer to the ED zone and growth of its temperature. It should be clarified that the gas-vapor shell of the ED, formed under the action of an electromagnetic field with an increase in voltage, has greater mobility of individual discharge elements — bubbles. Their constant movement around the discharge axis occurs due to the Lorentz forces and the dipole moment. This results in an intensive transfer of molecules from the interface “bubble — environment”. Another factor that makes a significant contribution to the evaporation of the electrolyte is the ionization of bubbles. In [9], it is shown that the ionization of the ED, which is well recorded especially in the upper part of the discharge, starts with the shell of the bubble. With growth of the discharge voltage, there is an increase in the ionization of the components, their surface energy and, consequently, a decrease in the energy of detachment of gas molecules from the surface of the bubbles.

Specificity of Electrolyte Flow Rate. When measuring the flow rate of 0.1 kg of electrolyte through the ED, the authors recorded the following features (Fig. 8). With an increase in voltage between the electrodes, the electrolyte flow rate was not constant and had different values. This was typical for all three studied electrolyte flow rates.

The greatest stability is shown by the mode $G = 1.20$ g/s (curve 2). However, at voltage $U = 340$ V, a sharp decrease in the electrolyte flow rate is observed — more than twice as compared to the initial.

At high initial electrolyte speed $G = 2.3$ g/s, with growth of discharge voltage $U = 20\text{--}300$ V, the flow rate increases. With a further growth of voltage U from 300 to 460 V, a slowdown in the electrolyte flow rate is also recorded. The slowdown in the flow rate can be most clearly seen at $G = 0.75$ g/s. In this case (curve 3), a clearly defined rise is observed. Here, the electrolyte flow rate decreases by up to two times.

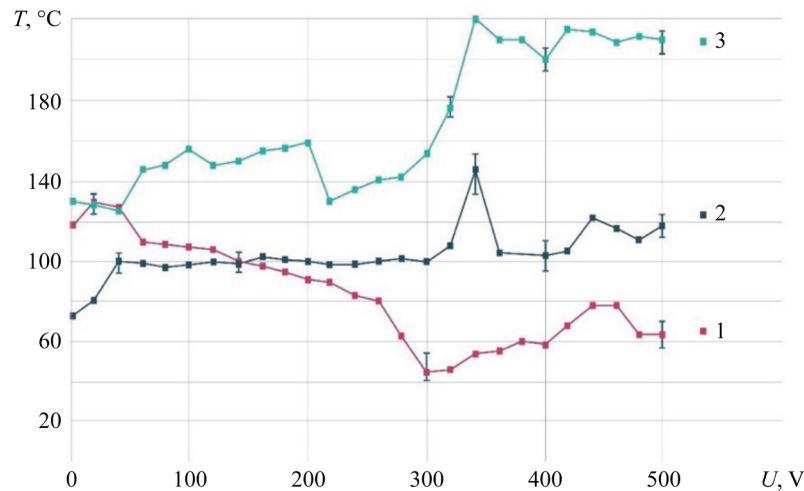


Fig. 8. Dependence of the time of passing 100 g of electrolyte through discharge on voltage; NaCl — 4 g/l; MA — KhVG steel; 1 — $G = 2.37$ g/s; 2 — $G = 1.20$ g/s; 3 — $G = 0.75$ g/s

Measuring ED Temperature Field with Thermal Imager. Measuring the ED zone with a thermal imager showed a temperature increase of up to 100°C . Electrolyte with an initial temperature of $23\text{--}26^{\circ}\text{C}$ was directed to the MA made of 08X18N9T stainless steel with a size of $100 \times 200 \times 1$ mm. In this case, the maximum temperature of the ED was recorded.

When studying the electrolyte-plasma discharge at different volumetric flow rates, concentrations and chemical compositions of the electrolyte, it was found that the ED temperature did not exceed 100°C (Fig. 9).

The characteristic features of the process are two key factors. The first is the proximity of the curves, the second is the decrease in temperature after reaching the maximum. The decrease in temperature after reaching the maximum can be explained by a change under the conditions of contact interaction, an increase in specific resistance, and the transition from an electrochemical process to an electrolytic-plasma process.

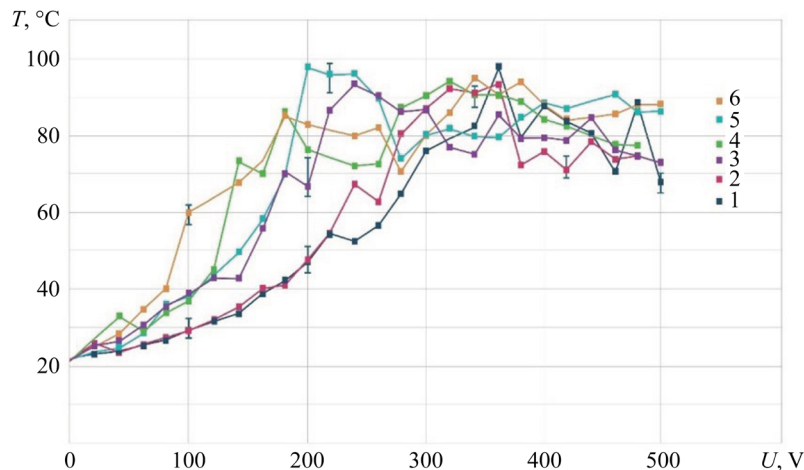


Fig. 9. Dependence of ED temperature on voltage; stainless steel 08X18N9T; 1 — $G = 0.94$ g/s; 2 — $G = 1.86$ g/s; 3 — $G = 2.78$ g/s; 4 — $G = 3.71$ g/s; electrolyte $(\text{NH}_4)_2\text{SO}_4$ — 2.7 g/l; 5 — $G = 1.86$ g/s; electrolytes $(\text{NH}_4)_2\text{SO}_4$ — 50 g/l and $\text{C}_6\text{H}_8\text{O}_7$ — 30 g/l; 6 — $G = 2.51$ g/s; electrolytes $(\text{NH}_4)_2\text{SO}_4$ — 15 g/l and $\text{C}_6\text{H}_8\text{O}_7$ — 15 g/l

It is noted that when the falling drops of electrolyte running down from the MA come into contact with the cathode plate fixed below, the maximum temperature is 167°C .

Study on Temperature on Metal Anode Surface. During jet flows of the electric discharge, an uneven temperature distribution is recorded on the surface of the MA. The periphery of the electrolytic discharge in the jet flows has a 15–20% higher temperature than in the central region of the electrolyte. The analysis of temperatures on the surface of the MA is presented in Figure 10.

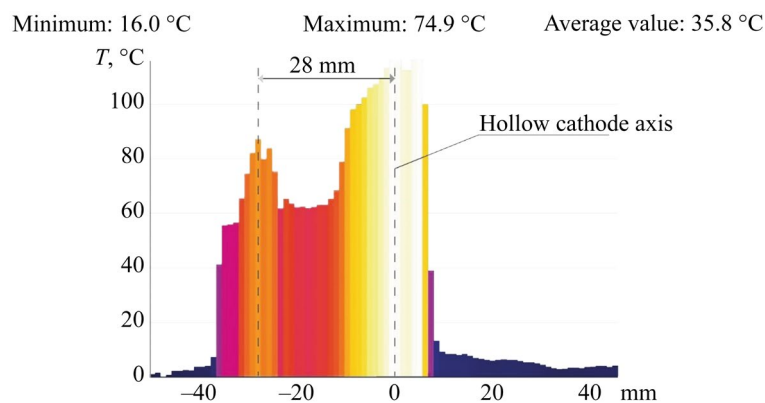


Fig. 10. MA surface temperature; anode — stainless steel 08X18N9T

Evaluation of ED Heat Flows. The analysis of the heat flow distribution shows that it consists of an incoming flow formed by heat generated by the Joule-Lenz law (Q_1) and heat generated by the oxidation of carbon in steel (Q_2). The outgoing flow consists of heat directed into the environment in the form of steam — Q_3 ; heat directed into the anode — Q_4 ; heat directed into the hollow cathode — Q_5 ; heat directed into the electrolyte — Q_6 ; heat directed into the environment in the form of radiation — Q_7 . The distribution of heat flows for the ED in the form of an ellipsoid truncated on both sides is shown in Figure 11. The maximum amount of heat Q_3 is directed into the environment in the form of steam and is about 58%. The flow Q_4 directed into the metal anode is also significant (about 21%).

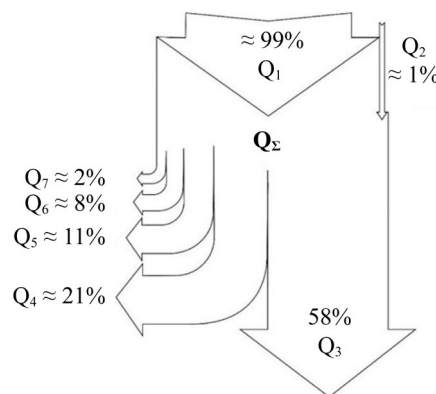


Fig. 11. Distribution of heat flows for an electric discharge in the form of an ellipsoid truncated on both sides

The calculation of the amount of heat for the heat balance equation shows the general picture of the distribution of heat flows in the range of operating voltages from 20 to 500 V (Fig. 12). The calculated curve shows that the amount of heat Q_6 , directed into the electrolyte, has a virtually constant character over the entire voltage range. At the same time, in the high voltage range, the values of Q_1 are almost 20 times higher than Q_6 . In general, the value of Q_6 is on average 10% of the value of Q_1 .

The calculated value of Q_3 in the range up to 260 V exceeds Q_1 . Obviously, the magnitude of exothermic reactions in this range is not taken into account and makes a significant contribution to the total heat flow. The value of Q_3 is on average 50–70% of Q_1 .

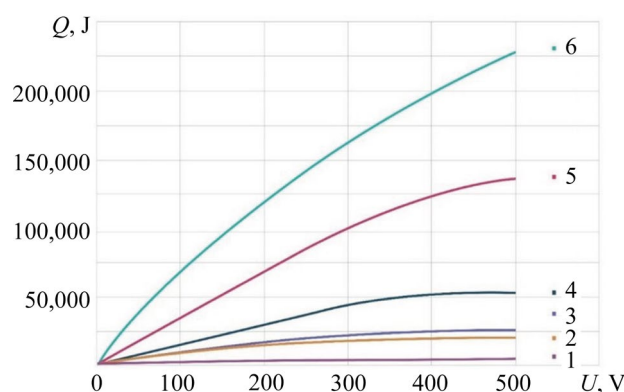


Fig. 12. Ratio of heat flows in the range of operating voltages from 20 to 500 V:

 1 — Q_7 ; 2 — Q_6 ; 3 — Q_5 ; 4 — Q_4 ; 5 — Q_3 ; 6 — Q_1

Discussion and Conclusion. As a result of the conducted study on the thermal state of the system formed by the electrolytic cathode and the metal anode, it can be confirmed that in the given geometric ratio of the metal anode and the hollow cathode and the studied volumetric flow rates of the electrolyte, the maximum temperatures on the anode do not exceed 100°C, and the maximum temperatures of the system are 167°C.

The results obtained are consistent with the data presented by other researchers and published recently. For example, in the study on plasma electrolytic jet polishing (PEP-Jet) of AISI 316L stainless steel [23], it is noted that the electrolyte temperature in the range of 68–90°C stabilizes the gas-vapor layer, which is consistent with the data obtained by the authors on the process temperatures corresponding to the boiling range of the electrolyte (up to 167°C). However, in [23], the emphasis is placed on corrosion resistance, and not on the complex heat balance, in contrast to the study. The data in [24] indicate that the optimum electrolyte temperature (80°C) provides efficient formation of the gas-vapor layer at voltage 300 V, which is close to the peak temperatures obtained in the ED ellipsoid zone, despite the difference in the research methods used. Paper [25] on the ESR of Inconel 718 alloy simulates the heat flow at the gas-liquid interface at a temperature of 70–85°C and a voltage of 250–350 V, which confirms the above conclusions about the main role of voltage in the formation of the heat flow. However, paper [25] does not consider the nonuniform temperature distribution over the anode surface. In [26], the authors consider ESR of 316L steel at 90°C. They focus on micro-level electrochemical reactions, but they do not analyze the electrohydraulic effect causing cavitation and shock waves, which slows down the electrolyte flow at low flow rates (0.75–1.2 g/s) and increases the temperature. It is a significant factor in the temperature growth at low electrolyte flow rates. This phenomenon is probably associated with the local specificity of the jet discharge, which requires further investigation [27].

The maximum recorded cathode temperature in the study was 167°C, which did not exceed the phase transformation temperature for most structural materials providing their operability. This is consistent with the findings of [24] and [25], which note that the process temperatures also remain below the critical values for the materials. The temperature data measured by various methods confirm that the process occurs in the electrolyte boiling region, which is consistent with the data of [23] and [26] on the temperature ranges of 68–90°C.

Another feature is the uneven distribution of the electrolyte temperature on the MA surface. The value of the electrolyte temperature spreading over the surface is not uniform or decreasing towards the periphery. It is noteworthy that its value falls in the center and increases at the periphery — the peripheral zones are 15–20% hotter than the central ones. A similar phenomenon has not been described by other researchers, since the temperature distribution was either not analyzed or was considered uniform. The cause-and-effect relationship of this effect remains unclear and requires further research. The study on this issue is the subject of subsequent research.

References

1. Quitzke S, Danilov I, Martin A, Morgenstern R, Lampke Th, Schubert A. Simulation-Assisted Process Design and Experimental Verification of Laterally Confined Oxide Areas Generated with Continuous Electrolytic Free Jet on EN AW-7075 Aluminum Alloy. *Micromachines*. 2023;14(2):293. <https://doi.org/10.3390/mi14020293>
2. Bagautdinova LN, Gaisin FM. A Multichannel Discharge in Conducting Liquid at Atmospheric Pressure. *High Temperature*. 2010;48:126–128. <https://doi.org/10.1134/S0018151X10010153>
3. Gaisin AIF, Son EE. Vapor-Air Discharges between Jet Electrolytic Cathode and Metal Anode at Low Pressure. *High Temperature*. 2010;48:447–450. <https://doi.org/10.1134/S0018151X10030223>
4. Nagulin KYu, Terent'ev AA, Belov MD, Gil'mutdinov AKh. Electrolytic-Plasma Jet Polishing of Additively Manufactured Gas Turbine Engine Components. *Russian Aeronautics*. 2022;65(4):822–830. <https://doi.org/10.3103/S1068799822040237>
5. Danilov I, Hackert-Oschätzchen M, Zinecker M, Meichsner G, Edelmann J, Schubert A. Process Understanding of Plasma Electrolytic Polishing through Multiphysics Simulation and Inline Metrology. *Micromachines*. 2019;10(3):214. <https://doi.org/10.3390/mi10030214>
6. Gaisin AIF, Gaisin FM, Basyrov RSh, Kayumov RR, Mirkhanov DN, Petryakov SYu. Electrophysical and Thermal Processes under Conditions of Discharge Combustion with a Liquid (Non-Metallic) Cathode. *High Temperature*. 2023;61(4):484–491. (In Russ.) <https://doi.org/10.31857/S004036442304004X>
7. Viet D Bui, Martin A, Berger Th, Steinert P, Schubert A. Antibacterial Surface Protection using Electrical Discharge Machining with Zinc Tool Electrode for Medical Devices. *Procedia CIRP*. 2024;125:278–283. <https://doi.org/10.1016/j.procir.2024.08.058>
8. Dyakov IG, Belkin VS, Shadrin SYu, Belkin PN. Heat Transfer Peculiarities at Anode Plasma Electrolytic Treatment of Cylindrical Pieces. *Electronic Processing of Materials*. 2014;50(4):65–75. (In Russ.) URL: <https://eom.usm.md/index.php/journal/article/view/eom.2014.50.4.65> (accessed: 10.02.2025).
9. Popov AI, Novikov VI, Radkevich MM. Characteristics of the Development of Electric Discharge between the Jet Electrolyte Cathode and the Metal Anode at Atmospheric Pressure. *High Temperature*. 2019;57(4):447–458. <https://doi.org/10.1134/S0018151X19030118>

10. Kulikov IS, Vashchenko SV, Kamenev AYa. *Electrolytic-Plasma Processing of Materials*. Minsk: Publ. House "Belaruskaya navuka"; 2010. 232 p. (In Russ.)
11. Witzke M, Rumbach P, Go DB, Sankaran RM. Evidence for the Electrolysis of Water by Atmospheric-Pressure Plasmas Formed at the Surface of Aqueous Solutions. *Journal of Physics D: Applied Physics*. 2013;46:129601. <https://doi.org/10.1088/0022-3727/45/44/442001>
12. Valentinčič J, Koroth JE, Zeidler H. Advancements in Surface Finish for Additive Manufacturing of Metal Parts: A Comprehensive Review of Plasma Electrolytic Polishing (PEP). *Virtual and Physical Prototyping*. 2024;19:1–23. <https://doi.org/10.1080/17452759.2024.2364222>
13. Radkevich MM, Novikov VI, Popov AI, Tyukhtyaev MI. The Analysis of Thermal Phenomena under Jet Focused Electrolytic Plasma Processing. *St. Petersburg Polytechnic University Journal: Physics and Mathematics*. 2016;254(4):141–150. (In Russ.) <https://doi.org/10.5862/JEST.254.15>
14. Krevsun EP, Kulikov IS. *Device for Electrolytic-Plasma Treatment of Conductive Products*. BY Patent No. 16101. 2012. (In Russ.)
15. Slovetskii DI, Terent'ev SD, Plekhanov VG. A Plasma-Electrolyte Metal Heating Mechanism. *High Temperature*. 1986;24(2):353–363. (In Russ.) URL: <https://www.mathnet.ru/rus/tvt4939> (accessed: 03.02.2025).
16. Alekseyev YuG, Korolyov AYU, Parshuto AE, Niss VS. Electrolyte-Plasma Treatment under Non-Stationary Mode in a High-Gradient Electric Field. *Science & Technique*. 2017;16(5):391–399. (In Russ.) <https://doi.org/10.21122/2227-1031-2017-16-5-391-399>
17. Quitzke S, Kröning O, Safranchik D, Zeidler H, Danilov I, Martin A, et al. Design and Setup of a Jet-Based Technology for Localized Small Scale Plasma Electrolytic Polishing. *Journal of Manufacturing Processes*. 2022;75:1123–1133. <https://doi.org/10.1016/j.jmapro.2022.01.064>
18. Danilov I, Paul R, Hackert-Oschätzchen M, Zinecker M, Quitzke S, Schubert A. Random Sequential Simulation of the Resulting Surface Roughness in Plasma Electrolytic Polishing of Stainless Steel. *Procedia CIRP*. 2020;95:981–986. <https://doi.org/10.1016/j.procir.2020.02.255>
19. Hackert-Oschätzchen M, Meichsner G, Zinecker M, Martin A, Schubert A. Micro Machining with Continuous Electrolytic Free Jet. *Precision Engineering*. 2012;36(4):612–619. <https://doi.org/10.1016/j.precisioneng.2012.05.003>
20. Nestler K, Böttger-Hiller F, Adamitzki W, Glowa G, Zeidler H, Schubert A. Plasma Electrolytic Polishing – An Overview of Applied Technologies and Current Challenges to Extend the Polishable Material Range. *Procedia CIRP*. 2016;42:503–507. <https://doi.org/10.1016/J.PROCIR.2016.02.240>
21. Guo QJ, Zhao YJ, Ni GH, Li L, Lin QF, Sui SY, et al. N₂/H₂ Non-Thermal Transferred Arc Plasma Nitriding Treatment of Stainless Steel at Atmospheric Pressure. *Plasma Chemistry and Plasma Processing*. 2020;40(6):1525–1537. <https://doi.org/10.1007/s11090-020-10103-0>
22. Barinov YuA, Shkol'nik SM. Discharge with a Liquid Nonmetallic Cathode (Tap Water) in Atmospheric-Pressure Air Flow. *Technical Physics*. 2016;86(11):155–158. (In Russ.) <https://doi.org/10.21883/jtf.2016.11.43833.1833>
23. Ghezri A, Pratama K, Scholl YV, Küenzi AM, Nelis T, Burger J, et al. Energy Efficient Jet Polishing via Electrolytic Plasma Enhances Corrosion Resistance in Stainless Steel. *MDPI*. 2024;8(6):289. <https://doi.org/10.24451/dspace/11365>
24. Gangqiang Ji, Longfei Ma, Liyun Wu. Effect of the Gas Layer Evolution on Electrolytic Plasma Polishing of Stainless Steel. *Scientific Reports*. 2024;14:22099. <https://doi.org/10.1038/s41598-024-74263-1>
25. Chuanqiang Zhou, Ning Qian, Honghua Su, Zhao Zhang, Wenfeng Ding, Jiu-hua Xu. Effect of Energy Distribution on the Machining Efficiency and Surface Morphology of Inconel 718 Nickel-Based Superalloy Using Plasma Electrolytic Polishing. *Surface and Coatings Technology*. 2022;441(15):128506. <https://doi.org/10.1016/j.surfcoat.2022.128506>
26. Gangqiang Ji, Longfei Ma, Sunan Zhang, Juan Zhang, Liyun Wu. Study of Electrochemical Behavior and a Material Removal Mechanism During Electrolytic Plasma Polishing of 316L Stainless Steel. *Materials*. 2025;18(6):1307. <https://doi.org/10.3390/ma18061307>
27. Sirota VV, Zaitsev SV, Limarenko MV, Churikov AS, Podgornyi DS. The Effect of the Introduction of B₄C on the Adhesive and Cohesive Properties of Self-Fluxing Coatings. *Construction Materials and Products*. 2024;7(6):5. <https://doi.org/10.58224/2618-7183-2024-7-6-5>

About the Authors:

Alexander I. Popov, Cand.Sci. (Eng.), Associate Professor of the Higher School of Mechanical Engineering, Peter the Great St. Petersburg Polytechnic University (29, Politekhicheskaya Str., St. Petersburg, 195251, Russian Federation), [SPIN-code](#), [ORCID](#), [ScopusID](#), [ResearcherID](#), [ResearchGate](#), popov_ai@spbstu.ru

Vitaly I. Novikov, Cand.Sci. (Eng.), Associate Professor of the Higher School of Mechanical Engineering, Peter the Great St. Petersburg Polytechnic University (29, Politekhnicheskaya Str., St. Petersburg, 195251, Russian Federation), Associate Professor of the Department of Forensic Science, St. Petersburg State University of Architecture and Civil Engineering (4, 2nd Krasnoarmeiskaya Str., St. Petersburg, 190005, Russian Federation), [SPIN-code](#), [ORCID](#), [ScopusID](#), [ResearcherID](#), [ResearchGate](#), novikov_vi@spbstu.ru

Dmitry N. Ivanov, Postgraduate Student, Higher School of Mechanical Engineering, Peter the Great St. Petersburg Polytechnic University (29, Politekhnicheskaya Str., St. Petersburg, 195251, Russian Federation), [SPIN-code](#), [ORCID](#), ivanov5.dn@edu.spbstu.ru

Igor A. Kozyrskiy, 4th year student majoring in Mechanical Engineering Technology, Higher School of Mechanical Engineering, Peter the Great St. Petersburg Polytechnic University (29, Politekhnicheskaya Str., St. Petersburg, 195251, Russian Federation), [ORCID](#), kozyrskij.i@edu.spbstu.ru

Claimed Contributorship:

AI Popov: conceptualization, supervision.

VI Novikov: formal analysis, investigation.

DN Ivanov: investigation, writing – original draft preparation.

IA Kozyrsky: investigation, writing – original draft preparation, visualization.

Conflict of Interest Statement: the authors declare no conflict of interest.

All authors have read and approved the final manuscript.

Об авторах:

Александр Иннокентьевич Попов, кандидат технических наук, доцент, «Высшая школа машиностроения» института машиностроения материалов и транспорта Санкт-Петербургского политехнического университета Петра Великого (195251, Российская Федерация, г. Санкт-Петербург, ул. Политехническая, д. 29), [SPIN-код](#), [ORCID](#), [ScopusID](#), [ResearcherID](#), [ResearchGate](#), popov_ai@spbstu.ru

Виталий Иванович Новиков, кандидат технических наук, доцент, «Высшая школа машиностроения» института машиностроения, материалов и транспорта Санкт-Петербургского политехнического университета Петра Великого (195251, Российская Федерация, г. Санкт-Петербург, ул. Политехническая, 29), доцент, кафедра «Судебных экспертиз» Санкт-Петербургского государственного архитектурно-строительного университета (190005, Российская Федерация, г. Санкт-Петербург, ул. 2-я Красноармейская, 4), [SPIN-код](#), [ORCID](#), [ScopusID](#), [ResearcherID](#), [ResearchGate](#), novikov_vi@spbstu.ru

Дмитрий Николаевич Иванов, аспирант, «Высшая школа машиностроения» института машиностроения материалов и транспорта Санкт-Петербургского политехнического университета Петра Великого (195251, Российская Федерация, г. Санкт-Петербург, ул. Политехническая, д. 29), [SPIN-код](#), [ORCID](#), ivanov5.dn@edu.spbstu.ru

Игорь Алексеевич Козырский, студент 4 курса, «Высшая школа машиностроения» института машиностроения материалов и транспорта Санкт-Петербургского политехнического университета Петра Великого (195251, Российская Федерация, г. Санкт-Петербург, ул. Политехническая, д. 29), [ORCID](#), kozyrskij.i@edu.spbstu.ru

Заявленный вклад авторов:

А.И. Попов: разработка концепции, научное руководство.

В.И. Новиков: формальный анализ. проведение исследования.

Д.Н. Иванов: проведение исследования, написание черновика рукописи.

И.А. Козырский: проведение исследования, написание черновика рукописи, визуализация.

Конфликт интересов: авторы заявляют об отсутствии конфликта интересов.

Все авторы прочитали и одобрили окончательный вариант рукописи.

Received / Поступила в редакцию 10.04.2025

Reviewed / Поступила после рецензирования 14.05.2025

Accepted / Принята к публикации 26.05.2025

MACHINE BUILDING AND MACHINE SCIENCE МАШИНОСТРОЕНИЕ И МАШИНОВЕДЕНИЕ



UDC 621.03.01

Original Theoretical Research

<https://doi.org/10.23947/2687-1653-2025-25-2-112-119>

A Method for Monitoring the Reliability of Technical Systems by Identifying the Entropy of the Causes of their Failures

Alexander T. Rybak , Svetlana V. Teplyakova ✉, Anastasiya V. Olshevskaya ,
Alexey S. Prutskov

Don State Technical University, Rostov-on-Don, Russian Federation

✉ svet-tp1@mail.ru

EDN: BSPTKA

Abstract

Introduction. Under designing, a large safety margin of components and units is included at the calculation stage, which does not exclude premature failures that occur at random. The consequences of such failures are not only economic losses, but also threats to the safety of people and the environment. In modern literature, the topic of assessing the reliability of machines, considered as complex probabilistic systems that take into account not only the dynamic parameters under operation, but also the processes of manufacturing the components of the system, is not sufficiently covered. Therefore, to provide for the targeted management of the reliability of machines as complex technical systems, it is required to apply the principles of cybernetics. The research objective is to study the method of monitoring the reliability of technical systems by identifying the entropy of the causes of their failures.

Materials and Methods. The materials for the study were statistical data on machine part failures obtained through long-term observation of the working condition of basic parts of lifting-and-shifting machines, as well as road and construction machines. The paper used mathematical statistics and probability theory — a parametric method for assessing reliability with a simplified approach, which assumes the deterministic behavior of the machine as a system with a predetermined functioning that does not depend on external circumstances. The value of the safety margin is taken at a level greater than one.

Results. The degree of impact of the uncertainty of the reference values of the operating process, design features, manufacturing technique of machine parts and the malfunctions that occur in them, on the final probability of failure-free operation and reliability of machines is determined.


Discussion and Conclusion. The analysis of the theory of verification calculations of machines confirmed the compliance of the obtained results with regulatory requirements. The conducted studies have proven that machines are deterministic systems, whose behavior is specified in advance by the calculation. Therefore, it can be argued that the developed method of monitoring the reliability of technical systems, based on identifying the entropy of the causes of failures, will allow establishing a quantitative and qualitative relationship between the design, material, size, manufacturing technique of machine parts, and failures that occur in them.

Keywords: reliability control system, entropy, machine, failure, determined system

Acknowledgements. The authors would like to thank the Editorial board and reviewers for their attentive attitude to the article and the comments indicated, which allowed us to improve its quality.

For Citation. Rybak AT, Teplyakova SV, Olshevskaya AV, Prutskov AS. A Method for Monitoring the Reliability of Technical Systems by Identifying the Entropy of the Causes of their Failures. *Advanced Engineering Research (Rostov-on-Don)*. 2025;25(2):112–119. <https://doi.org/10.23947/2687-1653-2025-25-2-112-119>

Метод контроля надежности технических систем путем выявления энтропии причин их отказов

А.Т. Рыбак , С.В. Теплякова ✉, А.В. Ольшевская , А.С. Пруцков 

Донской государственный технический университет, г. Ростов-на-Дону, Российская Федерация

✉ svet-tpl@mail.ru

Аннотация

Введение. При конструировании на этапе проведения расчетов закладывается большой запас прочности деталей и узлов, что не исключает преждевременные отказы, имеющие случайный характер. Последствиями таких отказов являются не только экономические потери, но и угрозы безопасности людям и окружающей среде. В современной литературе недостаточно освещена тема оценки надежности машин, рассматриваемых как сложные вероятностные системы, учитывающие не только динамические параметры при эксплуатации, но и технологические процессы изготовления составных деталей системы. Поэтому для обеспечения целенаправленного управления надежностью машин, как сложных технических систем, необходимо применять принципы кибернетики. Цель данной работы — исследование метода контроля надежности технических систем путем выявления энтропии причин их отказов.

Материалы и методы. Материалами для исследования послужили статистические данные отказов деталей машин, полученные путем многолетнего наблюдения за работоспособным состоянием базовых деталей подъемно-транспортных, дорожных и строительных машин. В работе применялась математическая статистика и теория вероятностей — параметрический метод оценивания надежности по упрощенному подходу, предполагающему детерминированное поведение машины как системы с заранее определенным функционированием, не зависящим от внешних обстоятельств. Значение запаса прочности принято на уровне больше единицы.

Результаты исследования. Определена степень влияния неопределенности исходных значений процесса эксплуатации, конструктивных особенностей, технологии изготовления деталей машин и возникающих в них неисправностей на итоговую вероятность безотказной работы и надежность машин.

Обсуждение и заключение. Анализ теории проверочных расчетов машин подтвердил соответствие полученных результатов нормативным требованиям. Проведенные исследования доказывают, что машины являются детерминированными системами, поведение которых заранее определяется расчетом. Поэтому можно утверждать, что разработанный метод контроля надежности технических систем, основанный на выявлении энтропии причин отказов, позволит устанавливать количественную и качественную взаимосвязь между конструкцией, материалом, размером, технологией изготовления деталей машин и отказами, возникающими в них.

Ключевые слова: система контроля надежности, энтропия, машина, отказ, детерминированная система

Благодарности. Авторы выражают благодарность редакции журнала и рецензентам за внимательное отношение к статье и указанные замечания, которые позволили повысить ее качество.

Для цитирования. Рыбак А.Т., Теплякова С.В., Рудой Д.В., Ольшевская А.В., Пруцков А.С. Энтропия как интегральный показатель надежности сложных технических систем. *Advanced Engineering Research (Rostov-on-Don)*. 2025;25(2):112–119. <https://doi.org/10.23947/2687-1653-2025-25-2-112-119>

Introduction. Technological progress and the constant complication of technical systems and equipment make reliability a key factor in determining the efficiency of their operation. The importance of providing the required level of reliability of complex technical facilities is due not only to the possible emergence of economic costs, but also to the evolution of safety threats to people and the environment.

Conducting strength calculations when designing machines shows the adoption of significant reserve factors of parts, eliminating the possibility of breakdowns. Therefore, it can be mistakenly assumed that malfunctions and failures are caused by errors in design and/or low quality of manufactured mechanisms. Indeed, miscalculations by designers and calculators, poorly manufactured parts or materials can be the cause of individual breakdowns and malfunctions [1]. During the refining process, the vast majority of errors are eliminated, but this does not lead to a significant increase in the reliability of the machine [2].

As previously conducted studies show, the causes of failures are random, and the factors affecting the level of randomness may include changes in the following parameters: the interval between failures, the order of failure of parts or units, the time it takes to restore the machine functionality, etc. Therefore, a machine, as a complex system, exhibits various degrees of uncertainty while in operation, which is associated with entropy and makes it a probabilistic system [3]. The conducted analysis of the literature showed insufficient elaboration of the issue of monitoring the level of dependence of the reliability of a complex system not only on the operation process, but also on the manufacturing of the components of the system.

The method of managing the reliability level of technical systems with targeted identification of the entropy of the causes of failures, linking the design, material, size, manufacturing technique and operating features of parts, will allow predicting the frequency and intensity of failures, and this will have a positive effect on the level of failure-free operation of the entire mechanism.

Therefore, the objective of the presented research is to study the method of monitoring the reliability of technical systems through identifying the entropy of the causes of failures, that allow establishing quantitative and qualitative relationships between the designs, materials, sizes, and manufacturing techniques of machine parts with the failures that occur in them.

Materials and Methods. The materials for the study were data on failures of basic parts of lifting-and-shifting, road and construction machines, obtained as a result of long-term monitoring of their condition. The analysis of such information has confirmed that the practical level of reliability of machines is provided in the process of their design. Certain decisions taken in the process of designing and refining machines ultimately determine their reliability as a combination of trouble-free operation, durability and maintainability [4–5]. As practice shows, machine failures are fairly common phenomena that affect safety and the amount of damage caused to varying degrees (Fig. 1).

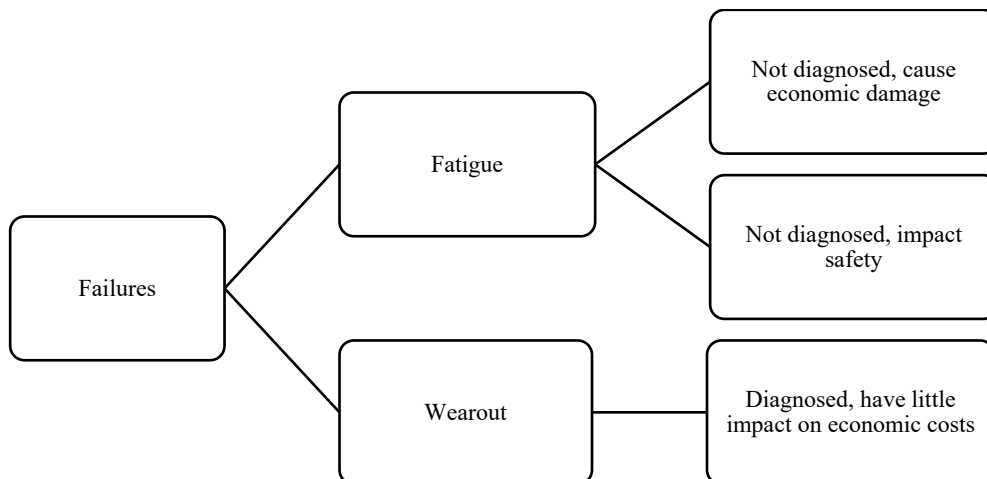


Fig. 1. Reasons for machine failures

As is known, at present, reliability calculations for machine components and parts are not performed. At the same time, the designer determines (albeit unconsciously) the reliability of parts, components and the machine as a whole — by establishing certain dimensions and shape of parts, accepting the value of the safety margin, assigning the grade of steel, heat treatment mode, surface purity, the nature of the mating and interaction with other parts, [6]. Therefore, the reliability parameters of machines manufactured in strict accordance with technical specifications are completely determined by the design organization — the author of the machine design [7].

In the process of serial production, deviations from drawings, technical conditions, obvious and hidden defects, etc., are possible. In some cases, engineering specifications contain unclear technical conditions for the manufacture and acceptance of parts and units, which allow for their free interpretation towards deterioration in quality. In order to eliminate obvious defects as much as possible, prior to putting the machines into operation, they are pre-run under load [8]. However, numerous machines do not undergo running-in due to the lack of required areas. Therefore, at the initial stage of machine operation, so-called running-in failures occur, whose frequency depends on the quality of the machine manufacture and gradually decreases to zero. Poor assembly quality leads to the need for additional maintenance of machines during the initial period of their operation.

It should be noted that running-in failures are caused by the most serious defects in the manufacture of machines. However, hidden defects (poor quality of heat treatment and welding, below-standard strength of the materials used, poorly executed sealing, etc.) manifest themselves in additional failures [9]. Thus, the design organization determines all the parameters of machine reliability, i.e., failure-free operation, durability and maintainability throughout their entire service life [10–12]. The manufacturer to a greater or lesser extent reduces the degree of reliability of machines, which manifests itself mainly at the beginning of their operation.

Even more significant damage is caused by so-called premature failures, which result in significant economic costs and can also be dangerous to human health and life [13].

As practice shows, reliability as a science does not lose its relevance over time, and ultimately, the objective of reliability management is to identify its quantitative parameters and actively affect them. This management consists in making the connection between the operation of machines, their design and manufacture [14].

Issues of rational control of complex probabilistic systems of any nature (from complex automatic self-guided systems to a living organism or community) with dynamic parameters are considered by cybernetics. These control processes include the collection, transmission, storage and processing of information. When analyzing a complex system, information from the external environment is also taken into account, which affects the behavior and state of the system [15]. Control is based on the principle of feedback, which allows the controlled process to be linked to the system under consideration.

Based on the principles of cybernetics, the process of machine operation can be controlled by less downtime, reduction of the volume of repair work and increase of the service life [16]. To provide the control process on the part of the manufacturer and/or design institute, it is necessary to set up feedback, i.e., to get comprehensive information on the operational reliability of the machine. To obtain reliable results, installations are used that allow resource tests to be performed under conditions close to real ones.

The question arises about the content and specificity of information suitable for targeted management of machine reliability for studying the method of monitoring the reliability of technical systems through identifying the entropy of the causes of failures in order to take into account the measure of uncertainty of the physical system under consideration [17]. In cybernetics, this value is entropy, which is defined as the sum of products of the probabilities of various states of the system multiplied by the logarithms of these probabilities taken with the opposite sign.

$$H = - \sum_{i=1}^n P_i \cdot \log P_i, \quad (1)$$

where P_i — probability of the i -th state of the system; n — number of possible states of the system.

Entropy allows taking into account the amount of the eliminated uncertainty. The opposite sign shows the direction of the processes to indicate the nonequivalence of the direct (failure occurrence) and reverse (performance restoration) processes in real operating conditions.

Machines, as complex systems, consist of elements — parts. Each part/unit of machines can be considered as a simple system, which is in two states: serviceable or faulty. Thus, it becomes clear that the degree of uncertainty of the operation of the i -th part can be determined using formula [18, 19]:

$$H = - [K_{ip} \cdot \log K_{ip} + K_{in} \cdot \log K_{in}], \quad (2)$$

where K_{ip} — readiness coefficient of the i -th part; K_{in} — probability of a faulty condition of a part.

The readiness coefficient of a part is determined by the following relationship:

$$K_{ip} = \frac{T_i}{T_i + T_{iB}}, \quad (3)$$

where T_i — mean time between failures of the i -th part, i.e., its average time of nonfailure operation; T_{iB} — average time to restore the machine when the i -th part fails.

Relative duration of downtime of a part:

$$K_{in} = 1 - K_{ip}, \quad (4)$$

or

$$K_{in} = \frac{T_{iB}}{T_i + T_{iB}}. \quad (5)$$

The reliability of a part is determined by its service life. If $t = Tp$ — service life of a part, then the service life distribution law:

$$Q_{(t)} = Tp \{Tp < t\}. \quad (6)$$

This function is the probability of failure of the part before moment Tp . It completely determines the reliability of this part [20, 21].

And the distribution density of this function is called the failure rate:

$$q_{(t)} = \frac{dQ_{(t)}}{dt}. \quad (7)$$

The following approximate relationship exists between the cycles to failure of a part and its reliability indicators:

$$T_{(t)} = \frac{[1 - Q_{(t)}]^2}{q(t)}. \quad (8)$$

In the statistical reliability theory, the reliability parameters of a part are expressed by the probability of failure-free operation $F(t)$ and failure rate $\lambda(t)$, which are determined from the following formulas:

$$F(t) = 1 - Q(t), \quad (9)$$

$$\lambda(t) = \frac{q(t)}{F(t)}. \quad (10)$$

Hence,

$$Q(t) = 1 - F(t), \quad (11)$$

$$q(t) = F(t)\lambda(t). \quad (12)$$

Substituting the expression for $Q(t)$ and $q(t)$ into equation (7), we obtain

$$T(t) = \frac{q(t)}{\lambda(t)}. \quad (13)$$

Then, the part readiness coefficient

$$K_{ip} = \frac{F_1(t)}{F_1(t) + \lambda_1(t)T_{ib}}, \quad (14)$$

and the relative duration of downtime of the part

$$K_{ip} = \frac{\lambda_1(t) \cdot T_{ib}}{F_1(t) + \lambda_1(t)T_{ib}}. \quad (15)$$

We substitute expressions (11) and (12) into (2) and obtain an equation for the entropy of the part:

$$H_1(t) = - \left[\frac{F_1(t)}{F_1(t) + \lambda_1(t)T_{ib}} \log \frac{F_1(t)}{F_1(t) + \lambda_1(t)T_{ib}} + \frac{\lambda_1(t) \cdot T_{ib}}{F_1(t) + \lambda_1(t)T_{ib}} \log \frac{\lambda_1(t) \cdot T_{ib}}{F_1(t) + \lambda_1(t)T_{ib}} \right]. \quad (16)$$

Understanding that the failures of machine parts are independent of each other, the machine from a cybernetic point of view can be represented as a complex system obtained by combining simple systems — the parts that make up the machine.

Therefore, according to the entropy addition theorem, when combining independent systems, their entropies are added up. This means that the entropy of the machine operation is determined by the following formula:

$$H(t) = \sum_{i=1}^m H_i(t), \quad (17)$$

where m — number of parts that make up a machine.

Substituting value $H_i(t)$ here, we obtain the formula for determining the failure entropy of the entire machine:

$$H_1(t) = \sum_{i=1}^m \left[\frac{F_1(t)}{F_1(t) + \lambda_1(t)T_{ib}} \log \frac{F_1(t)}{F_1(t) + \lambda_1(t)T_{ib}} + \frac{\lambda_1(t) \cdot T_{ib}}{F_1(t) + \lambda_1(t)T_{ib}} \log \frac{\lambda_1(t) \cdot T_{ib}}{F_1(t) + \lambda_1(t)T_{ib}} \right]. \quad (18)$$

The authors of the article believe that the entropy value obtained for the entire machine with a significant exhausted resource will tend to unity.

Research Results. As an example, the study determined the entropy of one of the basic parts of a loader — a boom, whose availability factor (probability that the loader boom is currently in serviceable condition), adopted by the manufacturer, is equal to $K_{ip} = 0.9$, and the relative duration of downtime is $K_{in} = 0.1$. The entropy of the part, according to dependence (2), will be

$$H = -[0.9 \log 0.9 + 0.1 \log 0.1] = 0.14.$$

As the readiness coefficient increases to $K_{ip} = 0.95$, entropy H tends to zero:

$$H = -[0.95 \log 0.95 + 0.05 \log 0.05] = 0.08.$$

If we consider the issue of replacing the boom, the duration will be approximately one work shift, but the costs in this case will be high, since they include the purchase of a new boom (approximately 112 thousand rubles). Repairing the boom is cheaper in terms of components, but its duration increases by an order of magnitude depending on the complexity of the repair.

That is, if we consider a loader boom, for which the availability factor declared by the manufacturer is equal to $K_{ip} = 0.9$, and the relative duration of downtime is $K_{in} = 0.1$, then entropy will be:

$$H_1(t) = - \left[\frac{0.9}{0.9 \cdot 0.1 \cdot 10} \log \frac{0.9}{0.9 \cdot 0.1 \cdot 10} + \frac{0.1 \cdot 10}{0.9 \cdot 0.1 \cdot 10} \log \frac{0.1 \cdot 10}{0.9 \cdot 0.1 \cdot 10} \right] = \\ = - (0.47 \log 0.47 + 0.5 \log 0.5) = - (0.32 + (-28)) = 0.6.$$

Thus, the degree of impact of the uncertainty of the initial values on the final probability of failure-free operation and, as a consequence, on the reliability of the machine is determined. A method for monitoring the reliability of technical systems based on identifying the entropy of the causes of failures, taking into account the quantitative and qualitative relationships between the design, material, dimensions and manufacturing technology of machine parts with the failures that occur in them, is developed.

Discussion and Conclusion. The study of the method of monitoring the reliability of technical systems by identifying the entropy of the causes of failures is a method of simplifying calculations, consisting in the determination of the machine operation [5]. The use of entropy in calculations allows taking into account the amount of the uncertainty of the relationship between quantitative and qualitative characteristics with design features, materials, dimensions, and processes of manufacturing machine parts, and the malfunctions that arise in them.

The conducted study of this relationship shows that the entropy of the loader operation, changing over time, is determined by the reliability characteristics and conditions of restoration of the machine components (units and parts).

The entropy of a complex machine system grows with the extension of its lifetime. This is confirmed by the increase in the frequency of fatigue processes, plastic deformations, and the degree of wear. When a certain level of entropy is reached, the operation of the machine is limited, and a major overhaul is performed, which helps to reduce the entropy of the machine operation.

In the process of targeted management of the operational reliability of the machine, the accuracy of the incoming information about the state of the system is very important. Such information should contain the actual, time-varying reliability (failure-free operation and maintainability) of all the components of the machine — units and parts.

Obviously, achieving zero entropy of a machine as a complex system is possible not only by analyzing quantitative indicators of component reliability, but also through identifying the causes of failures. Then, the volume of information under study when studying a sample lot of objects (parts, units, machines), obtained under operation, increases significantly. Conducting a special analysis allows us to determine the causes of component failures and provide clear recommendations for their elimination.

Thus, the authors have proven that the method of monitoring the reliability of technical systems by identifying the entropy of the causes of failures considered in the research provides for effective control of the reliability of complex systems, taking into account not only the operational causes of failures, but also design features, materials, dimensions, and manufacturing of parts. The application of this method of reliability control of complex systems will make it possible to develop a reliability management system with identification of failure causes. This will make it possible to consider the machine not as a probabilistic system, but as a deterministic system, where the change in reliability is precalculated. Although the need for reliability management is decreasing, reliability control will probably remain an important requirement to prevent possible errors in machine design.

References

1. Ferrian F, Cornetti P, Marsavina L, Sapor A. Finite Fracture Mechanics and Cohesive Crack Model: Size Effects through a Unified Formulation. *Frattura ed Integrità Strutturale*. 2022;16(61):496–509. <https://doi.org/10.3221/IGF-ESIS.61.33>
2. Kasyanov VE. *Principles of the Creation of an Absolute Trouble-Free Machine*. Deposited Manuscript, No. 1-B2014. Moscow: VINITI RAN; 2014. 9 p. (In Russ.)
3. Doronin SV, Reizmunt EM, Rogalev AN. Erratum to: “Problems on Comparing Analytical and Numerical Estimations of Stressed-Deformed State of Structure Elements”. *Journal of Machinery Manufacture and Reliability*. 2018;47(4):387–387. <https://doi.org/10.3103/S1052618818040167>
4. Makhutov NA, Albagachiev AYU, Alekseeva SI, Ahhmetzhanov RS, Baranov YuV, Vanin GA, et al. *Durability, Resource, Survivability and Safety of Machines*. Monograph. Moscow: LIBROKOM; 2008. 574 p. (In Russ.)
5. Trukhanov VM. Calculation of Design Reliability of Technical Systems on Gradual Breakdowns. *Testing. Diagnostics*. 2015;(1):70–72. <https://doi.org/10.14489/td.2015.01.pp.070-072>

6. Lepikhin AM, Moskvichev VV, Doronin SV. Reliability, Survivability and Safety for Complex Technical Systems. *Computational Technologies*. 2009;14(6):58–70. (In Russ.) URL: <http://www.ict.nsc.ru/jct/annotation/1333> (accessed: 13.01.2025).
7. Lepikhin AM, Moskvichev VV, Doronin SV, Makhutov NA. Probabilistic Modeling of Safe Crack Growth and Estimation of the Durability of Structures. *Fatigue & Fracture of Engineering Materials & Structures*. 2000;23(5):395–401. <https://doi.org/10.1046/j.1460-2695.2000.00303.x>
8. Klyuev VV. *Non-Destructive Testing*. Handbook. In 8 vol. 2nd rev. ed. Moscow: Mashinostroenie; 2008. 560 p. (In Russ.)
9. Lepikhin AM. Non-Destructive Testing and Risk Assessment of Welding Defects at the Equipment Operation Stage. *Voprosy Materialovedeniya*. 2007;51(3):208–213.
10. Birger IA. *Technical Diagnostics*. 2nd ed. Moscow: LENAND; 2018. 238 p. (In Russ.)
11. Klyuev VV (ed), Lozovsky VN, Savilov VP. *Diagnostics of Machine Parts and Mechanisms*. In 2 parts. Part 1. Moscow: Spektr; 2017. 176 p. (In Russ.)
12. Zaitseva M, Popov S, Marchenko J, Dontsov N, Nemtseva E. Truck Maintenance Frequency Optimization, Taking into Account an Increase in Its Operational Reliability. In book: Guda A (ed). *Networked Control Systems for Connected and Automated Vehicles*, Vol. 2. Cham: Springer; 2023. P. 1863–1871.
13. Deryushev VV, Teplyakova SV, Zaitseva MM. Production Facilities Safety Assessment according to the Maximum Values of Machine Reliability. *Safety of Technogenic and Natural Systems*. 2023;7(2):58–69. <https://doi.org/10.23947/2541-9129-2023-7-2-58-69>
14. Teplyakova SV. Justification of the Concept of Creating Practically Trouble-Free Machines. *University News. North-Caucasian Region. Technical Sciences Series*. 2021;210(2):41–45. <https://doi.org/10.17213/1560-3644-2021-2-41-45>
15. Shambadal P. *Development and Applications of the Concept of Entropy*. Moscow: Nauka; 1967. 278 p. (In Russ.)
16. Deryushev VV, Zaitseva MM, Evseev DZ, Kosenko EE. Concentration of Thermal Stresses in Metal Materials and Constructions under Local Heating. *Materials Science Forum*. 2019;974:729–734. <https://doi.org/10.4028/www.scientific.net/MSF.974.729>
17. Kasyanov VE, Kosenko EE, Kosenko VV, Demchenko DB, Khvan RV. Checking the Adequacy of the Technical and Economic Model for Ensuring a Target Life of an Individual Production Machine. *IOP Conference Series: Materials Science and Engineering*. 2021;1083:012066. <http://doi.org/10.1088/1757-899X/1083/1/012066>
18. Dulesov AS, Fedorenko NS, Baishev AV. Estimation of the Possibilities of Measuring the Amount of Entropy in the Analysis of the Reliability of Technical Systems. *Vestnik of KhSU*. 2021;35(1):43–48.
19. Klyuev SV, Slobodchikova NA, Saidumov MS, Abumuslimov AS, Mezhdidov DA, Khezhev TA. Application of Ash and Slag Waste from Coal Combustion in the Construction of the Earth Bed of Roads. *Construction Materials and Products*. 2024;7(6):3. <https://doi.org/10.58224/2618-7183-2024-7-6-3>
20. Zhangabay N, Giyasov A, Ibraimova U, Tursunkululy T, Kolesnikov A. Construction and Climatic Certification of an Area as a Prerequisite for Development of Energy-Efficient Buildings and Their External Wall Constructions. *Construction Materials and Products*. 2024;7(5):1. <https://doi.org/10.58224/2618-7183-2024-7-5-1>
21. Zhangabay N, Bakhbergen S, Aldiyarov Zh, Tursunkululy T, Kolesnikov A. Analysis of Thermal Efficiency of External Fencing Made of Innovative Ceramic Blocks. *Construction Materials and Products*. 2024;7(3):1. <https://doi.org/10.58224/2618-7183-2024-7-3-1>

About the Authors:

Alexander T. Rybak, Dr.Sci. (Eng.), Professor of the Department of Technologies and Equipment for Processing Agricultural Products, Don State Technical University (1, Gagarin Sq., Rostov-on-Don, 344003, Russian Federation), [SPIN-code](#), [ORCID](#), [ScopusID](#), [ResearchGate](#), 2130373@mail.ru

Svetlana V. Teplyakova, Cand.Sci. (Eng.), Associate Professor of the Department of Transport Systems Operation and Logistics, Don State Technical University (1, Gagarin Sq., Rostov-on-Don, 344003, Russian Federation), [SPIN-code](#), [ORCID](#), [ScopusID](#), [ResearchGate](#), svet-tpl@yandex.ru

Anastasiya V. Olshevskaya, Cand.Sci. (Eng.), Deputy Dean of the Agro-Industrial Faculty, Associate Professor of the Department of Technologies and Equipment for Processing Agricultural Products, Don State Technical University, Deputy Head of the Don Valley Territorial Cluster Development Center of the Rostov Region (1, Gagarin Sq., Rostov-on-Don, 344003, Russian Federation), [SPIN-code](#), [ORCID](#), [ScopusID](#), [ResearchGate](#), oav.donstu@gmail.com

Alexey S. Prutskov, Engineer of the Don Valley Territorial Cluster Development Center of the Rostov Region (1, Gagarin Sq., Rostov-on-Don, 344003, Russian Federation), [SPIN-code](#), [ORCID](#), [ScopusID](#), prutskov.aleksey@yandex.ru

Claimed Contributorship:

AT Rybak: supervision, validation.

SV Teplyakova: conceptualization, formal analysis.

AV Olshevskaya: validation, data curation.

AS Prutskov: writing – original draft preparation, writing – review & editing.

Conflict of Interest Statement: the authors declare no conflict of interest.

All authors have read and approved the final manuscript.

Об авторах:

Александр Тимофеевич Рыбак, доктор технических наук, профессор, кафедра «Технологии и оборудование переработки продукции агропромышленного комплекса» Донского государственного технического университета (344003, Российская Федерация, г. Ростов-на-Дону, пл. Гагарина, 1), [SPIN-код](#), [ORCID](#), [ScopusID](#), [ResearchGate](#), 2130373@mail.ru

Светлана Викторовна Теплякова, кандидат технических наук, доцент, кафедра «Эксплуатация транспортных систем и логистика» Донского государственного технического университета (344003, Российская Федерация, г. Ростов-на-Дону, пл. Гагарина, 1), [SPIN-код](#), [ORCID](#), [ScopusID](#), [ResearchGate](#), svet-tpl@yandex.ru

Анастасия Владимировна Ольшевская, кандидат технических наук, заместитель декана, факультет «Агропромышленный», доцент, кафедра «Технологии и оборудование переработки продукции агропромышленного комплекса» Донского государственного технического университета, заместитель руководителя Центра развития территориального кластера «Долина Дона» Ростовской области (344003, Российская Федерация, г. Ростов-на-Дону, пл. Гагарина, 1), [SPIN-код](#), [ORCID](#), [ScopusID](#), [ResearchGate](#), oav.donstu@gmail.com

Алексей Сергеевич Прутков, инженер Центра развития территориального кластера «Долина Дона» Ростовской области (344003, Российская Федерация, г. Ростов-на-Дону, пл. Гагарина, 1), [SPIN-код](#), [ORCID](#), [ScopusID](#), prutskov.aleksey@yandex.ru

Заявленный вклад авторов:

А.Т. Рыбак: научное руководство, валидация результатов.

С.В. Теплякова: разработка концепции, формальный анализ.

А.В. Ольшевская: валидация результатов, курирование данных.

А.С. Прутков: написание черновика рукописи, написание рукописи – рецензирование и редактирование.

Конфликт интересов: авторы заявляют об отсутствии конфликта интересов.

Все авторы прочитали и одобрили окончательный вариант рукописи.

Received / Поступила в редакцию 21.03.2025

Reviewed / Поступила после рецензирования 12.04.2025

Accepted / Принята к публикации 16.04.2025

INFORMATION TECHNOLOGY, COMPUTER SCIENCE AND MANAGEMENT ИНФОРМАТИКА, ВЫЧИСЛИТЕЛЬНАЯ ТЕХНИКА И УПРАВЛЕНИЕ



UDC 004.8

Original Empirical Research

<https://doi.org/10.23947/2687-1653-2025-25-2-120-128>

Forecasting Delivery Time of Goods in Supply Chains Using Machine Learning Methods

 Vladislav K. Rezvanov¹ , Oksana M. Romakina¹ , Ekaterina V. Zaytseva²
¹ National Research University ITMO, Saint Petersburg, Russian Federation² Empress Catherine II Saint Petersburg Mining University, Saint Petersburg, Russian Federation omromakina@itmo.ru

EDN: QBDMMA

Abstract

Introduction. Trade development requires the implementation of artificial intelligence and machine learning technologies to improve the accuracy of delivery forecasts. The scientific research published to date in this area appears insufficient for two reasons. First, it focuses primarily on global supply chains, although the issue is relevant for local businesses as well. Second, forecasting typically requires large amounts of data for machine learning and significant computing resources that are not available to the majority of companies. The presented study aims to fill these gaps and demonstrate the efficiency of using open, accessible data and known algorithms. The research objective is to describe a pattern of appropriate selection of the least resource-intensive delivery forecasting model based on the analysis of machine learning algorithms.

Materials and Methods. The open data set DataCo Smart supply chain for big data analysis on deliveries in online trade was used. To process and analyze the information, methods of data cleaning, eliminating multicollinearity, normalization and coding of categorical features were applied. The following algorithms were used with the cleaned data: Decision tree, Random Forest, k-nearest neighbors, Naïve Bayes, Linear discriminant analysis, XGBoost, CatBoost, LightGBM, AdaBoost, and Perceptron.

Results. The basic algorithm for the delivery forecasting model was the Decision Tree algorithm. This choice was due to its high accuracy, ease of use, and low risk of overfitting. The model evaluation showed a high determination coefficient close to one (0.986). Low values of the mean square error (0.0367) and mean absolute error (0.0324) were recorded. The model showed satisfactory results in terms of time spent on training (3.3087 s) and forecasting (0.0051 s). Actual and predicted values almost perfectly matched. Deviations from actual values were minimal.

Discussion and Conclusion. The proposed model is efficient and has a high predictive ability. High-quality forecasting of delivery time is possible without the use of extensive databases and powerful computing resources. The study opens up the prospect of high-quality organization of logistics operations for small and medium enterprises. In further research, it is advisable to integrate weather data, traffic conditions and other indicators into the model. Using such information in real time will increase the adaptability and accuracy of forecasting.

Keywords: delivery time forecasting model, delivery forecast for small and medium enterprises, error in delivery forecasting, decision tree for logistics challenges

Acknowledgements. The authors would like to thank the Editorial board of the journal and the reviewers for their attentive attitude to the article and the comments that improved its quality.

For citation. Rezvanov VK, Romakina OM, Zaytseva EV. Forecasting Delivery Time of Goods in Supply Chains Using Machine Learning Methods. *Advanced Engineering Research (Rostov-on-Don)*. 2025;25(2):120–128. <https://doi.org/10.23947/2687-1653-2025-25-2-120-128>

Прогнозирование сроков доставки товаров в цепях поставок с использованием методов машинного обучения

В.К. Резванов¹ , О.М. Ромакина¹  , Е.В. Зайцева² 

¹ Национальный исследовательский университет ИТМО, г. Санкт-Петербург, Российская Федерация

² Санкт-Петербургский горный университет императрицы Екатерины II, г. Санкт-Петербург, Российская Федерация

 omromakina@itmo.ru

Аннотация

Введение. Развитие торговли требует внедрения технологий искусственного интеллекта и машинного обучения для повышения точности прогнозов доставки. Опубликованные на сегодня научные изыскания в этой области представляются недостаточными по двум причинам. Первая: рассматриваются главным образом глобальные цепи поставок, хотя вопрос актуален и для локальных бизнесов. Вторая: прогнозирование, как правило, требует больших объемов данных для машинного обучения и значительных вычислительных ресурсов, недоступных основной массе компаний. Представленное исследование призвано восполнить эти пробелы и показать эффективность использования открытых, доступных данных и известных алгоритмов. Цель работы — описать схему обоснованного выбора наименее ресурсоемкой модели прогнозирования доставки на основе анализа алгоритмов машинного обучения.

Материалы и методы. Использовался набор открытых данных DataCo Smart supply chain for big data analysis¹ о поставках в онлайн-торговле. Для обработки и анализа информации задействовали методы очистки данных, устранения мультиколлинеарности, нормализации и кодирования категориальных признаков. С очищенными данными работали алгоритмы: Decision tree, Random forest, K-nearest neighbors, Naive Bayes, Linear discriminant analysis, XGBoost, CatBoost, LightGBM, AdaBoost и Perceptron².

Результаты исследования. Базовым алгоритмом для модели прогнозирования доставки стал алгоритм дерева решений (Decision Tree). Этот выбор обусловлен высокой точностью, простотой использования и низким риском переобучения. Оценка модели показала высокий и близкий к единице коэффициент детерминации (0,986). При этом фиксируются низкие значения среднеквадратичной ошибки (0,0367) и средней абсолютной ошибки (0,0324). Модель показала удовлетворительные результаты по времени, затраченному на обучение (3,3087 с) и на прогнозирование (0,0051 с). Фактические и предсказанные значения почти идеально совпали. Отклонения от фактических значений оказались минимальными.

Обсуждение и заключение. Предложенная модель эффективна и обладает высокой предсказательной способностью. Качественное прогнозирование сроков доставки товара возможно без привлечения обширных баз данных и мощных вычислительных ресурсов. Исследование открывает перспективу качественной организации логистических операций для средних и малых предприятий. В дальнейших изысканиях целесообразно интегрировать в модель данные о погоде, дорожной ситуации и другие показатели. Использование такой информации в режиме реального времени повысит адаптивность и точность прогнозирования.

Ключевые слова: модель прогнозирования сроков доставки, прогноз доставки для малых и средних предприятий, ошибка в прогнозировании доставки, дерево решений для логистических задач

Благодарности. Авторы выражают благодарность редакции и рецензентам за внимательное отношение к статье и замечания, которые позволили повысить ее качество.

Для цитирования. Резванов В.К., Ромакина О.М., Зайцева Е.В. Прогнозирование сроков доставки товаров в цепях поставок с использованием методов машинного обучения. *Advanced Engineering Research (Rostov-on-Don)*. 2025;25(2):120–128. <https://doi.org/10.23947/2687-1653-2025-25-2-120-128>

Introduction. In the context of trade development, the relevance of accurate forecasting of delivery time increases. The inefficiency of traditional planning methods is due to the uncertainty related to the effect of various factors. It is obvious that the use of artificial intelligence (AI) in logistics can significantly improve the accuracy of forecasts and reduce operating costs. According to the international consulting organization McKinsey & Company, enterprises using AI for supply chain management can reduce forecast errors by 20–50%, which ultimately reduces costs by 10–15%³.

¹ Constante F, Silva F, Pereira A. DataCo Smart Supply Chain for Big Data Analysis. *Mendeley Data*. <https://doi.org/10.17632/8gx2fvg2k6.5>

² «Дерево решений», «Метод случайного леса», «Метод к ближайших соседей», «Наивный байесовский классификатор», «Линейный дискриминантный анализ», «Экстремальный градиентный бустинг», «Категориальный бустинг», «Облегченный градиентный машинный бустинг», «Адаптивный бустинг», «Перцептрон» (англ.)

³ DocShipper Group. *How AI is Changing Logistics & Supply Chain in 2025?* URL: <https://docshipper.com/logistics/ai-changing-logistics-supply-chain-2025/> (accessed: 22.03.2025).

Published scientific papers on this topic mainly consider large-scale, global supply chains [1]. Various approaches to forecasting delivery time are actively discussed, but research usually focuses on complex and resource-intensive models that are inaccessible to the majority of enterprises — small and medium-sized ones. At the same time, the problem is indeed a challenge for local, small businesses that are badly in need of saving resources. This is facilitated by better settings of logistics processes in general and, in particular, accurate delivery time forecasting. Companies with limited information and computing capabilities have few tools to improve the situation. The presented study is intended to fill this gap. The research objective is to determine the most efficient and least resource-intensive machine learning model for forecasting delivery time.

Materials and Methods. The study used a structured dataset of sales, deliveries, customers, and financials. The open-source DataCoSupplyChainDataset is hosted by DataCo Global in the free Mendeley Data cloud repository. The basics in this dataset are order and delivery dates, customer information, order financials, and delivery status.

Before analysis and modeling, the data were pre-processed — cleaned and transformed. To achieve the set goal, correlations were first identified and multicollinearity was eliminated on the basis of the correlation matrix (Fig. 1).

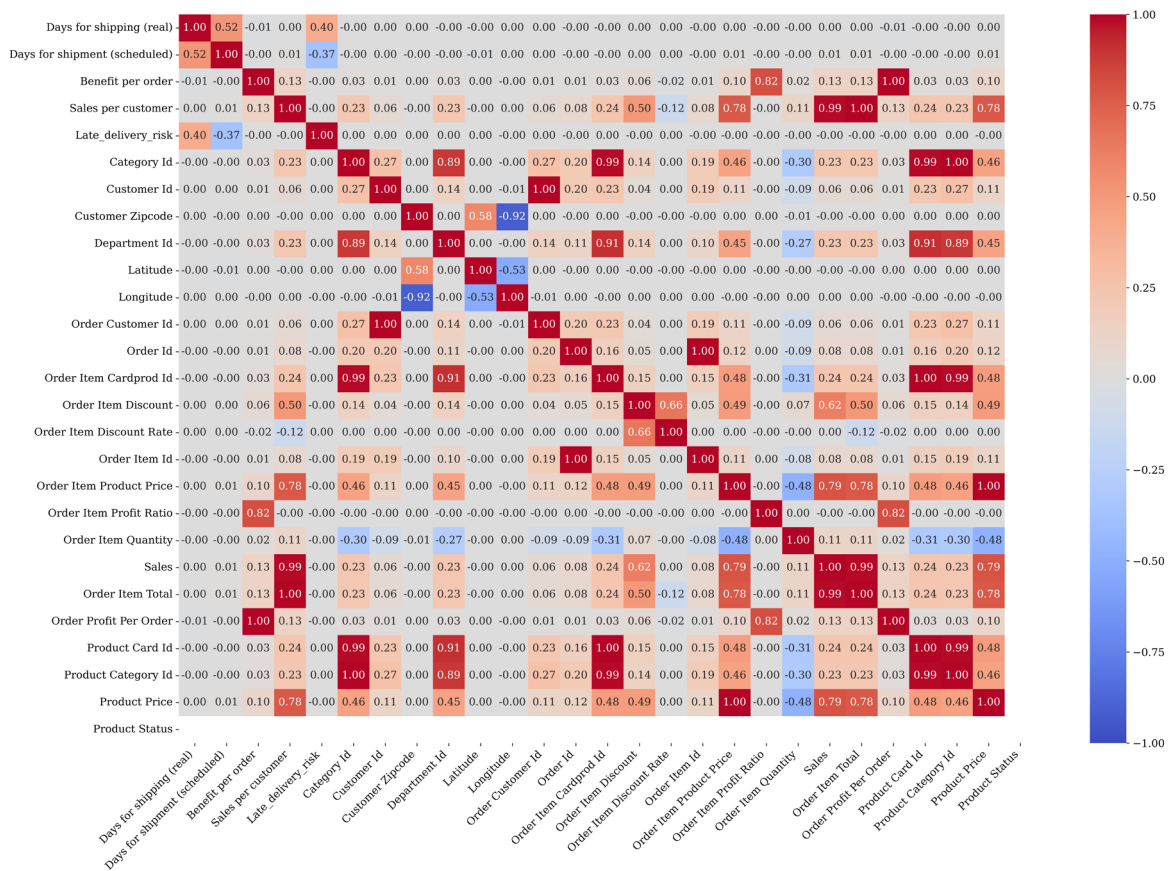


Fig. 1. Correlation matrix

The matrix allowed us to identify several pairs of features with a correlation coefficient equal to 1. This indicates their complete duplication. These pairs of features are presented below.

1. Customer_id and order_customer_id.
2. Sales_per_customer and order_item_total.
3. Benefit_per_order and order_profit_per_order.
4. Order_item_cardprod_id (ID of product card in the order) and product_card_id (product card ID).
5. Category_id and product_category_id.
6. Order_item_product_price (product price in the order) and product_price.

To eliminate duplication, the following features have been removed:

- benefit_per_order;
- sales_per_customer;
- order_item_cardprod_id;
- order_item_product_price;
- product_category_id;
- order_customer_id.

It was also found that the `product_status` (product availability) feature has only one unique value (0), i.e., the product is always available. This feature was also removed.

To analyze multicollinearity between numerical features, the variance inflation factor (VIF) was used [2]. Features with VIF higher than 5 indicate a strong relationship with other features, which can distort the results of the analysis and models. To avoid this problem, such features were removed or combined. This reduced data redundancy and increased the stability of the model.

After preliminary processing, we selected the main numerical and categorical features for further analysis and model building.

Numerical features included such indicators as sales, profit, discounts, and quantity of goods in the order. Categorical features included delivery status, customer segment, and delivery mode.

For features with VIF above 5, further analysis was performed to identify redundant relationships. If a feature could be expressed through others, it was replaced by a combination of simpler features. Examples are presented below.

1. $\text{Sales} = \text{product_price} * \text{order_item_quantity}$. Since sales revenue depends directly on the product price (`product_price`) and the quantity of goods (`order_item_quantity`), it is decided to use this expression to replace redundant features.

2. $\text{Order_item_discount} = \text{sales} * \text{order_item_discount_rate}$. The discount on the product (`order_item_discount`) depends directly on the volume of sales revenue and the discount rate (`order_item_discount_rate`), which makes this feature also redundant.

3. $\text{Order_item_total} = \text{sales} - \text{order_item_discount}$. Here, the total order amount (`order_item_total`) is expressed through the sales revenue and the discount on the product, which has reduced data duplication.

4. $\text{Order_profit_per_order} = \text{order_item_total} * \text{order_item_profit_ratio}$. The profit per order (`order_profit_per_order`) is linked to the total cost of the item and the profit ratio per item (`order_item_profit_ratio`), which makes it possible to calculate it using other attributes.

Missing values in the `order_zipcode` column were replaced with `customer_zipcode`.

The data in the `days_for_shipping_real` column was converted to a normal floating-point number.

In the original dataset, the features “delivery status”, “customer segment”, and “delivery mode” were categorical, which made it difficult to use numerical machine learning models. Using the Label Encoder⁴ method, these features were converted to a numeric format:

- the categories “shipped”, “in transit”, and “delivered” of the `delivery_status` feature were mapped to values 0, 1, and 2, respectively;
- the categories of the `customer_segment` feature were also assigned unique numeric values.

The described approach provides preserving the differences between categories, and at the same time using the categories in the machine learning process.

When selecting the optimal machine learning model for predicting delivery time, a number of machine learning algorithms were implemented. Decision tree [3] is one of the most common machine learning algorithms used for tasks related to decision making based on a set of features. Taking into account the values of some features, the algorithm divides the data into smaller subgroups and then structures them in the form of a decision tree.

The algorithm works as follows.

1. Before the first step, the root node of the decision tree contains the source dataset.
2. At each step of the algorithm, a feature is selected that provides the most efficient division of data into subsets and one or more of its threshold values. The data is divided into groups according to the selected feature values. The process is repeated until leaf nodes that contain the final solutions and are not subject to further decomposition are reached.

Thus, each node of the tree is a decision point at which the data is divided on the basis of the value of some feature. The branches of the tree correspond to the possible results of such a division.

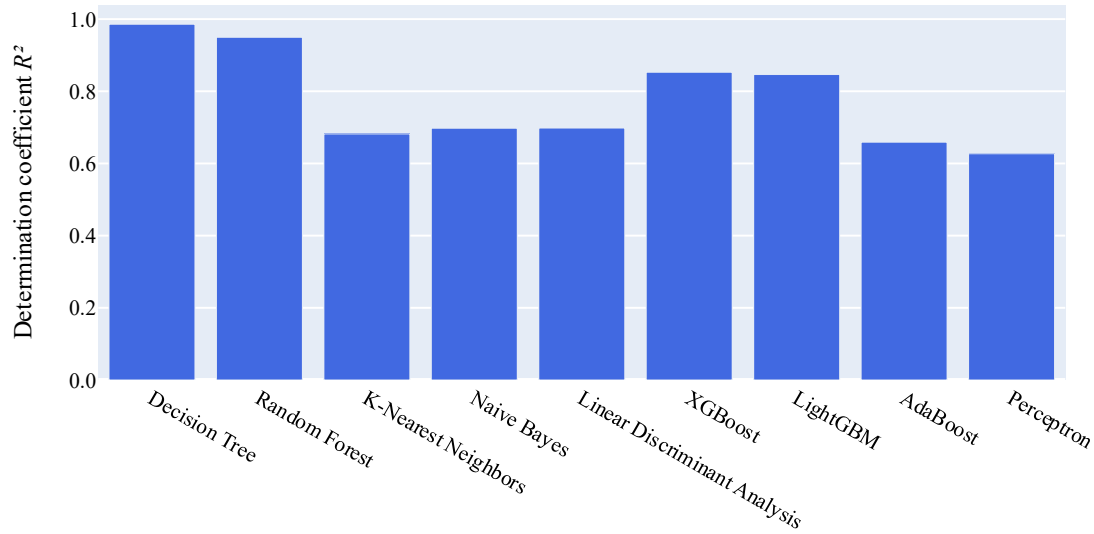
The key point of the algorithm is the determination of the data partitioning feature at each step.

Preliminary experiments showed that the Gini criterion provided the best accuracy of data partitioning within the framework of the task, therefore it was used in the presented work.

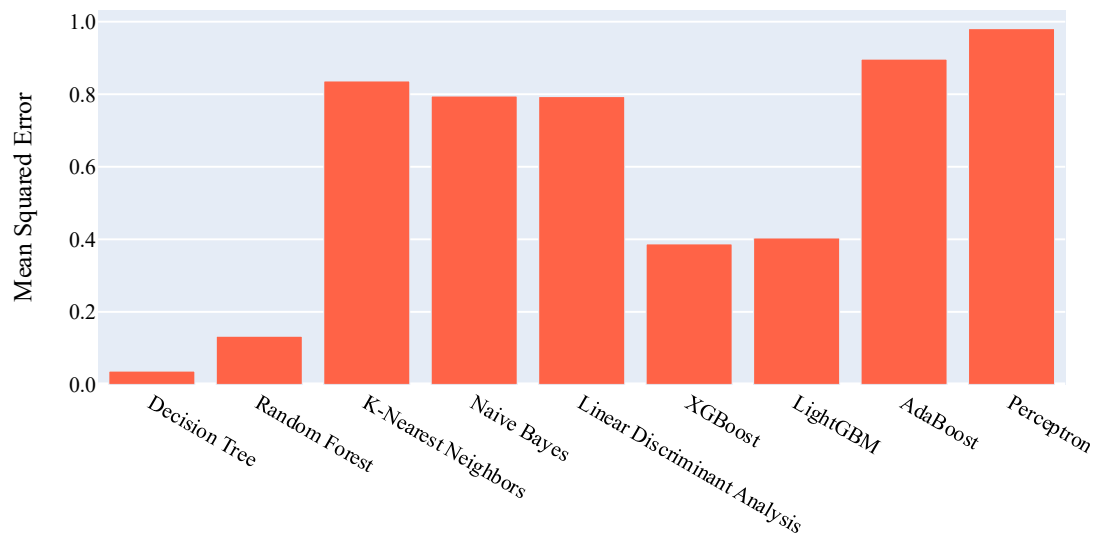
To determine the optimal algorithm, Random Forest [4], K-Nearest Neighbors [5], Naive Bayes [6], Linear Discriminant Analysis [7], XGBoost [8], CatBoost [9], LightGBM [10], AdaBoost [11] and Perceptron [12] were tested on the prepared data set. These algorithms were selected due to their widespread use and proven efficiency in solving forecasting problems. Each model was tested on the same dataset after the same preprocessing procedure. To evaluate the efficiency of the models, the following metrics were used: R^2 (determination coefficient), mean square error (MSE), mean absolute error (MAE), as well as the time spent on training and forecasting. The listed metrics provide for an objective comparison of the accuracy and resource intensity of the algorithms, and the selection of the optimal model for forecasting delivery time.

⁴ Label Encoder: the method transforms data representing categorical values into integers 0, 1, 2, etc., corresponding to each category.

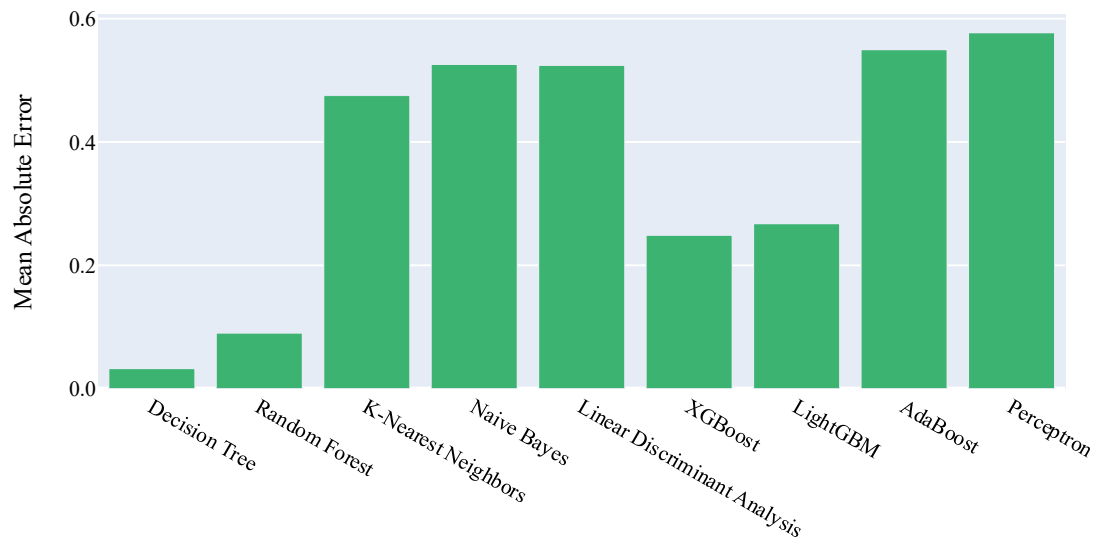
Research Results. Figure 2 shows the quality assessment of the models described above using the metrics listed. Decision Tree and Random Forest demonstrated the highest accuracy. However, the simplicity and interpretability of Decision Tree, as well as its lower tendency to overfitting [13] compared to more complex models, should be taken into account. In this regard, the Decision Tree algorithm was used to predict the delivery time of goods.



a)



b)



c)

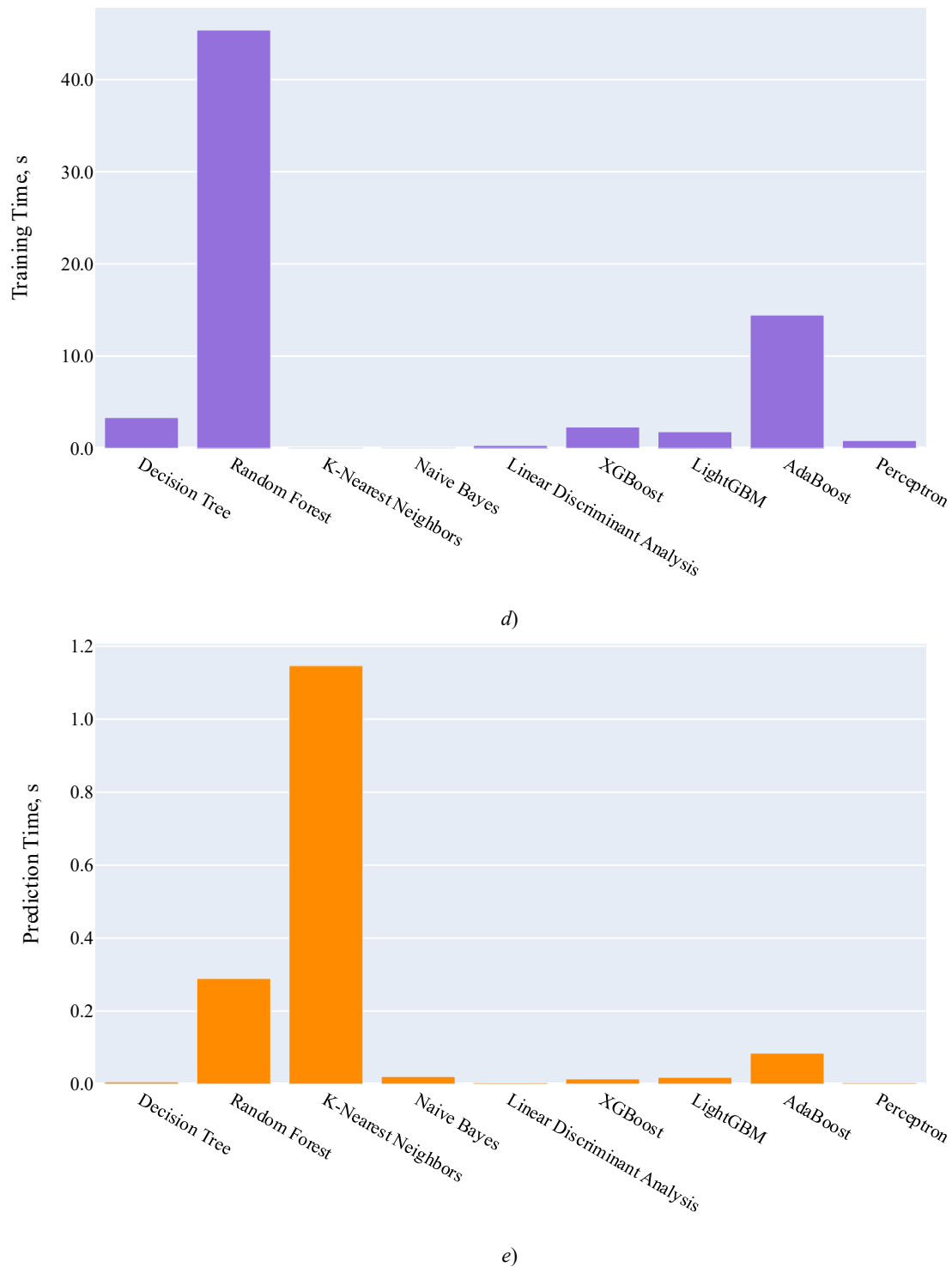


Fig. 2. Model quality assessment:

a — model quality assessment using R^2 metric; *b* — model quality assessment using MSE metric; *c* — model quality assessment using MAE metric;

d — training time, s; *e* — prediction time, s

Thus, testing the Decision tree model gave the following results:

- determination coefficient — 0.986;
- mean square error (MSE) — 0.0367;
- mean absolute error (MAE) — 0.0324;
- training time — 3.3087 s;
- prediction time — 0.0051 s.

High R^2 value and low MSE and MAE values indicate high accuracy and efficiency of the model.

Consider the agreement between the actual values and the values predicted by the model (Fig. 3).

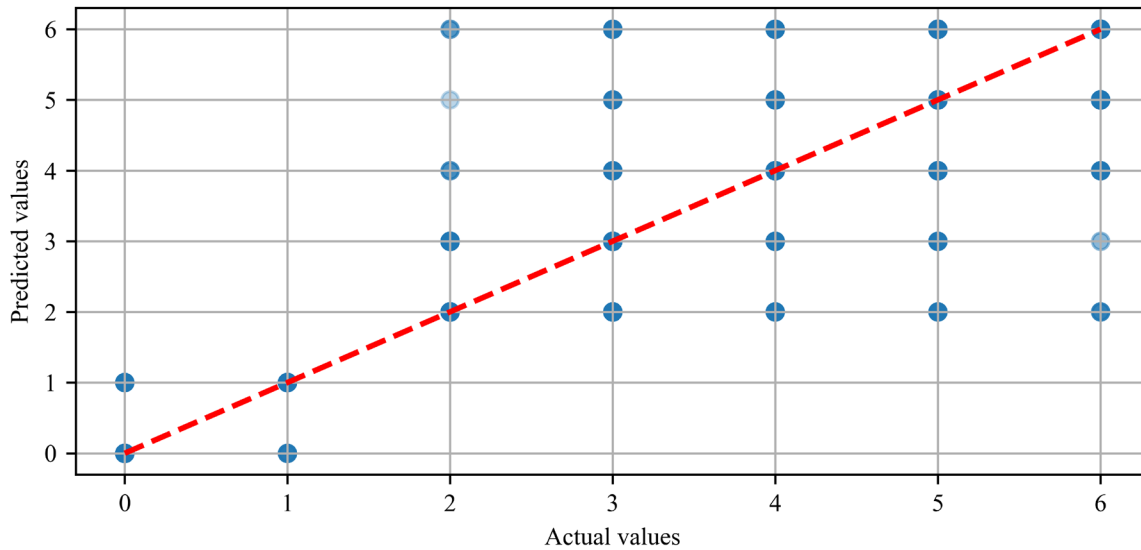


Fig. 3. Actual vs. predicted values chart

As you can see, the blue dots (predicted values) are located close to the red dashed line, which is the line of perfect agreement between the actual and predicted values. This indicates high accuracy of the prediction of values. This indicates high accuracy of the prediction of values.

The dense arrangement of dots along the dashed line refers to the absence of significant biases towards overestimation or underestimation of indicators. This shows a balance between the predicted and actual values.

The clustering of points along the diagonal suggests that deviations from the actual values are minimal. Thus, we can reasonably speak of extremely minor errors and high predictive ability of the model.

Discussion and Conclusion. The experimental results have shown that the decision tree-based model is capable of predicting the delivery time of goods with high accuracy. This is confirmed by high R^2 values and low MSE and MAE values. It was also established that the model was trained and made a forecast quite quickly, i.e., it was well suited for use under real conditions. In this sense, it is especially valuable that the operations have been implemented with minimal computational resources.

Let us note the basic conditions for achieving good results:

- high-quality data preprocessing;
- elimination of multicollinearity;
- application of optimal data partitioning criterion.

The scientific significance of the presented research should be considered from both theoretical and applied perspectives. In the first case, we are talking about the possibility of successful application of simple and effective machine learning models in logistics. It is shown that these models can provide the required accuracy of forecasts, significantly reduce operating costs, and optimize enterprise resources. The authors of the presented paper select from nine algorithms, each of which may be optimal for solving one or another logistical (or, more broadly, economic) problem of the enterprise. We will list only some of the logistical problems that can be attempted to be solved using the approach described in this paper:

- selection of delivery scheme taking into account requirements for product freshness;
- selection of delivery scheme taking into account the costs of fuels and lubricants;
- optimization of purchases taking into account warehousing costs;
- formation of salary policy in the logistics department;
- forecasting the liquidity of goods.

This leads to the second — applied — potential of the scientific research described in the article. The expected final practical effect is better controllability and profitability of logistics. This is especially important for small and medium businesses. Large corporations employ their own staff of analysts and programmers, create their own databases or purchase exclusive information to build effective logistics. Small companies can use the data sets and known algorithms they have accumulated in the course of their work for the same purposes. However, we note that the proposed approach can also be used as a basic model for more complex supply chain management systems.

Further research could focus on integrating additional data sources, such as current traffic conditions, weather conditions, and macroeconomic indicators. Using this information in real time could improve the forecast accuracy and adaptability of models.

References

1. Korchagina E, Korchagina D, Romakina O, Arsenieva A. Application of Artificial Intelligence Technologies in Logistics and Global Supply Chain Management: Analysis of Foreign Scientific Publications. *RISK: Resources, Information, Supply, Competition*. 2024;(1):29–33.
2. Midi H, Bagheri A. Robust Estimations as a Remedy for Multicollinearity Caused by Multiple High Leverage Points. *Journal of Mathematics and Statistics*. 2009;5(4):311–318. <https://doi.org/10.3844/JMSSP.2009.311.321>
3. Patel HH, Prajapati P. Study and Analysis of Decision Tree Based Classification Algorithms. *International Journal of Computer Sciences and Engineering*. 2018;6(10):74–78. <https://doi.org/10.26438/ijcse/v6i10.7478>
4. Louppe G. *Understanding Random Forests: From Theory to Practice*. PhD diss. Liège: University of Liège; 2014. 213 p. <https://doi.org/doi:10.13140/2.1.1570.5928>
5. Zhongheng Zhang. Introduction to Machine Learning: k-nearest neighbors. *Annals of Translational Medicine*. 2016;4(11):218–218. <https://doi.org/10.21037/atm.2016.03.37>
6. Taheri S, Mammadov M. Learning the Naive Bayes Classifier with Optimization Models. *International Journal of Applied Mathematics and Computer Science*. 2013;23(4):727–739. <https://doi.org/10.2478/amcs-2013-0059>
7. Jianhang Zhou, Qi Zhang, Shaoning Zeng, Bob Zhang, Leyuan Fang. Latent Linear Discriminant Analysis for Feature Extraction via Isometric Structural Learning. *Pattern Recognition*. 2023;149:110218. <https://doi.org/10.1016/j.patcog.2023.110218>
8. Tianqi Chen, Carlos Guestrin. XGBoost: A Scalable Tree Boosting System. In: *Proc. 22nd ACM SIGKDD International Conference on Knowledge Discovery and Data Mining*. San Francisco: ACM; 2016. P. 785–794. <https://doi.org/10.1145/2939672.2939785>
9. Prokhorenkova L, Gusev G, Vorobev A, Dorogush A, Gulin A. CatBoost: unbiased boosting with categorical features. *Advances in Neural Information Processing Systems*. 2018;31:6638–6648. <https://doi.org/10.48550/arXiv.1706.09516>
10. Guolin Ke, Qi Meng, Thomas Finley, Taifeng Wang, Wei Chen, Weidong Ma, et al. LightGBM: A Highly Efficient Gradient Boosting Decision Tree. In: *Proc. 31st International Conference on Neural Information Processing Systems (NeurIPS)*. Long Beach, CA: Curran Associates Inc.; 2017. P. 3149–3157. URL: https://www.researchgate.net/publication/378480234_LightGBM_A_Highly_Efficient_Gradient_Boosting_Decision_Tree (accessed: 22.02.2025).
11. Jianghua Duan, Hongfei Ye, Hongyu Zhao, Zhiqiang Li. Deep Cascade AdaBoost with Unsupervised Clustering in Autonomous Vehicles. *Electronics*. 2023;12(1):44. <https://doi.org/10.3390/electronics12010044>
12. Ke-Lin Du, Chi-Sing Leung, Wai Ho Mow, MNS Swamy. Perceptron: Learning, Generalization, Model Selection, Fault Tolerance, and Role in the Deep Learning Era. *Mathematics*. 2022;10(24):4730. <https://doi.org/10.3390/math10244730>
13. Zadvornaya IA, Romakina OM. Application of the Algorithm “Decision Trees” to Analysis of Personal Information of Potential Bank Clients. *Cloud of Science*. 2019;6(3):415–424.

About the Authors:

Vladislav K. Rezvanov, graduate student of the Applied Computer Science Faculty, ITMO University (49, Kronverksky Ave., St. Petersburg, 197101, Russian Federation), [ORCID](#), [ResearchGate](#), waweda299@gmail.com

Oksana M. Romakina, Cand.Sci. (Phys.-Math.), Associate Professor of the Applied Computer Science Faculty, ITMO University (49, Kronverksky Ave., St. Petersburg, 197101, Russian Federation), [SPIN-code](#), [ORCID](#), [ScopusID](#), [ResearcherID](#), [ResearchGate](#), omromakina@itmo.ru

Ekaterina V. Zaitseva, Cand.Sci. (Eng.), Associate Professor of the Computer Science and Computer Technology Department, Empress Catherine II Saint Petersburg Mining University (2, 21st Line, St. Petersburg, 199106, Russian Federation), [SPIN-code](#), [ORCID](#), [ScopusID](#), [ResearcherID](#), [ResearchGate](#), Zaitseva_EV@pers.spmi.ru

Claimed Contributorship:

VK Rezvanov: investigation, validation, writing – original draft preparation.

OM Romakina: conceptualization, supervision.

EV Zaitseva: validation, writing – review & editing.

Conflict of Interest Statement: the authors declare no conflict of interest.

All authors have read and approved the final manuscript.

Об авторах:

Владислав Константинович Резванов, магистрант, факультет «Прикладная информатика» Национального исследовательского университета «ИТМО» (197101, Российская Федерация, г. Санкт-Петербург, Кронверкский пр., 49а), [ORCID](#), [ResearchGate](#), waweda299@gmail.com

Оксана Михайловна Ромакина, кандидат физико-математических наук, доцент, факультет «Прикладная информатика» национального исследовательского университета «ИТМО» (197101, Российская Федерация, г. Санкт-Петербург, Кронверкский пр., 49 а), [SPIN-код](#), [ORCID](#), [ScopusID](#), [ResearcherID](#), [ResearchGate](#), omromakina@itmo.ru

Екатерина Викторовна Зайцева, кандидат технических наук, доцент, кафедра «Информатика и компьютерные технологии» Санкт-Петербургского горного университета императрицы Екатерины II (199106, Российская Федерация, Санкт-Петербург, 21-я линия Васильевского острова, 2), [SPIN-код](#), [ORCID](#), [ScopusID](#), [ResearcherID](#), [ResearchGate](#), Zaytseva_EV@pers.spmi.ru

Заявленный вклад авторов:

В.К. Резванов: проведение исследования, анализ результатов, подготовка черновика научной статьи.

О.М. Ромакина: разработка концепции, научное руководство.

Е.В. Зайцева: валидация результатов, оформление научной статьи.

Конфликт интересов: авторы заявляют об отсутствии конфликта интересов.

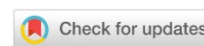
Все авторы прочитали и одобрили окончательный вариант рукописи.

Received / Поступила в редакцию 12.03.2025

Reviewed / Поступила после рецензирования 07.04.2025

Accepted / Принята к публикации 13.04.2025

INFORMATION TECHNOLOGY, COMPUTER SCIENCE AND MANAGEMENT ИНФОРМАТИКА, ВЫЧИСЛИТЕЛЬНАЯ ТЕХНИКА И УПРАВЛЕНИЕ



UDC 538.915;538.958

Original Theoretical Research

<https://doi.org/10.23947/2687-1653-2025-25-2-129-141>

Ab initio Calculations of the Electronic-Energy Structure and Optical Properties of Lanthanum and Neodymium Pyrozoirconates

Anatoliy A. Lavrentyev¹ , Boris V. Gabrelian¹ , Vu Van Tuan² ,Ksenia F. Kalmykova¹ ¹ Don State Technical University, Rostov-on-Don, Russian Federation² Institute for Computational Science and Artificial Intelligence, Van Lang University,
Ho Chi Minh City, Vietnam✉ alavrentyev@donstu.ru

EDN: MJOLRM

Abstract

Introduction. Compounds with lanthanum and neodymium ($\text{La}_2\text{Zr}_2\text{O}_7$ and $\text{Nd}_2\text{Zr}_2\text{O}_7$) have low thermal conductivity, high permittivity and melting point, stability and resistance to defects. They can be used for thermal insulation of metal components in turbines and air engines. Also, these compounds are widely studied from the point of view of the development of materials science, particularly, for the improvement of laser technology and optics. However, the physical properties of $\text{La}_2\text{Zr}_2\text{O}_7$ and $\text{Nd}_2\text{Zr}_2\text{O}_7$ have not been sufficiently studied experimentally. This gap is intended to be filled by the presented study. The research objective includes model calculations of the electronic structure and optical properties of $\text{La}_2\text{Zr}_2\text{O}_7$ and $\text{Nd}_2\text{Zr}_2\text{O}_7$.

Materials and Methods. Based on model calculations within the framework of the density functional theory, the electron-energy structure of pyrozoirconates $\text{La}_2\text{Zr}_2\text{O}_7$ and $\text{Nd}_2\text{Zr}_2\text{O}_7$, containing Zr and having the crystal structure of pyrochlore was investigated. The parameters of the crystal lattice of $\text{La}_2\text{Zr}_2\text{O}_7$ taken from the literature were used in the calculations. Due to the lack of experimental data, the parameters for $\text{Nd}_2\text{Zr}_2\text{O}_7$ were calculated by minimizing the forces acting on the atoms of the compound. A combined exchange-correlation potential was used, taking into account the strong interactions of *d*- and *f*-electrons of La and Nd atoms with a correction in the form of a modified Becke-Johnson meta-potential. *Wien2K* software package was used for the calculations.

Results. The densities of electron states of all atoms of the studied compounds were obtained. The calculated densities of valence electron states of the compounds were compared to the experimental X-ray photoelectron spectra. At zero energy, the optical characteristics of $\text{La}_2\text{Zr}_2\text{O}_7$ and $\text{Nd}_2\text{Zr}_2\text{O}_7$ were calculated. Firstly, it was the permittivity: for $\text{La}_2\text{Zr}_2\text{O}_7$ — 8.4334, for $\text{Nd}_2\text{Zr}_2\text{O}_7$ — 8.501; secondly, refraction: for $\text{La}_2\text{Zr}_2\text{O}_7$ — 2.904, for $\text{Nd}_2\text{Zr}_2\text{O}_7$ — 2.916; thirdly, reflection: for $\text{La}_2\text{Zr}_2\text{O}_7$ — 23.786%, for $\text{Nd}_2\text{Zr}_2\text{O}_7$ — 23.935%. High optical absorption coefficient ($>10^5 \text{ cm}^{-1}$) was recorded in the ranges: from 5 to 14 eV, from 14 to 28 eV, and from 28 to 40 eV. Peak extinction values were in the ranges from 5 to 13 eV, from 14 to 28 eV, and from 28 to 40 eV. $\text{La}_2\text{Zr}_2\text{O}_7$ and $\text{Nd}_2\text{Zr}_2\text{O}_7$ crystals could absorb photons in a wide energy range (4–10 eV).

Discussion and Conclusion. The study supplemented the concept of the properties of $\text{La}_2\text{Zr}_2\text{O}_7$ and $\text{Nd}_2\text{Zr}_2\text{O}_7$ with new experimental data. The densities of electron states and optical spectra of $\text{La}_2\text{Zr}_2\text{O}_7$ and $\text{Nd}_2\text{Zr}_2\text{O}_7$ compounds were calculated. This made it possible to explain features of the experimental X-ray photoelectron spectra of the compounds. In the approximation of the modified Becke-Johnson potential, the values of the widths of the forbidden bands of the compounds corresponding to the experimental ones were obtained. The research is fundamental and can open up prospects for creating more efficient, reliable and functional materials, laser and optical devices.

Keywords: electron energy structure, properties of the pyrochlore group, modified Becke-Johnson meta-potential, lanthanum and neodymium pyrozoirconates, optical properties of $\text{La}_2\text{Zr}_2\text{O}_7$ and $\text{Nd}_2\text{Zr}_2\text{O}_7$, X-ray photoelectron spectra

Acknowledgments. The authors would like to thank the reviewers, whose critical evaluation of the submitted materials and suggestions for improvement contributed significantly to the quality of this article.

For Citation. Lavrentyev AA, Gabrelian BV, Vu Van Tuan, Kalmykova KF. *Ab initio* Calculations of the Electronic-Energy Structure and Optical Properties of Lanthanum and Neodymium Pyrozoirconates. *Advanced Engineering Research (Rostov-on-Don)*. 2025;25(2):129–141. <https://doi.org/10.23947/2687-1653-2025-25-2-129-141>

Оригинальное теоретическое исследование

***Ab initio* расчеты электронно-энергетической структуры и оптических свойств пироцирконатов лантана и неодима**

А.А. Лаврентьев¹  , Б.В. Габрельян¹ , Ву Ван Туан² , К.Ф. Калмыкова¹ 

¹ Донской государственный технический университет, г. Ростов-на-Дону, Российская Федерация

² Институт вычислительной науки и искусственного интеллекта, Университет Ван Ланг, г. Хошимин, Вьетнам

 alavrentyev@donstu.ru

Аннотация

Введение. Соединения с лантаном и неодимом ($\text{La}_2\text{Zr}_2\text{O}_7$ и $\text{Nd}_2\text{Zr}_2\text{O}_7$) обладают низкой теплопроводностью, высокой диэлектрической проницаемостью и температурой плавления, стабильностью и устойчивостью к дефектам. Их можно применять для теплоизоляции металлических компонентов в турбинах и воздушных двигателях. Также указанные соединения широко исследуются с точки зрения развития материаловедения, в частности совершенствования лазерной техники и оптики. Однако физические свойства $\text{La}_2\text{Zr}_2\text{O}_7$ и $\text{Nd}_2\text{Zr}_2\text{O}_7$ недостаточно экспериментально изучены. Этот пробел призвано восполнить представленное исследование. Цель работы — модельные расчеты электронной структуры и оптических свойств $\text{La}_2\text{Zr}_2\text{O}_7$ и $\text{Nd}_2\text{Zr}_2\text{O}_7$.

Материалы и методы. На основе модельных расчетов в рамках теории функционала плотности исследована электронно-энергетическая структура пироцирконатов $\text{La}_2\text{Zr}_2\text{O}_7$ и $\text{Nd}_2\text{Zr}_2\text{O}_7$, содержащих Zr и имеющих кристаллическую структуру пирохлора. В расчетах использовались взятые из литературы параметры кристаллической решетки $\text{La}_2\text{Zr}_2\text{O}_7$. Из-за отсутствия экспериментальных данных параметры для $\text{Nd}_2\text{Zr}_2\text{O}_7$ рассчитывались через минимизацию сил, действующих на атомы соединения. Применяется комбинированный обменно-корреляционный потенциал, учитывающий сильные взаимодействия *d*- и *f*-электронов атомов La и Nd с поправкой в форме модифицированного метапотенциала Беке-Джонсона. Для расчетов использовался пакет программ *Wien2K*.

Результаты исследования. Получены плотности электронных состояний всех атомов исследованных соединений. Сравниваются рассчитанные плотности валентных электронных состояний соединений с экспериментальными рентгеновскими фотоэлектронными спектрами. При нулевой энергии рассчитаны значения оптических характеристик $\text{La}_2\text{Zr}_2\text{O}_7$ и $\text{Nd}_2\text{Zr}_2\text{O}_7$. Во-первых, это диэлектрическая проницаемость: для $\text{La}_2\text{Zr}_2\text{O}_7$ — 8,4334, для $\text{Nd}_2\text{Zr}_2\text{O}_7$ — 8,501. Во-вторых, преломление: для $\text{La}_2\text{Zr}_2\text{O}_7$ — 2,904, для $\text{Nd}_2\text{Zr}_2\text{O}_7$ — 2,916. В-третьих, отражение: для $\text{La}_2\text{Zr}_2\text{O}_7$ — 23,786 %, для $\text{Nd}_2\text{Zr}_2\text{O}_7$ — 23,935 %. Высокий оптический коэффициент поглощения ($>10^5 \text{ см}^{-1}$) фиксируется в областях: от 5 до 14 эВ, от 14 до 28 эВ и от 28 до 40 эВ. Пиковые значения экстинкции приходятся на области от 5 до 13 эВ, от 14 до 28 эВ и от 28 до 40 эВ. Кристаллы $\text{La}_2\text{Zr}_2\text{O}_7$ и $\text{Nd}_2\text{Zr}_2\text{O}_7$ могут поглощать фотоны в широком диапазоне энергий (4–10 эВ).

Обсуждение и заключение. Исследование дополнило представления о свойствах $\text{La}_2\text{Zr}_2\text{O}_7$ и $\text{Nd}_2\text{Zr}_2\text{O}_7$ новыми экспериментальными данными. Рассчитаны плотности электронных состояний и оптические спектры соединений $\text{La}_2\text{Zr}_2\text{O}_7$ и $\text{Nd}_2\text{Zr}_2\text{O}_7$. Это позволило объяснить особенности экспериментальных рентгеновских фотоэлектронных спектров соединений. В приближении модифицированного метапотенциала Беке-Джонсона получены значения ширины запрещенных полос соединений, соответствующие экспериментальным. Исследование относится к фундаментальным и может открыть перспективы создания более эффективных, надежных и функциональных материалов, лазерных и оптических устройств.

Ключевые слова: электронная энергетическая структура, свойства группы пирохлоров, модифицированный метапотенциал Беке-Джонсона, оптические свойства $\text{La}_2\text{Zr}_2\text{O}_7$ и $\text{Nd}_2\text{Zr}_2\text{O}_7$

Благодарности. Авторы выражают благодарность рецензентам, чья критическая оценка представленных материалов и высказанные предложения по их совершенствованию способствовали значительному повышению качества статьи.

Для цитирования. Лаврентьев А.А., Габрельян Б.В., Туан Ву Ван, Калмыкова К.Ф. *Ab initio* расчеты электронно-энергетической структуры и оптических свойств пироцирконатов лантана и неодима. *Advanced Engineering Research (Rostov-on-Don)*. 2025;25(2):129–141. <https://doi.org/10.23947/2687-1653-2025-25-2-129-141>

Introduction. Lanthanum and neodymium pyrochlorates — $\text{La}_2\text{Zr}_2\text{O}_7$ and $\text{Nd}_2\text{Zr}_2\text{O}_7$ — belong to the pyrochlorates group. The general formula of these materials is $\text{A}_2\text{B}_2\text{O}_7$. A and B are metallic cations that can be trivalent (like La and Nd), tetravalent (like Zr), divalent, and pentavalent [1]. Pyrochlorates have high dielectric constant. They exhibit unique magnetic [2], chemical, mechanical and electronic [3] properties. Due to this, they can be used as:

- ceramic coatings of thermal barriers, gas sensors, metal oxide transistors;
- solid electrolytes in fuel cells [4];
- immobilization carriers of actinides in nuclear waste;
- catalysts of oxidation reactions [5];
- elements of magnetic devices.

The research described in this paper was conducted taking into account the development of new technologies in the laser technology, optics and materials science [6]. The results of the work may open the way to the creation of more efficient, reliable and functional devices [7]. The studied oxides of complex chemical composition have significant stability, high melting point, high coefficient of thermal expansion [8], low thermal conductivity, excellent ionic conductivity, and resistance to defects [9]. From the practical perspective, it is important to use pyrochlorates $\text{Ln}_2\text{Zr}_2\text{O}_7$ as coatings to provide thermal insulation of metal components from hot gases [10] in turbines of marine electric generators and in aircraft engines [11].

Numerous papers (e.g., [12]) investigated physical properties of pyrochlorates, including mechanical and thermal ones. However, some of their properties are very difficult to evaluate and explain due to their strong dependence on the stoichiometry of the samples [10]. Calculations of the electron-energy structure of various pyrochlorates were performed within the framework of the density functional theory (e.g., [13]). These calculations used exchange-correlation potentials obtained in the local density approximation, the generalized gradient approximation, and pseudopotentials.

In [13], the importance of the Hubbard correction in calculating the unoccupied d - and f -states of heavy atoms is noted [14]. Nevertheless, even taking into account the correction, the width of the forbidden band obtained in the calculations often turns out to be smaller than the experimentally observed one [15]. Additional corrections must be taken into account, and this is exactly what the authors of the presented work have done.

Thus, additional experimental and theoretical studies on the electron-energy structure and physical properties of pyrochlorates are quite relevant and have practical significance.

Let us consider the crystal structure of pyrochlorate $\text{La}_2\text{Zr}_2\text{O}_7$ (space group $Fd-3m$, $Z = 8$) with the general formula $\text{Ln}_2^{3+}\text{Zr}_2^{4+}\text{O}_{16}\text{O}_2$ (O1 and O2 are oxygen atoms located in different crystallographic positions). It can be described as a structure of defective fluorite, in which the cations form a face-centered cubic (fcc) lattice, and 1/8 of the oxygen atom positions are unoccupied to provide charge neutrality (Fig. 1).

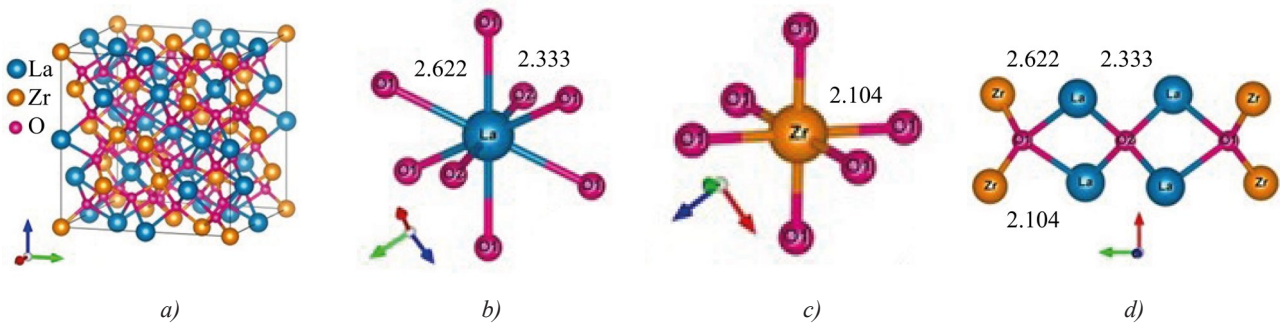


Fig. 1. Crystal structure and immediate environment of atoms in pyrochlorate $\text{La}_2\text{Zr}_2\text{O}_7$:

- a — unit cell in compound $\text{La}_2\text{Zr}_2\text{O}_7$; b — immediate environment of La atom;
 c — immediate environment of Zr atom; d — immediate environment of oxygen atoms O1 and O2.
 Distances between atoms are given in Å

Atoms in the crystal structure of $\text{La}_2\text{Zr}_2\text{O}_7$ are distributed over four unique crystallographic positions:

- La cations are in Wyckoff positions $16d$;
- Zr cations are in positions $16c$;
- oxygen O1 is in position $48f$;
- oxygen O2 is in position $8b$.

The positions of $8a$ nodes ($1/8, 1/8, 1/8$) are not occupied at all. Oxygen ions O2 in $8b$ nodes ($3/8, 3/8, 3/8$) are stable and tetrahedrally coordinated by the rare earth element cations La.

Oxygen ions O1 in positions $48f$ ($x, 1/8, 1/8$) are shifted towards the neighboring empty nodes $8a$, and they are surrounded by two La cations and two Zr cations (Fig. 1) [16]. The immediate environment of La cations consists of six oxygen atoms O1 (positions $48f$) and two oxygen atoms O2 (positions $8b$). La-O2 interatomic distance is shorter than La-O1 distance. Zr cations (Fig. 1) are surrounded by six O1 atoms (positions $48f$), located at equivalent distances in trigonal antiprisms with $3m$ (D_{3d}) point symmetry.

The crystal structures of $\text{Nd}_2\text{Zr}_2\text{O}_7$ and $\text{La}_2\text{Zr}_2\text{O}_7$ compounds coincide. Table 1 shows the crystal lattice parameters of the studied pyrochlores $\text{Ln}_2\text{Zr}_2\text{O}_7$ ($\text{Ln} = \text{La}, \text{Nd}$) with the space group $Fd-3m$, for which $a = b = c$, $\alpha = \beta = \gamma = 90^\circ$. For $\text{La}_2\text{Zr}_2\text{O}_7$, parameter a and the coordinates of oxygen O1 are taken from [15], and for $\text{Nd}_2\text{Zr}_2\text{O}_7$, they are calculated. The total energy of the crystal with different values of a was calculated, and the optimal value corresponding to the minimum of the total energy was determined. Then, the oxygen atoms were displaced within the unit cell and the position, for which the forces acting on the atoms became minimal, was determined.

Table 1

Crystal Structure Parameters of the Studied Compounds

Compound, lattice parameter	Wyckoff symbols	x/a	y/b	z/c
$\text{La}_2\text{Zr}_2\text{O}_7$ $a = 10.793 \text{ \AA}$ [15]				
La	$16d$	0.50000	0.50000	0.50000
Zr	$16c$	0.00000	0.00000	0.00000
O1	$48f$	0.33002	0.12500	0.12500
O2	$8b$	0.37500	0.37500	0.37500
$\text{Nd}_2\text{Zr}_2\text{O}_7$ $a = 10.6565 \text{ \AA}$				
Nd	$16d$	0.50000	0.50000	0.50000
Zr	$16c$	0.00000	0.00000	0.00000
O1	$48f$	0.33520	0.12500	0.12500
O2	$8b$	0.37500	0.37500	0.37500

Thus, some physical properties of pyrochlores, as well as the structure of compounds $\text{Nd}_2\text{Zr}_2\text{O}_7$ and $\text{La}_2\text{Zr}_2\text{O}_7$, have been considered in scientific literature in sufficient detail. However, physical properties of $\text{La}_2\text{Zr}_2\text{O}_7$ and $\text{Nd}_2\text{Zr}_2\text{O}_7$ have not been sufficiently studied experimentally. The presented research is intended to fill this gap. The objective of the work is to perform model calculations of the electronic structure and optical properties of $\text{La}_2\text{Zr}_2\text{O}_7$ and $\text{Nd}_2\text{Zr}_2\text{O}_7$.

Materials and Methods. *Ab initio* calculations of the electron-energy structure (EES) of $\text{La}_2\text{Zr}_2\text{O}_7$ and $\text{Nd}_2\text{Zr}_2\text{O}_7$ were performed within the framework of the density functional theory. The method of augmented plane waves with the addition of local orbitals *APW+lo* was used. For the implementation, *WIEN2k* [17] software package was applied, which used a full potential that did not have a predetermined form, such as *muffin-tin* potential.

When constructing the attached plane wave, we used the expansion by l inside the atomic sphere up to $l_{\max} = 10$. The following radii of the atomic spheres were used in the present calculations: $R_{(\text{La})} = 2.24 \text{ a.u.}$, $R_{(\text{Nd})} = 2.26 \text{ a.u.}$, $R_{(\text{Zr})} = 1.96 \text{ a.u.}$, $R_{(\text{O})} = 1.78 \text{ a.u.}$ ($1 \text{ a.u.} = 0.529117 \text{ \AA}$). The series of the expansion in plane waves was interrupted at the values of the wave vector determined by the relation $R_{\min}^{MT} k_{\max} = 7$, where R_{\min} — radius of the minimal atomic sphere. The charge density decomposed into a Fourier series up to value $G_{\max} = 12 \text{ (a.u.)}^{-1}$. The densities of electron states were obtained through integrating over 1,000 \vec{k} points in the irreducible Brillouin zone (BZ) using the tetrahedron method [18]. The self-consistency procedure was carried out until the change in the integral charge $q = \int |\rho_n - \rho_{n-1}| dr$ became less than $q \leq 0.0001$. Here, $\rho_{n-1}(r)$ and $\rho_n(r)$ are the electron densities obtained at iterations $n-1$ and n , respectively.

To calculate the exchange-correlation potential, the following were used:

- generalized gradient approximation (GGA) in the parameterization proposed in [19];
- modified Becke-Johnson potential, *mBJ* [20].

In addition to the above exchange-correlation potentials, the EES calculations took into account the strong Coulomb interaction of f -electrons at one node Nd [21] in *PBE+U* approximation [22] with $U = 5 \text{ eV}$. Thus, in the final version, the exchange-correlation potential models were used *PBE+U* and *mBJ+U* [23].

$\text{Nd}_2\text{Zr}_2\text{O}_7$ has an incomplete $4f$ -shell with four f -electrons, therefore, a spin-polarized EES calculation was performed. For La, Nd and Zr atoms, spin-orbit coupling (SOC) was taken into account. It resulted in splitting:

- $5p$ -states of La and Nd into $5p_{1/2}$ and $5p_{3/2}$ states;
- $4p^6$ -states of Zr into $4p_{1/2}$ and $4p_{3/2}$ states.

Research Results. The paper calculates the total and partial densities of electron states (DOS). Atom La has no f -electrons, while atom Nd has four f -electrons. Despite this difference, in the first approximation, the calculated total densities of electron states and the experimental X-ray photoelectron spectra of the valence bands of the studied compounds demonstrate a similar structure — four regions reflecting the contributions of s -, p -, d - and f -electrons of different elements [23].

Figure 2 provides comparing the experimental X-ray photoelectron spectrum (XPS) to the calculated total and partial densities DOS for compound $\text{La}_2\text{Zr}_2\text{O}_7$, and Figures 3–5 — for $\text{Nd}_2\text{Zr}_2\text{O}_7$. Zero of the energy scale corresponds to the top of the valence band E_V . The spectra were obtained at the Frantsevich Institute for Problems of Materials Science, National Academy of Sciences of Ukraine (Kyiv). The experimental features and equipment are described in [24].

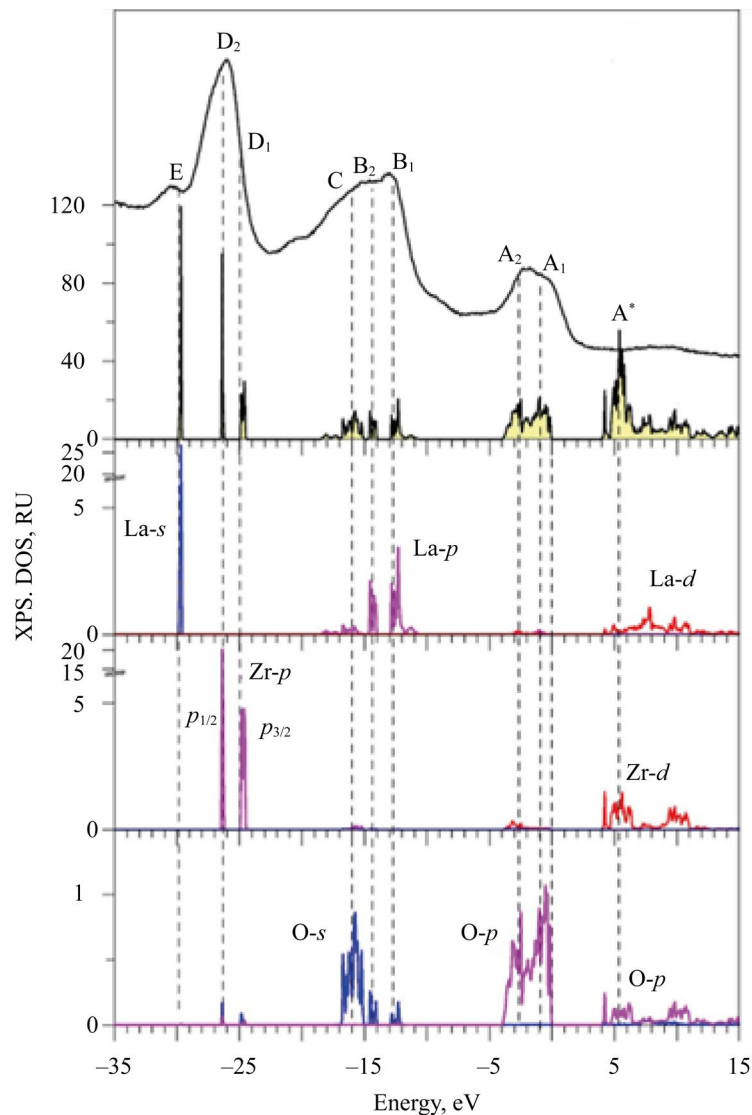


Fig. 2. Total and partial densities of states (DOS) calculated in *GGA-PBE-SOC* approximation in comparison with experimental X-ray photoelectron spectrum (XPS) of valence band of compound $\text{La}_2\text{Zr}_2\text{O}_7$

In Figure 2, in compound $\text{La}_2\text{Zr}_2\text{O}_7$, region 1 is shown— the upper part of the valence band from 0 to 4 eV. This region is formed mainly by $2p$ -states of oxygen with a small admixture of $4d$ -states of Zr, $5s$ -states of Zr, and $6s$ - and $5d$ -states of La.

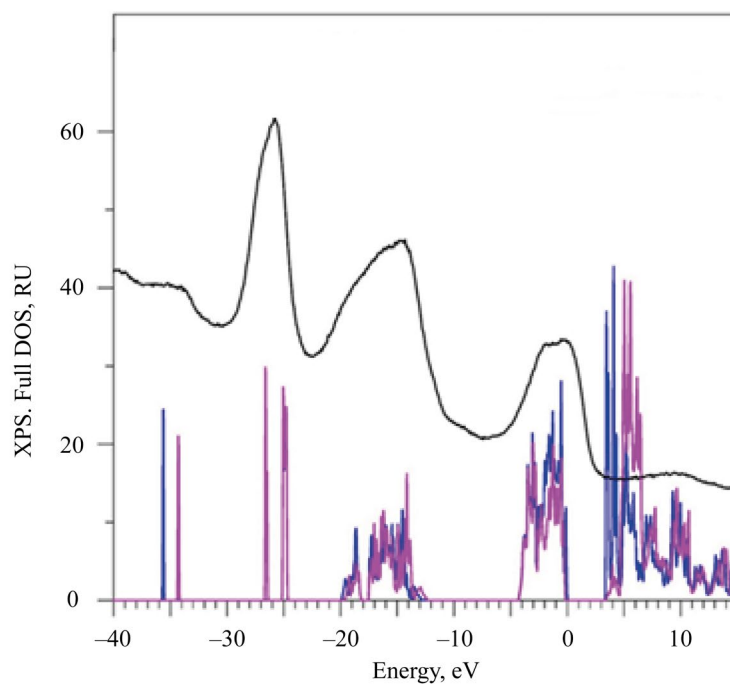


Fig. 3. Total densities of states (DOS) calculated in *GGA-PBE+U+SOC* approximation with spin up and spin down in comparison with the experimental X-ray photoelectron spectrum (XPS)

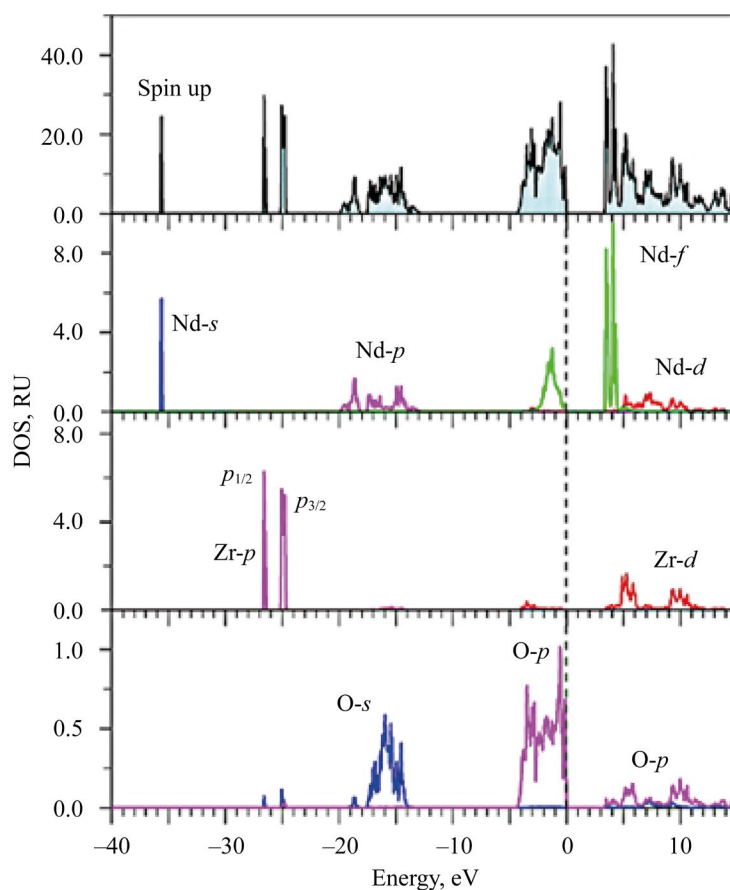


Fig. 4. Total and partial densities of states (DOS) of electrons for spin up in $\text{Nd}_2\text{Zr}_2\text{O}_7$ calculated in *GGA-PBE+U+SOC* approximation

Here, in $\text{Nd}_2\text{Zr}_2\text{O}_7$, at the top of the valence band, *f*-states of *Nd* with spin up are located. X-ray photoelectron spectrum (XPS) confirms the calculation. It is seen that the broad peak closest to the top of the valence band with elements A_1 and A_2 in $\text{La}_2\text{Zr}_2\text{O}_7$ and *A* in $\text{Nd}_2\text{Zr}_2\text{O}_7$ corresponds to $2p$ -states of oxygen atoms O1 and O2.

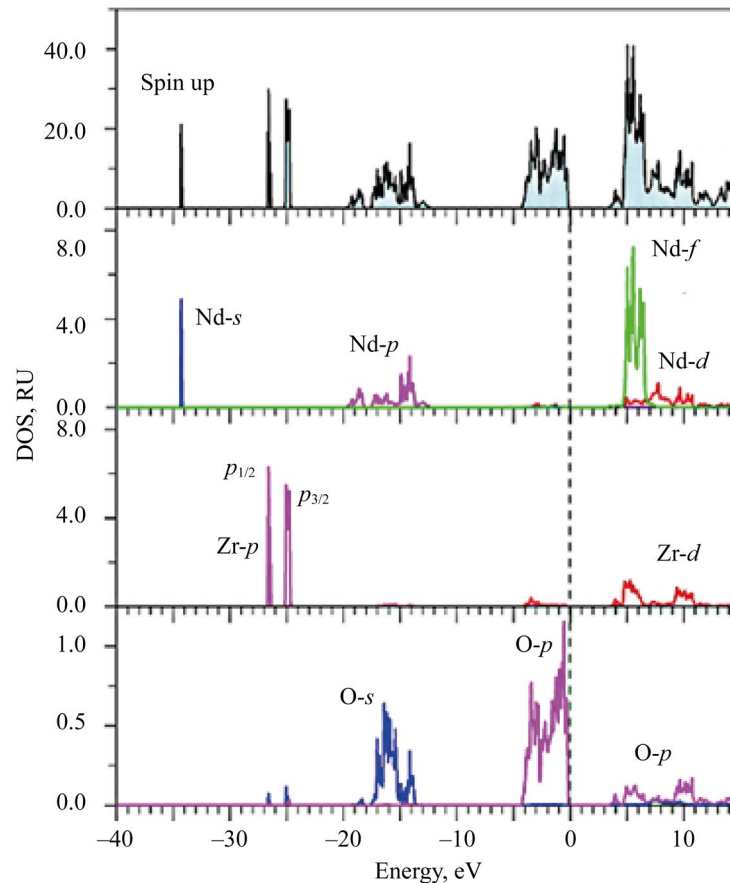


Fig. 5. Total and partial densities of states (DOS) of electrons for spin down in $\text{Nd}_2\text{Zr}_2\text{O}_7$ calculated in $\text{GGA-PBE}+U+\text{SOC}$ approximation

In regions 2, 12–18 eV from E_v in XPS, there is also a broad peak with features B_1 , B_2 and C for $\text{La}_2\text{Zr}_2\text{O}_7$ and B for $\text{Nd}_2\text{Zr}_2\text{O}_7$. The theoretical calculation shows the entire fine structure that forms the peak in XPS. $5p^6$ -states of La and Nd are split into $5p_{1/2}$ - and $5p_{3/2}$ -states. This splitting is already evident in free atoms La and Nd [25].

The spin-orbit splitting in a free atom is also present in a solid (Fig. 2) in the third panel from the bottom for the partial states of La. It is the spin-orbit splitting of the $5p$ -states of La that leads to the splitting of the $2s$ -states of oxygen. This is clearly seen in the very bottom panel of Figure 2, where the partial states of oxygen are shown. As Figure 2 shows, in the energy region ~12–18 eV, the deep-lying $5p$ -states of La interact with the $2s$ -states of oxygen. This interaction of deep-lying states in a solid is unusual and is related primarily to:

- spin-orbit splitting of the $5p$ -states of La;
- the fact that the $2s$ -wave function of oxygen is spatially and energetically strongly stretched.

The presence of structural elements B_1 , B_2 and C in the X-ray photoelectron spectrum coincides well with the calculations of the peak in the partial densities of the electron states of La and O.

The third energy region (from 24 to 27 eV) from E_v — peaks D_1 and D_2 in the X-ray photoelectron spectrum of $\text{La}_2\text{Zr}_2\text{O}_7$, C — in the spectrum of $\text{Nd}_2\text{Zr}_2\text{O}_7$. This region corresponds to the $4p$ -states of Zr, which are split in the atom into:

- $4p_{1/2}$ -state with energy 35 eV (N_2);
- $4p_{3/2}$ -states with energy 33 eV (N_3).

In the XPS curve of $\text{La}_2\text{Zr}_2\text{O}_7$, the splitting of the $4p$ -states of Zr is manifested as an asymmetry of the lines with elements D_1 and D_2 .

The deepest states of the valence bands of $\text{La}_2\text{Zr}_2\text{O}_7$ and $\text{Nd}_2\text{Zr}_2\text{O}_7$ are already semi-core states. The fourth energy region in the XPS spectrum (small peak E in Fig. 2, 3) is the $5s$ -states of La and Nd. Note that La $5s$ -state in $\text{La}_2\text{Zr}_2\text{O}_7$ is not split compared to the $5s$ -states of Nd with different spin directions (Fig. 3). The splitting of the $5s$ -states of Nd for spin up and spin down occurs under the action of the internal magnetic field. It is created by four $4f$ -electrons, which are aligned identically with spin up according to Hund's rule [26]. The broad influx of D in the XPS spectrum (Fig. 3) corresponds to the $5s$ -states of Nd.

The energy distribution of the electron states in the valence band $\text{La}_2\text{Zr}_2\text{O}_7$ correlates well with the electronegativity (EN) values of the elements [27] included in this compound (Table 2).

Table 2

Electronegativity of Elements Included in the Compounds under Study [27]

Element	O	Zr	La	Nd	Sm	Eu	Gd
EN	3.44	1.33	1.10	1.14	1.17	1.20	1.20

Thus, oxygen has the highest EN (3.44), therefore, it is quite natural that the upper part of the valence band is formed by the $2p$ -state of O. The admixture of the $4d$ - and $5s$ -states of Zr to the $2p$ -states of oxygen is insignificant, since the Zr-O1 bond is predominantly ionic in nature. The electronegativity of oxygen (EN = 3.44) is significantly higher than that of Zr (EN = 1.33). Due to this, the $4d$ - and $5s$ -electron densities of Zr are apparently attracted to the oxygen atom (O1), which is typical for the octahedral environment of the Zr atom by O1 atoms. There are also six O1 atoms in the environment of the La atom. The electronegativity of La (EN = 1.1) is significantly less than $EN^S = 3.44$. Admixture of $5d$ - and $6s$ -states of La is almost not observed. The bond between La and O1 atoms is predominantly ionic in nature, the share of covalence in this bond is very small.

The bottom of the conduction band in both compounds is formed mainly by unoccupied f - and d -states of La/Nd, as well as d -states of Zr (Fig. 2, 4, 5).

A well-known problem of calculations using the exchange-correlation potential in the *GGA*-approximation is the underestimation of the obtained value of the band gap. For some non-conducting compounds, the calculations even give a conducting state or, as in the case of $Nd_2Zr_2O_7$ in this calculation, a zero value of the band gap. Taking into account the strong interaction of f - electrons in Nd atom, e.g., within the framework of the *LDA+U* (or *GGA+U*) approximation in the EES calculations of $Nd_2Zr_2O_7$, leads to the appearance of a small forbidden band, but the value close to the experimental one can be obtained either in calculation schemes that consider multi-electron phenomena, or by using hybrid or metapotentials, such as the modified Becke-Johnson potential (*mBJ*) [28].

Table 3 gives the values of the widths of the forbidden bands E_g . They were calculated taking into account the spin-orbit splitting (SOC) of the electron states in the *La* and *Nd* atoms in the *GGA-PBE* approximations for $La_2Zr_2O_7$ (*GGA-PBE+SOC*) and *GGA+PBE+U+SOC* (with $U = 5\text{ eV}$ for $4f$ -states of *Nd*) for $Nd_2Zr_2O_7$.

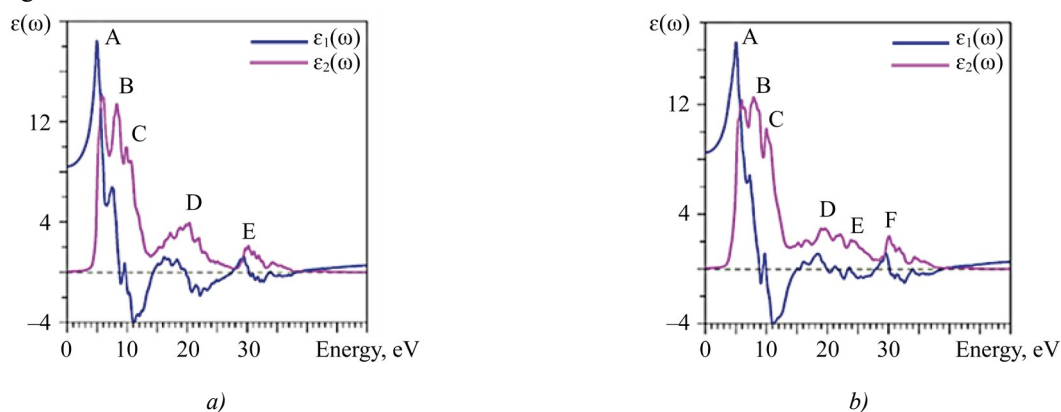
Table 3

Calculated Values of the Widths of Prohibited Bands E_g

Compound	Exchange-correlation potential	E_g , eV
$La_2Zr_2O_7$	<i>GGA-PBE+SOC</i>	3.928
$Nd_2Zr_2O_7$	<i>GGA-PBE+U+SOC</i>	3.393

The complex dielectric function $\varepsilon(\omega) = \varepsilon_1(\omega) + i\varepsilon_2(\omega)$ — the most important characteristic for calculating the optical response of materials to electromagnetic impact. The dielectric function, in principle, should include both transitions between bands and transitions within a band. Interband transitions are divided into direct and indirect. In these calculations, two factors are ignored. The first is intraband transitions, since they are important for metals, and the compounds under study are semiconductors. The second is the contribution of phonons and other quasiparticles included in indirect interband transitions. Only direct transitions between occupied and unoccupied states are considered. The cubic symmetry of the pyrochlore crystal structure determines only three non-zero (diagonal) elements of the dielectric tensor, and the values of all three of these elements are the same.

The calculated curves of the actual $\varepsilon_1(\omega)$ and imaginary $\varepsilon_2(\omega)$ parts of the permittivity for $La_2Zr_2O_7$ and $Nd_2Zr_2O_7$ are shown in Figure 6.

Fig. 6. Calculated actual (ε_1) and imaginary parts of permittivity: *a* — $La_2Zr_2O_7$; *b* — $Nd_2Zr_2O_7$

The spectral peaks of the absorbing part of the dielectric function correspond to the allowed dipole transitions between the valence band and the conduction band. To identify the fine structure elements, it is required to compare the values of the optical matrix elements. The observed structures correspond to those transitions that have large values of the optical matrix dipole transition elements. When calculating $\varepsilon_2(\omega)$, only dipole transitions within the atom, i.e., without crossover transitions, were taken into account. The interpretation of peaks *A, B, C, D, E, F* in Figure 6 for $\varepsilon_2(\omega)$ is given in Table 4.

Table 4

Interpretation of Major Peaks $\varepsilon_2(\omega)$

Compound	Peak	Energy, eV	Atom	Transition
La ₂ Zr ₂ O ₇	<i>A</i>	≈ 5	O	$p \rightarrow s(d)$
	<i>B</i>	≈ 8	O	$p \rightarrow s$
	<i>C</i>	≈ 10	O	$p \rightarrow s$
	<i>D</i>	≈ 20	O La	$p \rightarrow s$ $5p \rightarrow d$
	<i>E</i>	≈ 30	Zr	$4p \rightarrow d$
Nd ₂ Zr ₂ O ₇	<i>A</i>	5.07	O	$p \rightarrow s$
	<i>B</i>	7.8	O	$p \rightarrow s$
	<i>C</i>	10.2	O	$p \rightarrow s$
	<i>D</i>	19.09	O	$p \rightarrow s$
	<i>E</i>	24.02	Nd	$5p \rightarrow d$
	<i>F</i>	30.11	Zr	$4p \rightarrow d$

Figure 6 shows the process when electrons of *p*-symmetry in the upper part of the valence band (peak *A* in XPS) pass to states of *s*- and *d*-symmetry in the conduction band of the oxygen atom. This is how the highest peak of the curve of the imaginary part of the dielectric function $\varepsilon_2(\omega)$ is formed, covering the range 5–8 eV.

The second and third highest peaks of the curve $\varepsilon_2(\omega)$ — *B* and *C* with energies 8.28 and 9.86 eV, respectively. They are caused by transitions of oxygen valence *p*- electrons to free states of oxygen *s*-symmetry. Let us consider the wide maximum *D* on the curve $\varepsilon_2(\omega)$. The “picket-fence” of small additional peaks appeared due to transitions of oxygen *s*-symmetry electrons to free states of oxygen *p*-symmetry. In addition, in peak *D* (energy ~20 eV), there is a contribution from the transitions of the valence *5p*-electrons of *La* to the vacant *d*-states of *La* in the conduction band. Finally, small peak *E* (energy ~30 eV) corresponds to the transition of the valence *4p*-electrons of *Zr* to the unoccupied *d*-states of *Zr*. At zero energy, the calculated value $\varepsilon_2(0)$ for La₂Zr₂O₇ is 8.4334, and for Nd₂Zr₂O₇ — 8.501.

All other optical properties can be derived from $\varepsilon_1(\omega)$ and $\varepsilon_2(\omega)$. These include, for example: absorption coefficient $\alpha(\omega)$, refractive index $n(\omega)$, extinction coefficient $k(\omega)$, optical reflectivity $R(\omega)$, and energy loss spectrum $L(\omega)$ [28].

The high optical absorption coefficient $\alpha(\omega) > 10^5 \text{ cm}^{-1}$ [29] is recorded in three clearly defined regions: from 5 to 14 eV, from 14 to 28 eV and from 28 to 40 eV (Fig. 7). Apparently, such absorption may indicate the potential of using thin-film elements from La₂Zr₂O₇ and Nd₂Zr₂O₇.

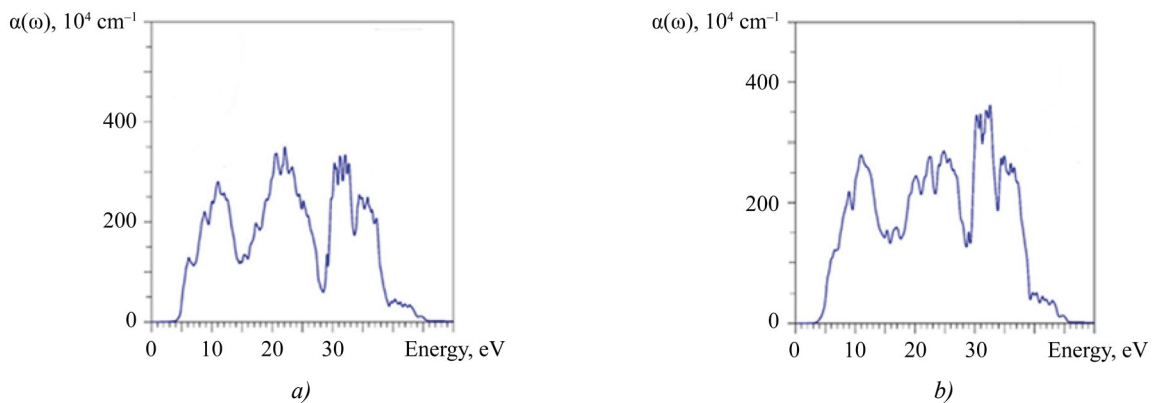


Fig. 7. Calculated absorption coefficient $\alpha(\omega)$: *a* — La₂Zr₂O₇; *b* — Nd₂Zr₂O₇

In addition, the optical absorption spectrum is characterized by a large number of peaks. They are formed due to transitions between occupied levels of the valence band and free levels of the conduction band, allowed by the selection rules ($\Delta l \neq 0$) and related to one atom (cross-transitions between neighboring atoms are unlikely). Such a picket-fence of small peaks on the curve $a(\omega)$ is undoubtedly related to the features of the above-described electron-energy structure of $\text{La}_2\text{Zr}_2\text{O}_7$ and $\text{Nd}_2\text{Zr}_2\text{O}_7$. Probably, it should be taken into account when using these compounds in optoelectronics.

The complex refractive index $N(\omega) = n(\omega) + ik(\omega)$ can be obtained from the complex dielectric function $\varepsilon(\omega)$, where the refractive index $n(\omega)$ depends mainly on the actual part $\varepsilon_1(\omega)$, and the extinction coefficient $k(\omega)$ depends on the imaginary part of the dielectric function $\varepsilon_2(\omega)$ [30].

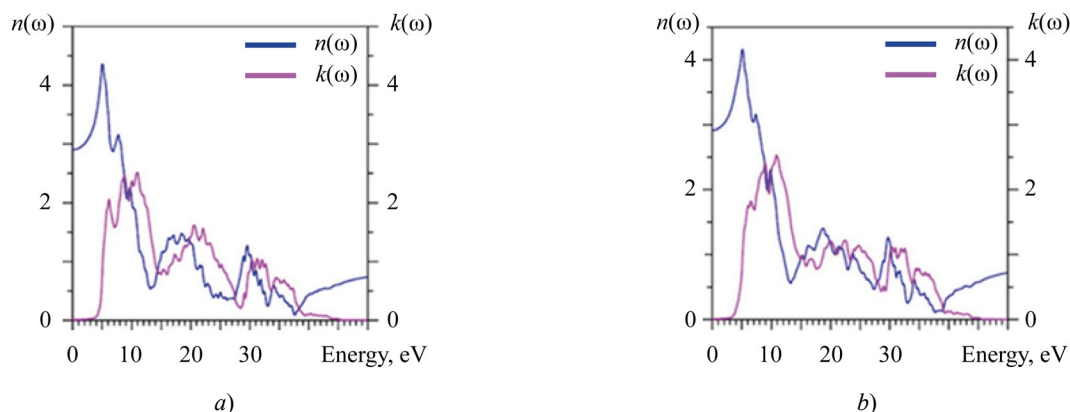


Fig. 8. Calculated refractive index $n(\omega)$ and extinction coefficient $k(\omega)$: a — $\text{La}_2\text{Zr}_2\text{O}_7$; b — $\text{Nd}_2\text{Zr}_2\text{O}_7$

At zero energy, the calculated value $n(0)$ (static refractive index) for $\text{La}_2\text{Zr}_2\text{O}_7$ is 2.904, and for $\text{Nd}_2\text{Zr}_2\text{O}_7$ — 2.916.

The extinction coefficient $k(\omega)$, responsible for the absorption of the electromagnetic wave incident on the crystal, is obtained from the imaginary part of the dielectric function $\varepsilon_2(\omega)$ (Fig. 6). Therefore, there are also three regions where value $k(\omega)$ increases from 5 to 13 eV, from 14 to 28 eV and from 28 to 40 eV. The attenuation of the intensity, represented by the extinction coefficient $k(\omega)$, starts with a decrease in the function $n(\omega)$ (Fig. 8). $\text{La}_2\text{Zr}_2\text{O}_7$ and $\text{Nd}_2\text{Zr}_2\text{O}_7$ crystals can absorb photons in a wide energy range (4–10 eV).

In general, the extinction coefficient of $\text{La}_2\text{Zr}_2\text{O}_7$ and $\text{Nd}_2\text{Zr}_2\text{O}_7$ is not isotropic and has three well-defined regions (energies are given above) where isotropic behavior of $k(\omega)$ is not observed. In these regions, the difference in $k(\omega)$ values is 25–50%.

The reflection coefficient $R(\omega)$ is shown in Figure 9. The spectrum $R(\omega)$ consists of three clearly defined energy regions. The same feature was noted for other optical characteristics. At zero energy, the calculated value $R(0)$ for $\text{La}_2\text{Zr}_2\text{O}_7$ is 23.786%, and for $\text{Nd}_2\text{Zr}_2\text{O}_7$ — 23.935%.

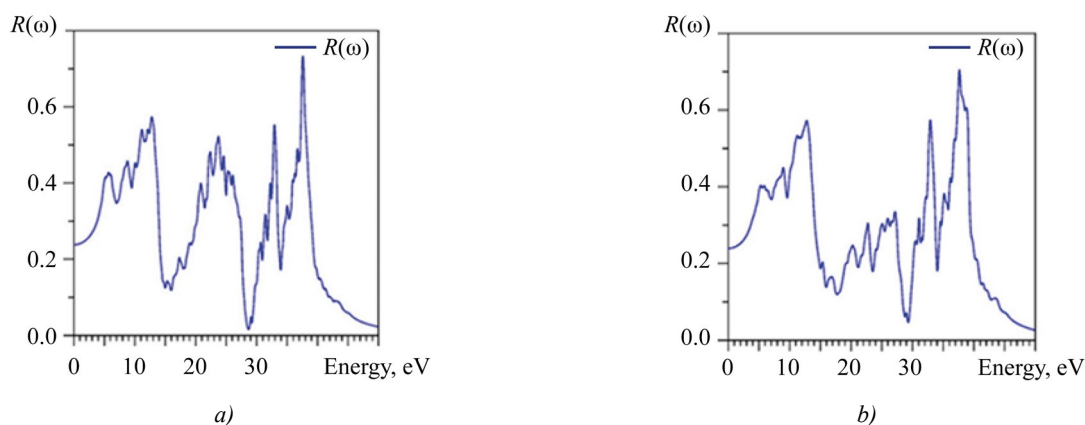


Fig. 9. Calculated reflection coefficient $R(\omega)$: a — $\text{La}_2\text{Zr}_2\text{O}_7$; b — $\text{Nd}_2\text{Zr}_2\text{O}_7$

It is evident from Figure 8 that incident photons with energy lower than the energy of the forbidden gap (~4 eV) are not absorbed. Photons with energy from 4 eV to ~40 eV are absorbed by $\text{La}_2\text{Zr}_2\text{O}_7$, $\text{Nd}_2\text{Zr}_2\text{O}_7$ crystals and excite electrons in the conduction band, while positively charged holes are formed in the valence band. However, part of the photon energy will be lost during thermalization, and it is reflected in the electron energy loss spectrum $L(\omega)$ shown in Figure 10.

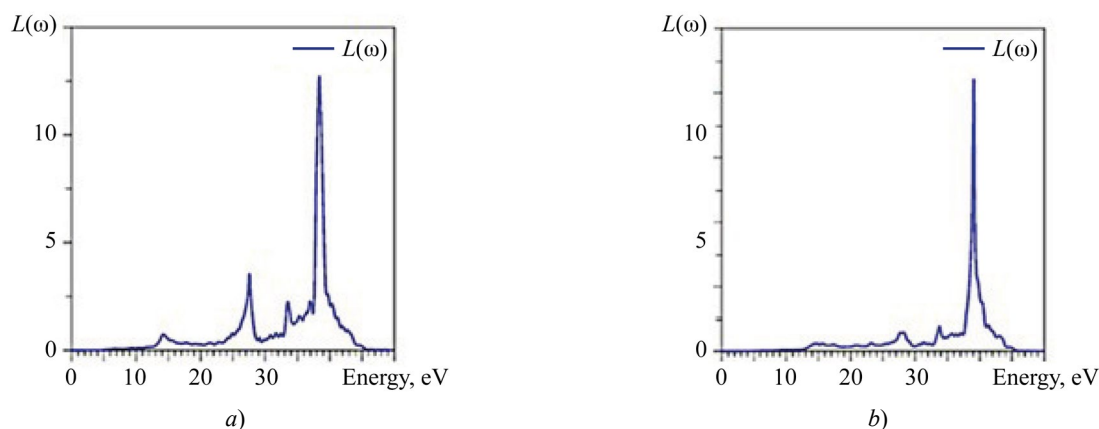


Fig. 10. Calculated spectrum of electron energy losses: *a* — $\text{La}_2\text{Zr}_2\text{O}_7$; *b* — $\text{Nd}_2\text{Zr}_2\text{O}_7$

The energy loss of the electron becomes significant at 14 eV (small peak), ~27 eV, ~33.5 eV. The largest value $L(\omega)$ is reached at 39 eV, which corresponds to a sharply decreasing edge of the absorption coefficient $\alpha(\omega)$ (Fig. 7).

Discussion and Conclusion. The calculation of the electron density states of the valence bands of $\text{La}_2\text{Zr}_2\text{O}_7$, $\text{Nd}_2\text{Zr}_2\text{O}_7$ gave two results:

- allowed us to explain all the main features of the experimental X-ray photoelectron spectra of these compounds in the energy range of ~35 eV from the top of the valence band;
- showed which electron symmetry determined the main features of the experimental spectra.

Together with the obtained densities of unoccupied states, the calculated densities of occupied states allowed us to define the optical coefficients of the compounds studied. It is extremely important to take into account the corrections in the exchange-correlation part of the potential (*GGA+U*, *mBJ*). Only with them it is possible to obtain the values of the widths of the forbidden bands that correspond to the experimental data. For $\text{Nd}_2\text{Zr}_2\text{O}_7$, calculations without corrections generally show a non-zero density of states at the Fermi level.

References

1. Chartier A, Meis C, Crocombette J, Corrales LR, Weber WJ. Atomistic Modeling of Displacement Cascades in $\text{La}_2\text{Zr}_2\text{O}_7$ Pyrochlore. *Physical Review B*. 2003;67:174102. <https://doi.org/10.1103/PhysRevB.67.174102>
2. Stanek CR, Minervini L, Grimes RW. Nonstoichiometry in $\text{A}_2\text{B}_2\text{O}_7$ Pyrochlores. *Journal of the American Ceramic Society*. 2002;85(11):2792–2798. <https://doi.org/10.1111/j.1151-2916.2002.tb00530.x>
3. Pirzada M, Grimes RW, Minervini L, Maguire JF, Sickafus KE. Oxygen Migration in $\text{A}_2\text{B}_2\text{O}_7$ Pyrochlores. *Solid State Ionics*. 2001;140:201–208. [https://doi.org/10.1016/S0167-2738\(00\)00836-5](https://doi.org/10.1016/S0167-2738(00)00836-5)
4. Tabira Y, Withers RL, Minervini L, Grimes RW. Systematic Structural Change in Selected Rare Earth Oxide Pyrochlores as Determined by Wide-Angle CBED and a Comparison with the Results of Atomistic Computer Simulation. *Journal of Solid State Chemistry*. 2000;153(1):16–25. <https://doi.org/10.1006/jssc.2000.8712>
5. Helean KB, Ushakov SV, Brown CE, Navrotsky A, Lian J, Ewing RC, et al. Formation Enthalpies of Rare Earth Titanate Pyrochlores. *Journal of Solid State Chemistry*. 2004;177(6):1852–1866. <https://doi.org/10.1016/j.jssc.2004.01.009>
6. Lian J, Zu XT, Kutty KVG, Chen J, Wang LM, Ewing RC. Ion-Irradiation-Induced Amorphization of $\text{La}_2\text{Zr}_2\text{O}_7$ Pyrochlore. *Physical Review B*. 2002;66:054108. <https://doi.org/10.1103/PhysRevB.66.054108>
7. Chen J, Lian J, Wang LM, Ewing RC, Wang RG, Pan W. X-ray Photoelectron Spectroscopy Study of Disorder in $\text{Gd}_2(\text{Ti}_{1-x}\text{Zr}_x)_2\text{O}_7$ Pyrochlores. *Physical Review Letters*. 2002;88:105901. <https://doi.org/10.1103/PhysRevLett.88.105901>
8. Yong Jiang, Smith JR, Odette GR. Prediction of Structural, Electronic and Elastic Properties of $\text{Y}_2\text{Ti}_2\text{O}_7$ and Y_2TiO_5 . *Acta Materialia*. 2010;58(5):1536–1543. <https://doi.org/10.1016/j.actamat.2009.10.061>
9. Winter MR, Clarke DR. Thermal Conductivity of Yttria-Stabilized Zirconia-Hafnia Solid Solutions. *Acta Materialia*. 2006;54(19):5051–5059. <https://doi.org/10.1016/j.actamat.2006.06.038>
10. Matteucci F, Cruciani G, Dondi M, Baldi G, Barzanti A. Crystal Structural and Optical Properties of Cr-Doped $\text{Y}_2\text{Ti}_2\text{O}_7$ and $\text{Y}_2\text{Sn}_2\text{O}_7$ Pyrochlores. *Acta Materialia*. 2007;55(7):2229–2238. <https://doi.org/10.1016/j.actamat.2006.11.008>
11. Uno M, Kosuga A, Okui M, Horisaka K, Muta H, Kurosaki K, et al. Photoelectrochemical Study of Lanthanide Zirconium Oxides, $\text{Ln}_2\text{Zr}_2\text{O}_7$ ($\text{Ln} = \text{La}, \text{Ce}, \text{Nd}$ and Sm). *Journal of Alloys and Compounds*. 2006;420:291–297. <https://doi.org/10.1016/j.jallcom.2005.10.072>
12. Ciomaga Hatnean M, Lees MR, Balakrishnan G. Growth of Single-Crystals of Rare-Earth Zirconate Pyrochlores, $\text{Ln}_2\text{Zr}_2\text{O}_7$ (with $\text{Ln} = \text{La}, \text{Nd}, \text{Sm}$, and Gd) by the Floating Zone Technique. *Journal of Crystal Growth*. 2015;418:1–6. <https://doi.org/10.1016/j.jcrysgro.2015.01.037>

13. Feng J, Xiao B, Wan CL, Qu ZX, Huang ZC, Chen JC, et al. Electronic Structure, Mechanical Properties and Thermal Conductivity of $\text{Ln}_2\text{Zr}_2\text{O}_7$ (Ln = La, Pr, Nd, Sm, Eu and Gd) Pyrochlore. *Acta Materialia*. 2011;59(4):1742–1760. <https://doi.org/10.1016/j.actamat.2010.11.041>
14. Zheng Li, Wei Pan. Electronic Structure and Transport Properties of $\text{La}_2\text{Zr}_2\text{O}_7$ Pyrochlore from First Principles. *Solid State Phenomena*. 2018;281:767–773. <https://doi.org/10.4028/www.scientific.net/SSP.281.767>
15. Liu B, Wang JY, Zhou YC, Liao T, Li FZ. Theoretical Elastic Stiffness, Structure Stability and Thermal Conductivity of $\text{La}_2\text{Zr}_2\text{O}_7$ Pyrochlore. *Acta Materialia*. 2007;55(9):2949–2957. <https://doi.org/10.1016/j.actamat.2006.12.035>
16. Subramanian MA, Aravamudan G, Subba Rao GV. Oxide Pyrochlores — A Review. *Progress in Solid State Chemistry*. 1983;15(2):55–143. [https://doi.org/10.1016/0079-6786\(83\)90001-8](https://doi.org/10.1016/0079-6786(83)90001-8)
17. Blaha P, Schwarz K, Tran F, Laskowski R, Madsen GKH, Marks LD. WIEN2k: an APW+lo Program for Calculating the Properties of Solids. *Journal of Chemical Physics*. 2020;152(7):074101. <https://doi.org/10.1063/1.5143061>
18. Blöchl PE, Jepsen O, Andersen OK. Improved Tetrahedron Method for Brillouin-Zone Integrations. *Physical Review B*. 1994;49(23):16223–16233. <https://doi.org/10.1103/PhysRevB.49.16223>
19. Perdew JP, Burke K, Ernzerhof M. Generalized Gradient Approximation Made Simple. *Physical Review Letters*. 1996;77(18):3865–3868. <https://doi.org/10.1103/PhysRevLett.77.3865>
20. Tran F, Blaha P. Accurate Band Gaps of Semiconductors and Insulators with a Semilocal Exchange-Correlation Potential. *Physical Review Letters*. 2009;102(22):226401. <https://doi.org/10.1103/PhysRevLett.102.226401>
21. Anisimov VI, Solov'yev IV, Korotin MA, Czyżyk MT, Sawatzky GA. Density-Functional Theory and NiO Photoemission Spectra. *Physical Review B*. 1993;48(23):16929–16934. <https://doi.org/10.1103/PhysRevB.48.16929>
22. Novák P, Boucher F, Gressier P, Blaha P, Schwarz K. Electronic Structure of the Mixed Valence System $(\text{YM})_2\text{BaNiO}_5$ (M = Ca, Sr). *Physical Review B*. 2001;63(23):235114. <https://doi.org/10.1103/PhysRevB.63.235114>
23. Hong Jiang. Band Gaps from the Tran-Blaha Modified Becke-Johnson Approach: A Systematic Investigation. *The Journal of Chemical Physics*. 2013;138(13):134115. <https://doi.org/10.1063/1.4798706>
24. Tuan V Vu, Khyzhun OY, Lavrentyev AA, Gabrelian BV, Kalmykova KF, Isaenko LI, et al. Electronic Band Structure and Optical Properties of $\text{Li}_2\text{In}_2\text{GeSe}_6$ Crystal. *Materials Today Communications*. 2023;35:105798. <https://doi.org/10.1016/j.mtcomm.2023.105798>
25. Lotz W. Electron Binding Energies in Free Atoms. *The Journal of the Optical Society of America*. 1970;60(2):206–210.
26. Lide DR (ed). *CRS Handbook of Chemistry and Physics*. 87th ed. Boca Raton; London; New York: CRC Press; Taylor & Francis; 2007. 2608 p.
27. Ambrosch-Draxl C, Sofo JO. Linear Optical Properties of Solids within the Full-Potential Linearized Augmented Planewave Method. *Computer Physics Communications*. 2006;175(1):1–14. <https://doi.org/10.1016/j.cpc.2006.03.005>
28. Khan SA, Reshak AH. Optoelectronic and Transport Properties of Zintl Phase $\text{KBa}_2\text{Cd}_2\text{Sb}_3$ Compound. *Computational Materials Science*. 2014;95:328–336. <https://doi.org/10.1016/j.commatsci.2014.07.031>
29. Boujnah M, Dakir O, Zaari H, Benyoussef A, Kenz AE. Optoelectronic Response of Spinel CdX_2O_4 with X = (Al, Ga, In) through the Modified Becke-Johnson Functional. *Journal of Applied Physics*. 2014;116(12):123703. <https://doi.org/10.1063/1.4896110>
30. Tuan V Vu, Lavrentyev AA, Doan V Thuan, Chuong V Nguyen, Khyzhun OY, Gabrelian BV, et al. Electronic Properties and Optical Behaviors of Bulk and Monolayer ZrS_2 : A Theoretical Investigation. *Superlattices and Microstructures*. 2019;125:205–213. <https://doi.org/10.1016/j.spmi.2018.11.008>

About the Authors:

Anatoliy A. Lavrentyev, Dr.Sci. (Phys.-Math.), Professor, Head of the Electrical Engineering and Electronics Department, Don State Technical University (1, Gagarin Sq., Rostov-on-Don, 344003, Russian Federation), [SPIN-code](#), [ORCID](#), [ScopusID](#), [ResearchGate](#), alavrentyev@donstu.ru

Boris V. Gabrelian, Cand.Sci. (Phys.-Math.), Associate Professor of the Computer and Automated Systems Software Department, Don State Technical University (1, Gagarin Sq., Rostov-on-Don, 344003, Russian Federation), [SPIN-code](#), [ORCID](#), [ScopusID](#), [ResearcherID](#), boris.gabrelian@gmail.com

Vu Van Tuan, Cand.Sci. (Phys.-Math.), Leading Researcher, Laboratory of Computational Physics, Institute of Computational Science and Artificial Intelligence, Van Lang University (69/68, Dang Thuy Tram Str. Ward 13, Binh Thanh District, Ho Chi Minh City, 70000, Vietnam), [ORCID](#), [ScopusID](#), vuvan.tuan@mail.ru

Ksenia F. Kalmykova, Teaching Assistant of the Electrical Engineering and Electronics Department, Don State Technical University (1, Gagarin Sq., Rostov-on-Don, 344003, Russian Federation), [SPIN-code](#), [ORCID](#), [ScopusID](#), [ResearchGate](#), 16ksy16@mail.ru

Claimed contributorship:

AA Lavrentyev: conceptualization, supervision, project administration.

BV Gabrelian: methodology, formal analysis, data curation, validation.

Vu Van Tuan: resources, validation, writing – original draft preparation.

KF Kalmykova: formal analysis, writing – review and editing.

Conflict of Interest Statement: the authors declare no conflict of interest.

All authors have read and approved the final version of manuscript.

Об авторах:

Анатолий Александрович Лаврентьев, доктор физико-математических наук, профессор, заведующий, кафедра «Электротехника и электроника» Донского государственного технического университета (344003, Российская Федерация, г. Ростов-на-Дону, пл. Гагарина, 1), [SPIN-код](#), [ORCID](#), [ScopusID](#), [ResearchGate](#), alavrentyev@donstu.ru

Борис Витальевич Габрельян, кандидат физико-математических наук, доцент, кафедра «Программное обеспечение вычислительной техники и автоматизированных систем» Донского государственного технического университета (344003, Российская Федерация, г. Ростов-на-Дону, пл. Гагарина, 1), [SPIN-код](#), [ORCID](#), [ScopusID](#), [ResearcherID](#), boris.gabrelian@gmail.com

Ву Ван Туан, кандидат физико-математических наук, ведущий научный сотрудник, «Лаборатория вычислительной физики» института вычислительной науки и искусственного интеллекта, Университет Ван Ланг, Хошимин, Вьетнам, [ORCID](#), [ScopusID](#), vuvan.tuan@mail.ru

Ксения Федоровна Калмыкова, ассистент, кафедра «Электротехника и электроника» Донского государственного технического университета (344003, Российская Федерация, г. Ростов-на-Дону, пл. Гагарина, 1), [SPIN-код](#), [ORCID](#), [ScopusID](#), [ResearchGate](#), 16ksyl6@mail.ru

Заявленный вклад авторов:

А.А. Лаврентьев: разработка концепции, научное руководство, административное руководство исследовательским проектом.

Б.В. Габрельян: разработка методологии, формальный анализ, курирование данных, валидация результатов.

Ву Ван Туан: предоставление ресурсов, валидация результатов, написание черновика рукописи.

К.Ф. Калмыкова: формальный анализ, написание рукописи – рецензирование и редактирование.

Конфликт интересов: авторы заявляют об отсутствии конфликта интересов.

Все авторы прочитали и одобрили окончательный вариант рукописи.

Received / Поступила в редакцию 10.03.2025

Reviewed / Поступила после рецензирования 03.04.2025

Accepted / Принята к публикации 14.04.2025

INFORMATION TECHNOLOGY, COMPUTER SCIENCE AND MANAGEMENT ИНФОРМАТИКА, ВЫЧИСЛИТЕЛЬНАЯ ТЕХНИКА И УПРАВЛЕНИЕ



UDC 519.688

Original Empirical Research

<https://doi.org/10.23947/2687-1653-2025-25-2-142-151>

Integration of Sensor Data and Mathematical Modeling of Underwater Robot Behavior Using a Digital Twin

Mikhail D. Gladyshev , Alexey V. Rybakov 

Astrakhan Tatishchev State University, Astrakhan, Russian Federation

✉ mih.gladyshev@gmail.com

EDN: LDXARH

Abstract

Introduction. Control of underwater robotic complexes (URC) is complicated by factors, such as inertia, stochastic disturbances, and lack of navigation infrastructure. Existing approaches to modeling and predicting URC behavior are known for their weak or absent integration of data from real sensors in real time. By eliminating this gap in integrated solutions, it is possible to combine physical models, digital twins, and visualization. A promising tool for overcoming the above limitations is a digital twin (DT), which provides an accurate digital representation of an object through the integration of data from physical sensors and mathematical models. The objective of the presented study is to develop a method for predicting the dynamics of the URC using a digital twin to improve the efficiency of autonomous control.

Materials and Methods. The basis of the study was the development of a mathematical model of the motion of an underwater robotic complex. It included differential kinematics, modeling of environmental resistance, and rotation dynamics. The following sensors were used to collect and process data: incremental encoders, a three-axis accelerometer, and a gyroscope. A proportional-integral differentiating (PID) controller was applied to control the motion along each axis. The Unity Game Environment was used to visualize and test the model. It created a digital twin module with the ability to display the system state in real time. The Arduino IDE platform was used as software for low-level programming, as well as MATLAB and Python for data analysis and graphing.

Results. To verify the model, experiments were conducted on a physical model. They were compared to the simulation of the object's behavior in a virtual environment. Graphs of discrepancies between physical and simulated trajectories were presented. Statistical metrics characterizing the accuracy of the digital twin were calculated. The maximum deviation in coordinates did not exceed 5.3 mm, the average angular deviation was 3.5°. This confirmed the reliability and practical applicability of the proposed model in autonomous control of a robotic complex. It was also found that the average error along X — 3.11 mm, along Y — 2.92 mm. The average error in angle Z — 1.8°. The response time was less than 10 ms. The stability of the digital twin to minor fluctuations in the data was provided by smoothing the input data, the stability of the system regulator, and adaptation of the model to the calibration values at the start of each cycle.

Discussion and Conclusion. Digital twins are suitable for predictive control and monitoring of an object under uncertainty. The proposed approach can be scaled for various types of robotic systems operating in aggressive and poorly predictable environments. Further research in this area may involve the introduction of adaptive and neural network control methods.

Keywords: digital twin of an autonomous robotic system, underwater robotic complex, predictive control, underwater robot

Acknowledgments. The authors would like to thank the editors and reviewers for their attentive attitude to the article and comments that allowed them to improve its quality.

For Citation. Gladyshev MD, Rybakov AV. Integration of Sensor Data and Mathematical Modeling of Underwater Robot Behavior Using a Digital Twin. *Advanced Engineering Research (Rostov-on-Don)*. 2025;25(2):142–151. <https://doi.org/10.23947/2687-1653-2025-25-2-142-151>

Интеграция сенсорных данных и математическое моделирование поведения подводного робота с использованием цифрового двойника

М.Д. Гладышев  , А.В. Рыбаков 

Астраханский государственный университет имени В.Н. Татищева, г. Астрахань, Российская Федерация

✉ mih.gladishev@gmail.com

Аннотация

Введение. Управление подводными робототехническими комплексами (ПРТК) осложняется такими факторами, как инерционность, стохастические возмущения и недостаток навигационной инфраструктуры. Существующие подходы к моделированию и прогнозированию поведения ПРТК известны слабой или отсутствующей интеграцией данных с реальных сенсоров в режиме реального времени. Устранив указанный пробел в комплексных решениях, можно объединить физические модели, цифровые двойники и визуализацию. Перспективный инструмент для преодоления названных выше ограничений — цифровой двойник (англ. digital twin, DT), обеспечивающий точную цифровую репрезентацию объекта через интеграцию данных от физических сенсоров и математических моделей. Цель представленного исследования — разработка метода прогнозирования динамики ПРТК с использованием цифрового двойника для повышения эффективности автономного управления.

Материалы и методы. Основа исследования — разработка математической модели движения подводного робототехнического комплекса. Она включает дифференциальную кинематику, моделирование сопротивления среды и динамики поворота. Для сбора и обработки данных использовались сенсоры: инкрементальные энкодеры, трехосевой акселерометр и гироскоп. Для управления движением по каждой оси действовали пропорционально-интегрально дифференцирующий (ПИД) регулятор. Для визуализации и проверки модели применялась игровая среда «Юнити» (Unity). В ней создали модуль цифрового двойника с возможностью отображения состояния системы в реальном времени. В качестве программного обеспечения использовалась платформа «Ардуино Ай-ди-и» (Arduino IDE) для низкоуровневого программирования, а также «Матлаб» (Matlab) и «Питон» (Python) для анализа данных и построения графиков.

Результаты исследования. Для верификации модели проводились эксперименты на физическом макете. Их сопоставили с симуляцией поведения объекта в виртуальной среде. Представлены графики расхождений между физическими и смоделированными траекториями. Рассчитаны статистические метрики, характеризующие точность цифрового двойника. Максимальное отклонение по координатам не превышает 5,3 мм, среднее угловое отклонение составило 3,5°. Это подтверждает достоверность и практическую применимость предложенной модели при автономном управлении робототехническим комплексом. Установлено также, что средняя ошибка по X — 3,11 мм, по Y — 2,92 мм. Средняя ошибка угла Z — 1,8°. Время реакции — менее 10 мс. Устойчивость цифрового двойника к незначительным флуктуациям в данных обеспечивается благодаря сглаживанию входных данных, стабильностью системного регулятора и адаптации модели к калибровочным значениям на старте каждого цикла.

Обсуждение и заключение. Цифровые двойники подходят для прогностического управления и наблюдения за объектом в условиях неопределенности. Предложенный подход целесообразно масштабировать для различных типов робототехнических систем, функционирующих в агрессивных и слабо предсказуемых средах. Дальнейшие исследования в этом направлении могут быть связаны с внедрением адаптивных и нейросетевых методов управления.

Ключевые слова: цифровой двойник автономной робототехнической системы, подводный робототехнический комплекс, предиктивное управление, подводный робот

Благодарности. Авторы выражают благодарность редакции и рецензентам за внимательное отношение к статье и замечания, позволившие повысить ее качество.

Для цитирования. Гладышев М.Д., Рыбаков А.В. Интеграция сенсорных данных и математическое моделирование поведения подводного робота с использованием цифрового двойника. *Advanced Engineering Research (Rostov-on-Don)*. 2025;25(2):142–151. <https://doi.org/10.23947/2687-1653-2025-25-2-142-151>

Introduction. In recent years, there has been growing interest in digital twin (DT) technology. These are virtual models closely related to physical objects and designed to display, analyze and predict their behavior in real time [1]. DT are widely used to solve applied problems in industry, energy and transport, especially if it is necessary to control and manage objects under conditions of high uncertainty [2]. With the spread of autonomous robotic systems, the digital twin becomes an important tool for providing reliable and sustainable management. It allows for the formation of a predictive model of the object's behavior, taking into account both internal parameters and external actions [3].

Of particular interest is the use of DT in the control of underwater robotic complexes (URC), where operating conditions are significantly complicated by poor visibility, lack of precise navigation, communication delays, high inertia, and noise in sensor data. All this reduces the efficiency of traditional closed-loop control systems [4]. There are publications on digital twins in the public domain, but the topic is still insufficiently developed in terms of using DT in underwater systems. Existing studies, as a rule, either do not cover predictive control tasks or do not take into account the specificity of the underwater environment and typical sensor errors [5]. Numerous papers are characterized by significant gaps related to the lack of integrated solutions for building digital twins of underwater robotic systems focused on stable predictive control and state assessment under conditions of noisy and incomplete data.

A stable assessment of the current state of the underwater robotic complex (URC) is required, and this can be provided by integrating sensor data — accelerometry, gyroscopy, encoder measurements, and other sources. However, due to the instability and noise typical of inertial sensors, it is necessary to implement algorithms for filtering, correcting and calibrating data at different stages of operation [5].

It should also be noted that in the literature on digital modeling and control of robotic systems, authors often focus on static models or limited control scenarios (e.g., on navigation or position stabilization). At the same time, a comprehensive approach to predicting the dynamic behavior of URC using digital twins in real time has not been sufficiently developed.

Based on the aforesaid, the objective of this study is to develop and apply a method for predicting the dynamic behavior of the URC using a digital twin to improve the efficiency of controlling an autonomous system when performing underwater engineering work.

Materials and Methods. To reach the research objective, a comprehensive model was implemented, including a physicomathematical description of the motion, sensor architecture, and visualization.

Scientific research made it possible to solve the following problems:

- construction of a generalized mathematical model of the motion of the URC taking into account the external environment and sensor architecture;
- formalization of the behavior of the autonomous system taking into account inertial and control effects;
- implementation of a feedback control system based on classical approaches to automatic control theory;
- assessment of the accuracy of the digital twin by analyzing the discrepancies between the physical and virtual behavior of the URC based on experiments;
- visualization of the digital twin in the Unity software environment with the ability to compare the indicators of virtual and physical trajectories.

Within the framework of the presented work:

- a mathematical model of the URC movement is created;
- data from sensors are collected and calibrated;
- a digital twin is implemented in the Unity environment;
- the model is experimentally verified;
- the results are analyzed, and the accuracy of the model is assessed.

The motion of the URC is described on the basis of differential kinematics and equations that take into account water resistance, inertial characteristics of the system, and control actions. The model is based on a system of second-order motion equations modified to take into account hydrodynamic resistance and correction coefficients obtained experimentally. Assumptions are made about the rigidity of the housing, insignificant drift, and quasi-stationary motion.

The system state vector includes coordinates: x , y , z , and heading angle θ , as well as linear and angular rates. The formulas used in the introduction describe kinematic relationships, feedback, resistance model, and control signals. PID controllers with parameters empirically selected on the basis of the system response are used for control along the longitudinal, transverse, and vertical axes.

A modular sensor system is used to collect data in real time. Its elements:

- 38S6G5-B-G24N encoders, 2000 pulses per revolution — to estimate linear displacement;
- LIS3DH three-axis accelerometer (measurement range $\pm 2g/\pm 4g/\pm 8g/\pm 16g$, I2C/SPI interfaces, sampling frequency up to 5.3 kHz) — to obtain acceleration and tilt data;
- gyroscope as part of the IMU module (inertial measurement unit) — to track angular speeds and orientation.

The sensor data was pre-filtered, calibrated (normalized relative to the zero position) and integrated into the digital twin model.

The key stage in building a digital twin is mathematical modeling of the movement of the underwater robotic complex. It allows predicting the behavior of the object in various environments [6]. This study considers a mobile URC with a rigid physical structure, moving in a flat (2D) or spatial (3D) coordinate system depending on the task scenario [7]. An independent drive for each of the tracks is used to control the movement, which allows for differential maneuvering [8].

To simulate the position and orientation of the URC on the plane, a kinematic model of a differential robot is used, based on the position of the center of mass (or center of geometry) of the robot [9]. Let x and y be the coordinates of the center of mass in the global coordinate system, θ — robot's orientation angle (angle between the longitudinal axis and the OX axis in the global system).

$$\dot{x} = v \cdot \cos(\theta), \quad (1)$$

$$\dot{y} = v \cdot \sin(\theta), \quad (2)$$

$$\dot{\theta} = w, \quad (3)$$

where v — linear speed of the center of mass (determined by encoder readings); w — angular speed (obtained from a gyroscope or calculated by the difference in track speeds).

The linear and angular speeds are related to the individual speeds of the right v_R and left v_L tracks:

$$v = \frac{v_R + v_L}{2}, \quad (4)$$

$$w = \frac{v_R - v_L}{L}, \quad (5)$$

where L — robot base (distance between tracks).

The robot's behavior is significantly affected by the underwater environment: water resistance, lifting force, viscous forces, friction forces. These effects are taken into account in the form of generalized disturbance $F_d(t)$ [10]. The system of differential equations takes the form:

$$m \cdot \ddot{r} = F_u(t) + F_d(t), \quad (6)$$

where M — robot's mass; \ddot{r} — position radius vector; $F_u(t)$ — control action from the drive system (determined by the PID controller or another algorithm); $F_d(t)$ — environmental disturbances (determined experimentally or set empirically).

Within the framework of the layout and digital model, the resistance of the environment can be taken into account in the form of a damped term:

$$F_d(t) = -k_u \cdot \dot{r}(t), \quad (7)$$

where k_u — coefficient of viscous resistance of the medium (adjustable parameter of the digital twin).

The physical model is equipped with encoders, therefore the positions and orientation of the URC in space are calculated through numerical integration of the speeds obtained from the left and right tracks:

$$\Delta s = \frac{\Delta s_L + \Delta s_R}{2}, \quad (8)$$

$$\Delta \theta = \frac{\Delta s_R - \Delta s_L}{L}, \quad (9)$$

where Δs_L , Δs_R — increments of distance according to encoder readings; Δs — increment of the center of mass; $\Delta \theta$ — change in orientation.

We use the current orientation $\Delta \theta$, to express the new position in the global coordinate system:

$$x_{t+1} = x_t + \Delta s \cdot \cos(\theta_t), \quad (10)$$

$$y_{t+1} = y_t + \Delta s \cdot \sin(\theta_t). \quad (11)$$

Mathematical modeling is a fundamental part of the development of a digital twin of an underwater complex [11]. The objective of modeling is to formalize the processes of movement [12], control and response to external actions with the possibility of further analysis of the stability and accuracy of execution of control actions [13].

The underwater robot is considered as a system with multiple inputs and outputs, located in an environment with a high level of inertia, delay and stochastic disturbances [14]. Control actions are implemented through thrust modules, and movements are tracked using encoders and inertial measurement units [15]. The model can be described as a system of second-order equations with position and speed feedback:

$$M\ddot{x}(t) + D\dot{x}(t) + Kx(t) = Bu(t), \quad (12)$$

where M — mass matrix (includes inertial characteristics); D — damping matrix (taking into account viscous resistance of water); K — stiffness matrix (includes elastic forces in the case of mechanical constraints); $x(t)$ — position and orientation vector in 3D space; $u(t)$ — control action (signals to the motors); B — control distribution matrix.

For rotational motion, the Euler model is used:

$$J\dot{\omega}(t) + \omega(t) + J\omega(t) = \tau(t), \quad (13)$$

where J — inertia tensor of the robot, $\omega(t)$ — angular speed (from the gyroscope), $\tau(t)$ — control moment.

When implementing a spot turn operation, as a rule, tracks with different directions of rotation are used. The difference in speeds on the right and left tracks sets the moment:

$$\tau_z = rF(w_L - w_R). \quad (14)$$

To set the angle of rotation, the expression is used:

$$Z(t) = \int_0^t w_z(t) dt. \quad (15)$$

The control system is implemented in the form of PID controllers for each axis (X, Y, Z):

$$u(t) = K_p e(t) + K_i \int_0^t e(t) dt + K_D \frac{de(t)}{dt}, \quad (16)$$

where $e(t) = x_{ref}(t) - x(t)$ — error between target and current position. Coefficients K_p, K_i, K_D are adjusted according to the optimality criterion.

Table 1

Regulator Coefficients for Position Stabilization

Axis	K_p	K_i	K_d
X	1.20	0.05	0.60
Y	1.00	0.04	0.50
Z	2.00	0.10	0.90

The physical model of the robot is implemented on the basis of Arduino Mega 2560 Pro. Microcontroller — ATmega 2560-16AU, 16 MHz, 256 KB FLash, with 54 digital inputs/outputs (I/O), 16 analog inputs, USB-UART interface CH340G. The complex is connected to sensors and a drive control system. Data is collected and transmitted to the digital environment via Serial port in the format of combined time-stamped lines.

The virtual implementation of the digital twin is created in Unity. C#-scripts are used to interpret the data, display the movements, rotations and behavior of the object in a three-dimensional environment. Axes, contours, coordinate values and trajectories are visualized. A model of a translucent robot that does not interact with other objects is used, which allow us to concentrate on comparing movements.

A data processor and a filtering system are implemented on the Unity side. Integration with correction based on sensor data is applied to calculate angles and coordinates. Individual blocks are implemented as scripts with the ability to scale the project. Standard metrics are used to statistically assess accuracy: standard deviation, maximum deviation, and average error in coordinates and angles.

Research Results. To verify the model in a digital environment, movements were simulated under successive control actions. Then, the trajectories of rectilinear and semicircular motion were compared (Fig. 1 and 3). The readings of the digital robot were compared to the ideal trajectory. The root-mean-square analysis showed a discrepancy when moving in a straight line (Fig. 2) and in a semicircle (Fig. 4).

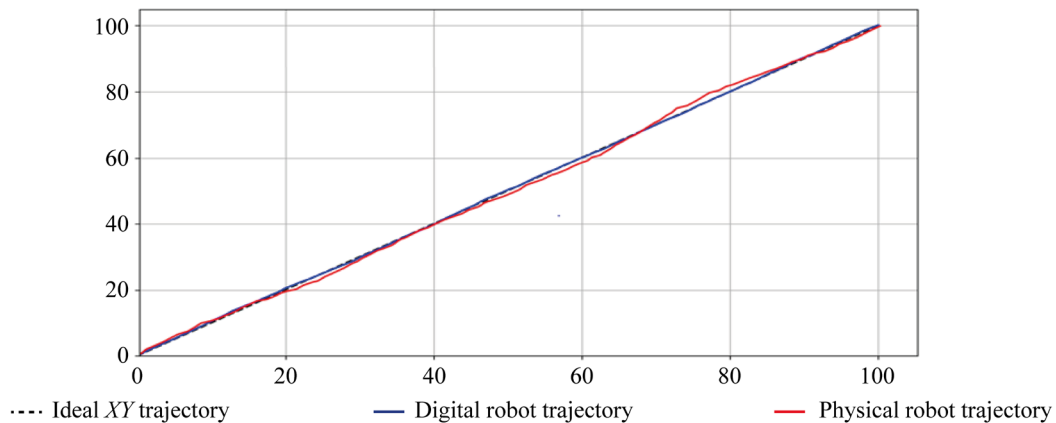


Fig. 1. Trajectories of motion in a straight line

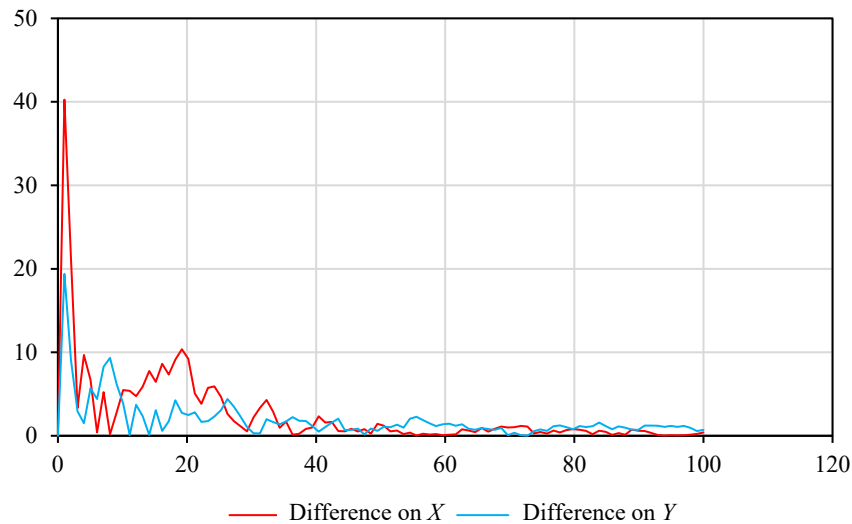


Fig. 2. Error (%) when measuring on a straight line

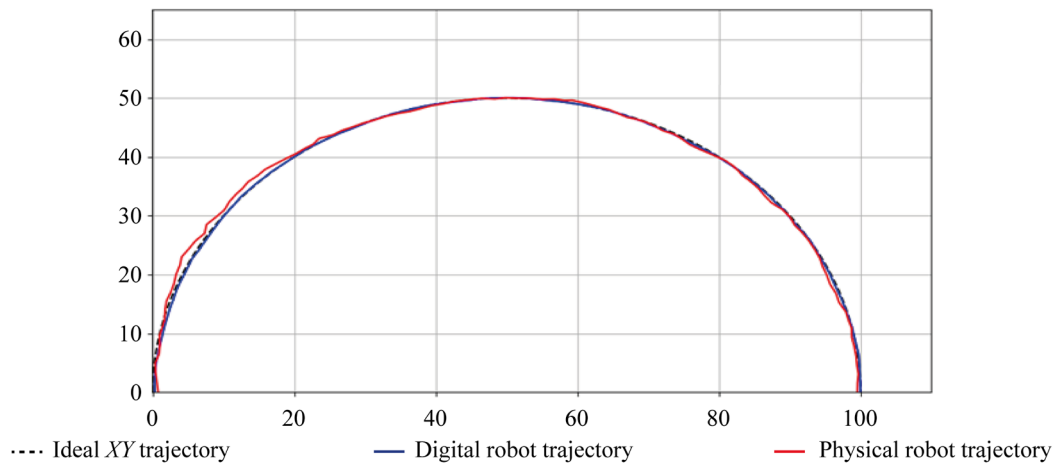


Fig. 3. Trajectories of movement in a semicircle

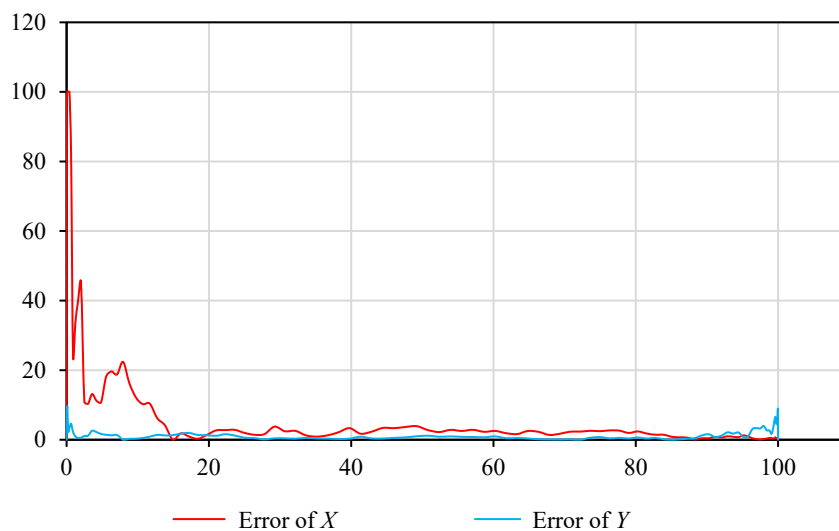


Fig. 4. Error (%) when measuring on a semicircle

The quality of displaying the URC behavior in the digital twin was assessed during experiments that included linear motion, the spot turn, and the trajectory with turns. In parallel, data from real sensors was recorded and compared to the parameters of the model in Unity. The results of measurements and comparisons are presented in Table 2.

Table 2

Deviation Indicators

Metric	Value
Maximum deviation of X	5.3 mm
Maximum deviation of Y	4.8 mm
Average angular deviation	3.5°

The digital twin was visualized in the Unity environment. This flexible 3D engine allowed us to embed data streams from physical sensors, display spatial movements, orientation, and also create scenarios for interaction with the external environment (Fig. 5).



Fig. 5. Robotic complex control program

Data from physical sensors (accelerometers, gyroscopes, encoders) was transmitted via a COM port (communications port) using a custom script in C#. Incoming data was divided into channels and displayed as parameters of the twin object.

The digital model in Unity used the same coordinate system and the same control structure as the implemented mathematical model. Its functions were:

- transmitting commands from the PID controller model to the virtual wheels;
- displaying position, tilt angle, speed;
- visual reproduction of movement based on integrated sensor data.

The solution allows creating a closed loop “model – reality – visualization” and provides consistency between the digital twin and the physical system (Fig. 6).

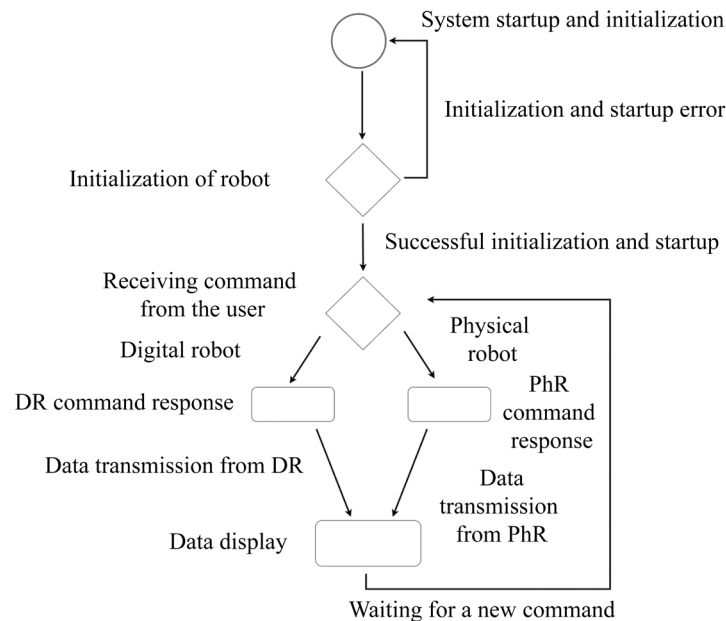


Fig. 6. Software operation algorithm: DR — digital robot, PhR — physical robot

The elements of the software operation algorithm are listed below.

System Startup and Initialization. The physical robot is turned on and connected via USB to a computer that collects and analyzes data, runs the main program, and initializes additional scripts:

- responsible for maintaining communication and collecting data,
- providing visualization.

All this takes place in Unity, after which the system is ready for work.

Robot Initialization. After the program is launched, its connection with the physical robot is established. Consequently, calibration occurs, and then the sensors and modules are launched: gyroscope, accelerometer, encoders, voltmeter, ammeter. A control message about the robot's readiness for launch and the start of data transmission is sent to Unity. After that, the stage of waiting for commands starts.

Receiving Command from the User. The value of the user interface entered into the program is analyzed and processed. The message is passed to intermediate scripts to perform the actions of the digital and physical robots.

Digital Robot's Command Response. The entered values and actions are recorded in the computer memory. Based on the embedded command execution algorithms and a mathematical model, the digital robot moves in digital space. At the same time, data on its position, speed and distance traveled, are recorded. After executing the command, the robot maintains its position and orientation in space.

Physical Robot's Command Response. Data is transmitted to the Arduino Mega microcontroller. Here, it is analyzed and, depending on the entered command and value, scripts are activated that are responsible for the operation of sensors: left and right encoders, accelerometers, and gyroscopes. Only after that does movement start at the user's command. During the execution of the command, the robot records its position and orientation in space and transmits data to the user interface program, where the data is visualized using a 3D model linked to the physical robot.

Data Collection and Display. At this stage, data on position, tilt angles, distance traveled and other parameters are collected from the digital and physical robots and visualized in the user interface program. After that, the program waits for a new command.

The described algorithm is based on the classical principles of closed-loop feedback control systems. The use of data from sensors (accelerometers, gyroscopes, encoders) allows for the implementation of a measuring element in the general structural form of control systems. The mathematical model integrated into Unity acts as an observer, tracking the behavior of the system and providing visual verification of the correctness of command execution.

The system is designed taking into account:

- linearization of the model of the URS motion in small neighborhoods of the trajectory;
- PID control of the angle of rotation and speed;
- filtering of sensor data using simple sliding windows and zero calibration corrections.

Formulas (17)–(19) present the indicators that are used to analyze the accuracy of the digital twin.

Absolute position error (in mm):

$$\Delta x(t) |x_{real}(t) - x_{digit}(t)|. \quad (17)$$

Root mean square orientation error (in degrees):

$$\Delta_{\theta} \frac{1}{n} \sum_{i=1}^n (\theta_{real,i} - \theta_{digit,i})^2. \quad (18)$$

Percentage deviation of the final position:

$$\varepsilon = \frac{\Delta x_{final}}{x_{real}} \cdot 100 \%. \quad (19)$$

As a result of experiments and analysis of sensor readings, additional parameters are obtained that characterize the error of the developed system (Table 3).

Table 3

Detected Errors in the System

Parameter	Value
Mean error on X	3.11 mm
Mean error on Y	2.92 mm
Average error of angle Z	1.8°
Maximum deviation	5.3 mm
Reaction time	<100 ms

The digital twin is resistant to minor fluctuations in the data due to the following factors:

- smoothing of input data;
- stability of the regulator implemented in the system;
- adaptation of the model to calibration values at the start of each cycle.

Discussion and Conclusion. A model of a digital twin of a robotic complex based on the integration of sensor data, mathematical modeling and 3D visualization has been developed and experimentally confirmed. Sustainable control and tracking of the behavior of the robotic complex have been implemented. The results of the comparative analysis of the digital model and the real system are presented. The results of the comparison have proven:

- a high degree of correspondence between the behavior of the digital twin and the real object;
- efficiency of the selected calibration and data processing algorithms;
- potential of using digital twins in debugging autonomous systems if physical testing is difficult.

The constructed model makes it possible to adequately assess the current state and predict the behavior of the URC under uncertainty. PID controllers provide stability during control, and visualization in Unity makes it possible to implement a digital twin as an interface for interaction with the system. Further development of this solution may be related to the implementation of adaptive and neural network control methods.

References

1. Meshkov AV, Gromov VS. Adaptive Nonlinear Motion Parameters Estimation Algorithm for Digital Twin of Multi-Link Mechanism Motion Trajectory Synthesis. *Scientific and Technical Journal of Information Technologies, Mechanics and Optics*. 2022;22(5):889–895. <https://doi.org/10.17586/2226-1494-2022-22-5-889-895>
2. Kubrikov MV. Digital Twin in the System of External Adaptive Control of Robot Manipulators. *Spacecrafts & Technologies*. 2023;7(2):171–176. <https://doi.org/10.26732/j.st.2023.2.10>
3. Kuzmenko VP, Soleniy SV. Development of a Digital Twin Model for a Hybrid Production Line for LED Lighting Devices Assembly. *Journal of Instrument Engineering*. 2022;65(10):725–734.
4. Jingsong Fan, Xiangqiang Zhong, Zhimin Di, Huajie Fang. Collaborative Operation of 6-DOF Industrial Robot Based on Digital Twin. *Journal of Physics: Conference Series*. 2022;2206(1):012019. <https://doi.org/10.1088/1742-6596/2206/1/012019>
5. Farhadi A, Lee S, Hinchy EP, O'Dowd N, McCarthy CT. The Development of a Digital Twin Framework for an Industrial Robotic Drilling Process. *Sensors*. 2022;22(19):7232. <https://doi.org/10.3390/s22197232>
6. Qinglei Zhang, Run Xiao, Zhen Liu, Jianguo Duan, Jiyun Qin. Process Simulation and Optimization of Arc Welding Robot Workstation Based on Digital Twin. *Machines*. 2023;11(1):53. <https://doi.org/10.3390/machines11010053>
7. Hang Wu, Zhaoming Liu, Long Cui, Lirong Guan, Hongwei Wang. Digital Twin of Non-Ferrous Metal Casting Robot. In book: M Chen, et al (eds). *Advances in Machinery, Materials Science and Engineering Application*. Amsterdam: IOS Press; 2022. 760 p. <https://doi.org/10.3233/ATDE220502>
8. Chanchaen R, Chairprabha K, Wuttisittikulij L, Asdomwised W, Saadi M, Phanomchoeng G. Digital Twin for a Collaborative Painting Robot. *Sensors*. 2022;23(1):17. <https://doi.org/10.3390/s23010017>
9. Banic MS, Simonovic M, Stojanović L, Rangelov D, Miltenovic A, Perić M. Digital Twin Based Lightweighting of Robot Unmanned Ground Vehicles. *Facta Universitatis. Series: Automatic Control and Robotics*. 2022;21(3):188. <https://doi.org/10.22190/FUACR221121015B>
10. Xin Liu, Du Jiang, Bo Tao, Guozhang Jiang, Ying Sun, Jianyi Kong, et al. Genetic Algorithm-Based Trajectory Optimization for Digital Twin Robots. *Frontiers in Bioengineering and Biotechnology*. 2022;9:793782. <http://doi.org/10.3389/fbioe.2021.793782>
11. Garg G, Kuts V, Anbarjafari G. Digital Twin for FANUC Robots: Industrial Robot Programming and Simulation Using Virtual Reality. *Sustainability*. 2021;13(18):10336. <http://doi.org/10.3390/su131810336>
12. Đoàn Thanh Xuân, Tran Van Huynh, Thanh-Hung Nguyen, Vu Toan Thang. Applying Digital Twin and Multi-Adaptive Genetic Algorithms in Human–Robot Cooperative Assembly Optimization. *Applied Sciences*. 2023;13(7):4229. <http://doi.org/10.3390/app13074229>
13. Sichao Liu, Xi Vincent Wang, Lihui Wang. Digital Twin-Enabled Advance Execution for Human-Robot Collaborative Assembly. *CIRP Annals — Manufacturing Technology*. 2022;71(1):25–28. <http://doi.org/10.1016/j.cirp.2022.03.024>
14. Kibira D, Weiss BA. Towards a Digital Twin of a Robot Workcell to Support Prognostics and Health Management. In: *Proc. 2022 Winter Simulation Conference at Singapore*. New York: IEEE; 2022. P. 2968–2979. <http://doi.org/10.1109/WSC57314.2022.10015371>
15. Xuan Liu, He Gan, Ying Luo, YangQuan Chen, Liang Gao. Digital-Twin-Based Real-Time Optimization for a Fractional Order Controller for Industrial Robots. *Fractal and Fractional*. 2023;7(2):167. <http://doi.org/10.3390/fractalfract7020167>

About the Authors:

Mikhail D. Gladyshev, postgraduate student majoring in Systems Analysis, Control and Information Processing, Statistics, Astrakhan Tatishchev State University (20a, Tatishcheva Str., Astrakhan, 414056, Russian Federation), Design Engineer, “Smelcom Robotics” LLC (8, Parizhskoi Kommuny Str., Astrakhan, 414050, Russian Federation), [SPIN-code](#), [ORCID](#), mih.gladyshev@gmail.com

Alexey V. Rybakov, Cand.Sci. (Phys.-Math.), Associate Professor of the Department of Information Technologies, Associate Professor of the Department of Materials Technology and Industrial Engineering, Astrakhan Tatishchev State University (20a, Tatishcheva Str., Astrakhan, 414056, Russian Federation), [SPIN-code](#), [ORCID](#), [ScopusID](#), [ResearcherID](#), rybakov_alex@mail.ru

Claimed Contributorship:

MD Gladyshev: conceptualization, methodology, software, investigation, formal analysis, visualization, writing – original draft preparation.

AV Rybakov: supervision, validation, resources, writing – review & editing, project administration.

Conflict of Interest: the authors declare no conflict of interest.

All authors have read and approved the final version of the manuscript.

Об авторах:

Михаил Дмитриевич Гладышев, аспирант направления «Системный анализ, управление и обработка информации, статистика» Астраханского государственного университета имени В. Н. Татищева» (414056, Российская Федерация, г. Астрахань, ул. Татищева, 20А), инженер-конструктор ООО «Смелком Роботикс» (414050, Российская Федерация, г. Астрахань, ул. Парижской Коммуны, 8), [SPIN-код](#), [ORCID](#), mih.gladyshev@gmail.com

Алексей Владимирович Рыбаков, кандидат физико-математических наук, доцент, кафедра «Информационных технологий», доцент, кафедра «Технологии материалов и промышленной инженерии» Астраханского государственного университета имени В.Н.Татищева, (414056, Российская Федерация, г. Астрахань, ул. Татищева, 20А), [SPIN-код](#), [ORCID](#), [ScopusID](#), [ResearcherID](#), rybakov_alex@mail.ru

Заявленный вклад авторов:

М.Д. Гладышев: разработка концепции, методологии и программного обеспечения, формальный анализ, валидация результатов, визуализация, написание черновика рукописи.

А.В. Рыбаков: научное руководство, валидация результатов, предоставление ресурсов, написание рукописи, административное руководство исследовательским проектом.

Конфликт интересов: авторы заявляют об отсутствии конфликта интересов.

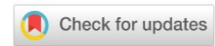
Все авторы прочитали и одобрили окончательный вариант рукописи.

Received / Поступила в редакцию 04.04.2025

Reviewed / Поступила после рецензирования 29.04.2025

Accepted / Принята к публикации 08.05.2025

INFORMATION TECHNOLOGY, COMPUTER SCIENCE AND MANAGEMENT ИНФОРМАТИКА, ВЫЧИСЛИТЕЛЬНАЯ ТЕХНИКА И УПРАВЛЕНИЕ



UDC 519.7

Original Empirical Research

<https://doi.org/10.23947/2687-1653-2025-25-2-152-164>

Approximate Synthesis of H_∞ – Controllers in Nonlinear Dynamic Systems over a Semi-Infinite Time Period

Andrei V. Panteleev , Aleksandra A. Yakovleva

Moscow Aviation Institute (National Research University), Moscow, Russian Federation

✉ ayakovleva982@gmail.com

EDN: IHQRUT

Abstract

Introduction. Problems and methods of finding H_∞ – control are the basis of modern control theory. They are actively used to develop robust controllers, especially in aircraft control systems under limited external actions. These methods allow for adapting control systems to changing environmental conditions, which is critically important for providing the reliability and safety of aircraft operation. Current research is aimed at improving approaches to the synthesis of controllers covering both linear and nonlinear dynamic systems. In this context, special attention is paid to the integration of new mathematical methods, such as linear matrix inequalities and frequency analysis, which allows for optimizing the system response to various external actions and providing protection against unexpected conditions. It is important to note that, despite the progress made in this area, significant problems remain unsolved regarding the analysis and synthesis of controllers for nonlinear systems. This necessitates further research and development in this promising area. In this paper, in order to fill the existing gap, sufficient conditions for the existence of control for one of the frequently encountered classes of nonlinear systems are formulated and proven, which will then be used as a theoretical basis for developing approximate algorithms for finding it.

Materials and Methods. The basic research tool was the H_∞ – control synthesis methods based on the minimax approach, which consisted in finding the control law under the worst external action. In this context, it was proposed to prove sufficient conditions for the existence of control using the extension principle. However, due to the computational difficulties that might arise when applying those conditions, it was decided to simplify the initial formulation of the problem. The simplification process was performed by approximate replacing the nonlinear system with another nonlinear system, which was similar in structure to the linear one, using the factorization procedure. This approach made it possible to use the solution of the Riccati equation, whose coefficients depended on the state vector, for the synthesis of controllers. To solve model examples and applied problems, a software package was developed using the MATLAB mathematical package.

Results. The article solved the problem of synthesis of H_∞ – control of the state of nonlinear continuous dynamic systems, linear in control and disturbance. Sufficient conditions for the existence of H_∞ – control were formulated and proved on the basis of the extension principle. An approximate method was proposed that provided solving the problem of finding control laws for dynamic systems that were nonlinear in state, similar to the methods used for linear systems. Analytical solutions were found for two model examples, which were illustrated by graphs of transient processes to demonstrate the results of numerical modeling of the considered nonlinear dynamic systems in the presence of external actions.

Discussion and Conclusion. The proposed approximate algorithm for synthesizing state and output controllers guarantees the required quality of transient processes and asymptotic stability of closed nonlinear control systems. This significantly expands the class of dynamic systems for which it is possible to synthesize controllers capable of resisting various external actions. The methods presented in this paper can be effectively applied to solve a variety of control problems, including the design of autopilots and automatic navigation systems for aircraft, even under conditions of limited external actions.

Keywords: H_∞ – control, nonlinear dynamic system, semi-infinite period of time, feedback control, controller synthesis

Acknowledgements. The authors would like to thank Irina Anatolyevna Kudryavtseva, Cand.Sci. (Phys.-Math.), Associate Professor, for assistance in preparing the text of the article.

For citation. Pantelev AV, Yakovleva AA. Approximate Synthesis of H_∞ – Controllers in Nonlinear Dynamic Systems over a Semi-Infinite Time Period. *Advanced Engineering Research (Rostov-on-Don)*. 2025;25(2):152–164. <https://doi.org/10.23947/2687-1653-2025-25-2-152-164>

Оригинальное эмпирическое исследование

Приближенный синтез H_∞ – регуляторов в нелинейных динамических системах на полубесконечном промежутке времени

А.В. Пантелеев , А.А. Яковлева  

Московский авиационный институт (национальный исследовательский университет), г. Москва, Российская Федерация

 ayakovleva982@gmail.com

Аннотация

Введение. Задачи и методы нахождения H_∞ – управления являются основой современной теории управления и активно используются для разработки робастных регуляторов, особенно в системах управления летательными аппаратами под ограниченными внешними воздействиями. Эти методы позволяют адаптировать системы управления к изменяющимся условиям окружающей среды, что критически важно для обеспечения надежности и безопасности работы летательных аппаратов. Текущие исследования направлены на усовершенствование подходов к синтезу регуляторов, охватывающих как линейные, так и нелинейные динамические системы. В этом контексте особое внимание уделяется интеграции новых математических методов, таких как линейные матричные неравенства и частотный анализ, что позволяет оптимизировать отклик системы на различные внешние воздействия и гарантировать защиту от непредвиденных условий. Важно отметить, что, несмотря на достигнутые успехи в данной области, остаются нерешенными значительные проблемы, касающиеся анализа и синтеза регуляторов для нелинейных систем. Это создает необходимость в дальнейших исследованиях и разработках в этой перспективной области. В данной работе, с целью заполнения существующего пробела, сформулированы и доказаны достаточные условия существования управления для одного из часто встречающихся классов нелинейных систем, которые затем будут использоваться в качестве теоретического обоснования для разработки приближенных алгоритмов его нахождения.

Материалы и методы. В качестве основного инструмента исследования используются методы синтеза H_∞ – управления, основанные на минимаксном подходе, заключающемся в нахождении закона управления в условиях наихудшего внешнего воздействия. В этом контексте предлагается доказать достаточные условия существования управления, используя принцип расширения. Однако из-за вычислительных трудностей, которые могут возникнуть при применении этих условий, было решено упростить исходную постановку задачи. Процесс упрощения осуществлялся путем приближенной замены нелинейной системы на другую нелинейную систему, которая по своей структуре схожа с линейной, с помощью процедуры факторизации. Такой подход позволяет применять решение уравнения Риккати, коэффициенты которого зависят от вектора состояния, для синтеза регуляторов. Для решения модельных примеров и прикладных задач был разработан программный комплекс с использованием математического пакета MATLAB.

Результаты исследования. В статье решена проблема синтеза H_∞ – управления состоянием нелинейных непрерывных динамических систем, линейных по управлению и возмущению; сформулированы и на основе принципа расширения доказаны достаточные условия существования H_∞ – управления. Предложен приближенный метод, позволяющий решать задачу нахождения законов управления для динамических систем, нелинейных по состоянию, аналогичный методам, применяемым для линейных систем. Найден аналитические решения двух модельных примеров, которые проиллюстрированы графиками переходных процессов для демонстрации результатов численного моделирования рассмотренных нелинейных динамических систем в присутствии внешних воздействий.

Обсуждение и заключение. Предложенный приближенный алгоритм синтеза регуляторов по состоянию и выходу гарантирует необходимое качество переходных процессов и асимптотическую устойчивость замкнутых нелинейных систем управления. Это значительно расширяет класс динамических систем, для которых возможно синтезирование регуляторов, способных противостоять различным внешним воздействиям. Методы, изложенные в данной работе, могут быть эффективно применены для решения множества задач управления, включая проектирование автопилотов и автоматических навигационных систем для летательных аппаратов, даже в условиях ограниченного воздействия извне.

Ключевые слова: H_∞ – управление, нелинейная динамическая система, полубесконечный промежуток времени, управление с обратной связью, синтез регуляторов

Благодарности. Авторы выражают признательность доценту, кандидату физико-математических наук Кудрявцевой Ирине Анатольевне за помощь в подготовке текста статьи.

Для цитирования. Пантелеев А.В., Яковлева А.А. Приближенный синтез H_∞ – регуляторов в нелинейных динамических системах на полубесконечном промежутке времени. *Advanced Engineering Research (Rostov-on-Don)*. 2025;25(2):152–164. <https://doi.org/10.23947/2687-1653-2025-25-2-152-164>

Introduction. Methods of modern control theory play an important role in the development of complex aerospace systems, providing their efficient operation. To achieve high productivity, stability and efficiency of such systems, it is necessary to develop algorithms for synthesizing controllers capable of operating under conditions of uncertainty in the description of external influences. The modern foundation for their development include the state space method, frequency analysis, and the approach based on linear matrix inequalities [1]. To solve problems of finding optimal control, sufficient optimality conditions in the form of the Bellman equation and the relations following from it in special cases are usually applied. Linear matrix inequalities can be used to search for H_∞ – controllers. They determine the existence of a regulator that satisfies certain performance criteria and provides the stability of the system to external influences. These criteria are usually associated with a norm, which is a measure of the sensitivity of the system to external disturbances. These criteria are usually related to H_∞ – norm, which is a measure of the sensitivity of the system to external disturbances. The problem is to find a regulator that minimizes this norm, while providing the stability of the system and satisfying the quality criterion of control. The solution method is based on finding the extremum of a convex objective function, where the conditions are presented in the form of linear matrix inequalities [2]. By using this method, it is possible to reduce the solution of complex systems of linear and nonlinear algebraic matrix equations of a certain type to the solution of convex optimization problems. However, the solution of linear matrix inequalities can be difficult when considering complex technical problems.

An alternative method based on stochastic minimax is presented in the anisotropic theory of stochastic robust control described in [3]. The main idea in applying this method is that robustness in stochastic control is reached by explicitly including different noise distribution scenarios in a single performance indicator to be optimized. Statistical uncertainty is expressed through entropy, and the robust quality indicator is selected in such a way as to make it possible to quantify the system's ability to suppress the worst external impact. The application of such an approach to solving complex systems of interrelated equations requires the development and use of specialized algorithms.

It should be noted that methods of H_∞ – optimization are used to solve numerous different applied problems, such as aircraft [4], helicopter [5], quadcopter [6] and multi-agent systems [7] control, robot stabilization [8], rocket engine design [9], where, when compared to other controllers, these methods show good results and lower error values under limited disturbances. It is also worth mentioning their use in filtering problems [10], state vector estimation [11] and neural network design [12]. Thus, the development and advancement of H_∞ – optimization methods are highly topical issues for research. Previously, the authors considered the problems of synthesizing H_∞ – controller [13] and H_∞ – observer [14] for linear dynamic systems, for the solution of which sufficient optimality conditions based on the expansion principle were used. Their application made it possible to justify the synthesis procedures and, as a result, to form step-by-step algorithms for solving problems.

Despite significant achievements in this area, a number of problems related to the analysis and synthesis of controllers for nonlinear systems remain unsolved. In this regard, the paper considers the problem of synthesis of controllers for nonlinear dynamic systems, linear in control and disturbance, on a semi-infinite time interval. The research objective is to formulate and prove sufficient conditions for the existence of control. This will not only create a basis for new research and development, but also fill existing gaps in the field of knowledge. Specifically, the work provides for the use of sufficient conditions as a theoretical justification for the formulation of approximate control search algorithms for the class of dynamic systems under consideration. To test the efficiency of the proposed algorithm, two model examples will be solved.

Materials and Methods. Let there be a mathematical model of the control object:

$$\dot{x}(t) = f(x(t)) + B_1(x(t))w(t) + B_2(x(t))u(t), \quad x(0) = \mathbf{0}, \quad (1)$$

and the model of the measuring system:

$$y(t) = C(x(t))x(t), \quad (2)$$

where $x \in R^n$ — state vector, $u \in R^q$ — control vector, $w \in R^p$ — external influences vector, $y \in R^m$ — output vector, $t \in T = [0, \infty)$ — current time, $\mathbf{0}$ — zero matrix-column of dimensions $(n \times 1)$. Assume that the continuously differentiable vector function $f(x)$ of dimensions $(n \times 1)$, as well as the matrix functions $B_1(x)$ of dimensions $(n \times p)$, $B_2(x)$ of dimensions $(n \times q)$, $C(x)$ of dimensions $(m \times n)$ are given. The model of the object is described by an equation that is nonlinear in state, but linear with respect to control and external influences.

It is implied that:

- a) $w(\cdot) \in L_2[0, \infty)$, $u(\cdot) \in L_2[0, \infty)$;
- b) $m \leq n$, $\text{rg } C(x) = m$;
- c) the origin of coordinates $x \equiv 0$ is the equilibrium point, e.g., $f(0) = 0$;
- d) $B_1(x) \neq 0$, $B_2(x) \neq 0$;

where O — zero matrix of corresponding dimensions.

An indicator describing the current behavior of the control object model (1) with measuring system (2) is defined:

$$\|z(t)\|^2 = y(t)^T S(x(t))y(t) + u^T(t)Q(x(t))u(t), \quad (3)$$

where for all $x \in R^n$ $Q(x) > 0$ — symmetric positive definite square matrix of order q , and $S(x) > 0$ — symmetric non-negative definite square matrix of order m . Functional (3) is quadratic in control, but non-quadratic in state.

Note that we are considering models of an object and a measuring system, the matrices in which depend on the state vector.

It is required to ensure the correctness of the condition:

$$\begin{aligned} \frac{\int_0^\infty \|z(t)\|^2 dt}{\int_0^\infty \|w(t)\|_p^2 dt} &= \frac{\int_0^\infty [y(t)^T S(x(t))y(t) + u^T(t)Q(x(t))u(t)] dt}{\int_0^\infty \|w(t)\|_p^2 dt} = \\ &= \frac{\int_0^\infty [x^T(t)C^T(x(t))S(x(t))C(x(t))x(t) + u^T(t)Q(x(t))u(t)] dt}{\int_0^\infty w^T(t)P(x(t))w(t) dt} \leq \gamma^2, \end{aligned} \quad (4)$$

where $\forall x \in R^n$ $P(x) > 0$ — symmetric square matrix of order p , $\gamma > 0$ — some number. As an additional condition, the necessity of fulfilling the property of asymptotic stability of the closed system “object-controller” is considered. Note that it is important to find the smallest value of parameter γ^* that provides the preservation of the required properties of the closed system. This is possible only if the conditions of minimizing the numerator and maximizing the denominator of the expression are simultaneously fulfilled (4).

We rewrite condition (4) in the form:

$$\begin{aligned} I(u, w) &= \int_0^\infty [\|z(t)\|^2 - \gamma^2 \|w(t)\|_p^2] dt = \\ &= \int_0^\infty [x^T(t)C^T(x(t))S(x(t))C(x(t))x(t) + u^T(t)Q(x(t))u(t) - \gamma^2 w^T(t)P(x(t))w(t)] dt \leq 0. \end{aligned} \quad (5)$$

This means that it is required to provide that inequality (5) is satisfied while minimizing control costs under conditions of maximum counteraction of external influences (disturbances).

Sufficient conditions for the existence of H_∞ – controllers

Assume that function $V(x) \in C^1(R^n)$ is known. Let us define the function:

$$\begin{aligned} R(x, u, w) &= \left(\frac{\partial V(x)}{\partial x} \right)^T [f(x) + B_1(x)w + B_2(x)u] + x^T C^T(x)S(x)C(x)x + \\ &\quad + u^T Q(x)u - \gamma^2 w^T P(x)w, \end{aligned} \quad (6)$$

$$\text{where } \frac{\partial V(x)}{\partial x} = \left(\frac{\partial V(x)}{\partial x_1}, \dots, \frac{\partial V(x)}{\partial x_n} \right)^T.$$

Theorem. If there exists function $V(x) \in C^1(R^n)$, satisfying conditions $V(0) = 0$ and

$$R(x, u^*(x), w^*(x)) = \min_u \max_w R(x, u, w) = 0 \quad \forall x \in R^n, \quad (7)$$

where

$$u^*(x) = -\frac{1}{2} Q^{-1}(x) B_2^T(x) \frac{\partial V(x)}{\partial x}, \quad w^*(x) = \frac{1}{2\gamma^2} P^{-1}(x) B_1^T(x) \frac{\partial V(x)}{\partial x}, \quad (8)$$

and function $V(x)$ is determined by solving a partial differential equation:

$$\begin{aligned} &\left(\frac{\partial V(x)}{\partial x} \right)^T f(x) - \frac{1}{4} \left(\frac{\partial V(x)}{\partial x} \right)^T B_2(x) Q^{-1}(x) B_2^T(x) \frac{\partial V(x)}{\partial x} + \\ &+ \frac{1}{4\gamma^2} \left(\frac{\partial V(x)}{\partial x} \right)^T B_1(x) P^{-1}(x) B_1^T(x) \frac{\partial V(x)}{\partial x} + x^T C^T(x)S(x)C(x)x = 0, \end{aligned} \quad (9)$$

then condition (4) is satisfied.

Proof. Suppose that the conditions of the theorem are satisfied. We find $\min_u \max_w R(x, u, w)$, applying the required conditions for an unconditional extremum, since no restrictions are imposed on the variables u, w :

$$\begin{aligned}\frac{\partial R(x, u, w)}{\partial u} &= B_2^T(x) \frac{\partial V(x)}{\partial x} - 2Q(x)u = 0, \\ \frac{\partial R(x, u, w)}{\partial w} &= B_1^T(x) \frac{\partial V(x)}{\partial x} - 2\gamma^2 P(x)w = 0.\end{aligned}$$

Solving the matrix equations, we obtain:

$$u^*(x) = -\frac{1}{2} Q^{-1}(x) B_2^T(x) \frac{\partial V(x)}{\partial x}, \quad w^*(x) = \frac{1}{2\gamma^2} P^{-1}(x) B_1^T(x) \frac{\partial V(x)}{\partial x},$$

where $u^*(x), w^*(x)$ — control structures of the object model and external influence (disturbance).

Since $\frac{\partial^2 R(x, u, w)}{\partial u^T \partial u} = 2Q(x) > 0 \quad \forall x \in R^n$ is true, then the sufficient conditions for the minimum in control are satisfied.

Also true are the sufficient conditions that guarantee the achievement of the maximum external influence w , since $\frac{\partial^2 R(x, u, w)}{\partial w^T \partial w} = -2\gamma^2 P(x) < 0 \quad \forall x \in R^n$.

In this case

$$R(x, u, w) = R(x, u^*(x), w^*(x)) - \gamma^2 [w - w^*(x)]^T P(x) [w - w^*(x)] + [u - u^*(x)]^T Q(x) [u - u^*(x)].$$

From this we get

$$R(x, u^*(x), w(x)) \leq R(x, u^*(x), w^*(x)) \leq R(x, u(x), w^*(x)), \quad (10)$$

i.e., the conditions for the presence of a saddle point are satisfied.

Assume that function $V(x) \in C^1(R^n)$ satisfies conditions $V(0) = 0$ and $R(x, u^*(x), w^*(x)) = 0$.

Then the relation that is fulfilled along the trajectories of system (1) is valid, namely:

$$\begin{aligned}& \left(\frac{\partial V(x(t))}{\partial x} \right)^T [f(x(t)) + B_1(x(t))w(x(t)) + B_2(x(t))u(x(t))] + \|z(t)\|^2 - \gamma^2 \|w(t)\|_p^2 = \\&= \frac{dV(x(t))}{dt} + \|z(t)\|^2 - \gamma^2 \|w(t)\|_p^2 = \underbrace{R(x(t), u^*(x(t)), w^*(x(t)))}_0 - \\& - \gamma^2 [w(t) - w^*(x(t))]^T P(x(t)) [w(t) - w^*(x(t))] + [u(t) - u^*(x(t))]^T Q(x(t)) [u(t) - u^*(x(t))].\end{aligned}$$

For $u = u^*(x)$, let us rewrite the left side of the inequality (10), i.e., $R(x, u^*(x), w(x)) \leq \underbrace{R(x, u^*(x), w^*(x))}_0$, in the form:

$$\frac{dV(x(t))}{dt} + \|z(t)\|^2 - \gamma^2 \|w(t)\|_p^2 \leq 0.$$

By integrating the left and right sides of the resulting inequality over the time interval from 0 to t_1 , we obtain:

$$V(x(t_1)) - V(x(0)) + \int_0^{t_1} \|z(t)\|^2 dt - \gamma^2 \int_0^{t_1} \|w(t)\|_p^2 dt \leq 0.$$

Since it is required to provide the fulfillment of the condition of asymptotic stability of the closed system, then $x(t_1) \rightarrow 0$ when $t_1 \rightarrow +\infty$, therefore $V(x(t_1)) \rightarrow V(0) = 0$. Since $x(0) = 0$ then $V(x(0)) \rightarrow V(0) = 0$. From this we can conclude that when $t_1 \rightarrow +\infty$ the inequality is valid:

$$\int_0^\infty \|z(t)\|^2 dt \leq \gamma^2 \int_0^\infty \|w(t)\|_p^2 dt,$$

indicating that condition (4) is satisfied, which was to be proved.

As a remark, we emphasize that when conditions $P(x) = E$, $\int_0^\infty \|w(t)\|^2 dt \leq 1$, i.e., the energy of external influences is

limited, an inequality of the form $\int_0^\infty \|z(t)\|^2 dt \leq \gamma^2$ is valid.

Approximate synthesis of H_∞ – state-based controllers using the SDRE method

Due to the nonlinearity of equation (9) and difficulties in obtaining its solution, a method based on the algebraic Riccati equation with coefficients dependent on the state vector is used for further analysis [15].

As a result of applying the factorization operation, we obtain a nonlinear system transformed to a structure similar to a linear one, with matrices dependent on the state vector.

It is known [16] that if $f(0) = 0$ and $f(x) \in C^1(R^n)$, then there exists matrix function $A(x)$, such that:

$$f(x) = A(x)x. \quad (11)$$

Notes

1. The factorization procedure for $n = 1$ is unique $\forall x \neq 0$, i.e., $A(x) = f(x) / x = a(x)$.
2. For $n > 1$, the factorization procedure yields a non-unique result [16]. For example, for $n = 2$, there are at least two options: $f(x) = A_1(x)x$ and $f(x) = A_2(x)x$, i.e., for a system of the form:

$$\begin{pmatrix} \dot{x}_1 \\ \dot{x}_2 \end{pmatrix} = \begin{pmatrix} f_1(x) \\ f_2(x) \end{pmatrix} + B_1(x)w + B_2(x)u$$

we obtain

$$\begin{pmatrix} \dot{x}_1 \\ \dot{x}_2 \end{pmatrix} = \underbrace{\begin{pmatrix} \frac{f_1(x)}{x_1} & 0 \\ \frac{f_2(x)}{x_1} & 0 \end{pmatrix}}_{A_1(x)} \begin{pmatrix} x_1 \\ x_2 \end{pmatrix} + B_1(x)w + B_2(x)u \text{ or } \begin{pmatrix} \dot{x}_1 \\ \dot{x}_2 \end{pmatrix} = \underbrace{\begin{pmatrix} 0 & \frac{f_1(x)}{x_2} \\ 0 & \frac{f_2(x)}{x_2} \end{pmatrix}}_{A_2(x)} \begin{pmatrix} x_1 \\ x_2 \end{pmatrix} + B_1(x)w + B_2(x)u.$$

3. If there are two parametrization options, i.e., $f(x) = A_1(x)x = A_2(x)x$, then there is an infinite family of options of the form [16]: $A(x, \alpha) = \alpha A_1(x) + (1 - \alpha)A_2(x) \forall \alpha$. The selection of parameter α allows for flexibility in designing the control system. The solution to the Riccati equation and the corresponding control become functions of this parameter.

As a result of factorization, the mathematical model of system (1) takes the form:

$$\dot{x}(t) = A(x(t))x(t) + B_1(x(t))w(t) + B_2(x(t))u(t), \quad x(0) = 0. \quad (12)$$

On the trajectories of system (12), functional (5) is specified.

It is assumed that system (12) is controllable and observable, i.e., $\forall x \in R^n$ the conditions are fulfilled point-to-point [16]:

$$\begin{aligned} \text{rg}[B_2(x) \ A(x)B_2(x) \ \dots \ A^{n-1}(x)B_2(x)] &= n, \\ \text{rg}[C^T(x) \ A^T(x)C^T(x) \ \dots \ (A^T(x))^{n-1}C^T(x)] &= n. \end{aligned}$$

Equation (9) takes the form:

$$\begin{aligned} &\left(\frac{\partial V(x)}{\partial x}\right)^T A(x)x - \frac{1}{4}\left(\frac{\partial V(x)}{\partial x}\right)^T B_2(x)Q^{-1}(x)B_2^T(x)\frac{\partial V(x)}{\partial x} + \\ &+ \frac{1}{4\gamma^2}\left(\frac{\partial V(x)}{\partial x}\right)^T B_1(x)P^{-1}(x)B_1^T(x)\frac{\partial V(x)}{\partial x} + x^T C^T(x)S(x)C(x)x = 0. \end{aligned} \quad (13)$$

Assume that

$$\frac{\partial V(x)}{\partial x} = 2K_2(x)x, \quad (14)$$

where $K_2(x) > 0$ unknown matrix function (for fixed $x \in R^n$, matrix $K_2(x)$ is a symmetric positive definite numerical matrix). Thus, an assumption is made not about the type of function $V(x)$, but only about the structure of its partial derivative.

Then, the control structures of the object and disturbance take the form:

$$\begin{aligned} u^*(x) &= -\frac{1}{2}Q^{-1}(x)B_2^T(x)\frac{\partial V(x)}{\partial x} = -Q^{-1}(x)B_2^T(x)K_2(x)x, \\ w^*(x) &= \frac{1}{2\gamma^2}P^{-1}(x)B_1^T(x)\frac{\partial V(x)}{\partial x} = \frac{1}{\gamma^2}P^{-1}(x)B_1^T(x)K_2(x)x. \end{aligned} \quad (15)$$

Equation (13) takes the form:

$$\begin{aligned} &2x^T K_2(x)A(x)x - x^T K_2(x)B_2(x)Q^{-1}(x)B_2^T(x)K_2(x)x + \\ &+ \frac{1}{\gamma^2}x^T K_2(x)B_1(x)P^{-1}(x)B_1^T(x)K_2(x)x + x^T C^T(x)S(x)C(x)x = 0, \end{aligned}$$

or

$$x^T [2K_2(x)A(x) - K_2(x)B_2(x)Q^{-1}(x)B_2^T(x)K_2(x) + \frac{1}{\gamma^2}K_2(x)B_1(x)P^{-1}(x)B_1^T(x)K_2(x) + C^T(x)S(x)C(x)]x = 0.$$

Applying the transpose operation, we obtain:

$$x^T [2A^T(x)K_2(x) - K_2(x)B_2(x)Q^{-1}(x)B_2^T(x)K_2(x) + \frac{1}{\gamma^2}K_2(x)B_1(x)P^{-1}(x)B_1^T(x)K_2(x) + C^T(x)S(x)C(x)]x = 0.$$

Summing up the last two expressions, we arrive at the equality:

$$x^T [2K_2(x)A(x) + 2A^T(x)K_2(x) - 2K_2(x)B_2(x)Q^{-1}(x)B_2^T(x)K_2(x) + \frac{2}{\gamma^2}K_2(x)B_1(x)P^{-1}(x)B_1^T(x)K_2(x) + 2C^T(x)S(x)C(x)]x = 0,$$

or finally:

$$x^T [K_2(x)A(x) + A^T(x)K_2(x) - K_2(x)B_2(x)Q^{-1}(x)B_2^T(x)K_2(x) + \frac{1}{\gamma^2}K_2(x)B_1(x)P^{-1}(x)B_1^T(x)K_2(x) + C^T(x)S(x)C(x)]x = 0. \quad (16)$$

Note that due to the dependence of all matrices on the state vector, the equality of the zero matrix in square brackets does not follow from (16).

By analogy with the case of a linear stationary system, it is proposed to solve the algebraic Riccati equation, all matrices in which are functions of the system's state vector (State Dependent Riccati Equation, SDRE). In this case, a positive definite solution to the Riccati equation is sought, generating a control law that guarantees that the system will be asymptotically stable in the vicinity of the equilibrium position. To check this property, the stability criterion by the roots of the characteristic equation, checked point-to-point, or the Routh–Hurwitz criterion, is used.

In the problem under consideration, it is proposed to solve the equation:

$$K_2(x)A(x) + A^T(x)K_2(x) - K_2(x)[B_2(x)Q^{-1}(x)B_2^T(x) - \frac{1}{\gamma^2}B_1(x)P^{-1}(x)B_1^T(x)]K_2(x) + C^T(x)S(x)C(x) = O, \quad (17)$$

i.e., to look for matrix $K_2(x) > 0$, that satisfies the Riccati equation, whose coefficients depend on x . Equation (17) is solved repeatedly for fixed $x \in R^n$. The coordinates of the state vector are determined in the process of integrating the differential equation (12) together with the controls of the object and the disturbances:

$$u^*(x) = -Q^{-1}(x)B_2^T(x)K_2(x)x, \quad w^*(x) = \frac{1}{\gamma^2}P^{-1}(x)B_1^T(x)K_2(x)x. \quad (18)$$

In this case, the solution to the Riccati equation must be such that the criterion $\sigma\{A(x) + [\frac{1}{\gamma^2}B_1(x)P^{-1}(x)B_1^T(x) - B_2(x)Q^{-1}(x)B_2^T(x)]K_2(x)\} \subset C^- \quad \forall x \in R^n$, is satisfied, where σ^- matrix spectrum, C^- — open left half-plane of the complex plane. Note that the stability criterion of a closed system can be replaced by checking the point-to-point fulfillment of the Routh-Hurwitz criterion.

Algorithm for approximate synthesis of H_∞ – controllers of state

Step 1. Set parameter $\gamma > 0$.

Step 2. Find the solution to the equation:

$$\dot{x}(t) = A(x(t))x(t) + B_1(x(t))w(t) + B_2(x(t))u(t), \quad x(0) = 0,$$

with controls

$$u(t) = u^*(x(t)) = -Q^{-1}(x(t))B_2^T(x(t))K_2(x(t))x(t),$$

$$w(t) = w^*(x(t)) = \frac{1}{\gamma^2}P^{-1}(x(t))B_1^T(x(t))K_2(x(t))x(t),$$

one of the numerical methods of integration with constant step h (explicit Euler method, Euler-Cauchy method, Adams-Bashforth, Milne, Hamming methods of various orders).

In this case, for each of the discrete moments of time $t_i = ih$, $i = 0, 1, 2, \dots$, solve the Riccati equation:

$$K_2(x)A(x) + A^T(x)K_2(x) - K_2(x)[B_2(x)Q^{-1}(x)B_2^T(x) - \frac{1}{\gamma^2}B_1(x)P^{-1}(x)B_1^T(x)]K_2(x) + C^T(x)S(x)C(x) = O,$$

for $x = x(t_i)$. As a result, find matrix $K_2(x)$ and use it to form control laws.

Step 3. Find the minimum γ^* . To do this, it is required to consistently decrease γ until the stability property of solutions of the differential equation

$$\dot{x}(t) = [A(x(t)) + \frac{1}{\gamma^2}B_1(x(t))P^{-1}(x(t))B_1^T(x(t)) - B_2(x(t))Q^{-1}(x(t))B_2^T(x(t))]K_2(x(t))x(t),$$

describing the dynamics of the system with the obtained controls, remains valid.

Research Results. To test the efficiency of the proposed approximate algorithm for synthesizing H_∞ – state-based controllers, two model examples were solved.

Model example No. 1. A one-dimensional case is considered, when equations (1), (2) and functional (5) have the form:

$$\dot{x}(t) = f(x) + B_1(x)w + B_2(x)u = A(x)x + B_1(x)w + B_2(x)u,$$

$$y = C(x)x,$$

$$I = \int_0^\infty [S(x(t))x^2(t) + Q(x(t))u^2(t) - \gamma^2 P(x(t))w^2(t)] dt.$$

Solution. The control structures follow from (18):

$$u^*(x) = -\frac{1}{Q(x)} B_2(x) K_2(x) x, \quad u^*(x) = -\frac{1}{Q(x)} B_2(x) K_2(x) x,$$

and equation (17) has the form:

$$2A(x)K_2(x) - K_2^2(x) \left[\frac{B_2^2(x)}{Q(x)} - \frac{1}{\gamma^2 P(x)} B_1^2(x) \right] + C^2(x)S(x) = 0.$$

Let us write the resulting quadratic equation in canonical form:

$$\left[\frac{B_2^2(x)}{Q(x)} - \frac{1}{\gamma^2 P(x)} B_1^2(x) \right] K_2^2(x) - 2A(x)K_2(x) - C^2(x)S(x) = 0.$$

The solution is as follows:

$$K_2(x) = \frac{2A(x) \pm \sqrt{4A^2(x) + 4C^2(x)S(x) \left[\frac{B_2^2(x)}{Q(x)} - \frac{1}{\gamma^2 P(x)} B_1^2(x) \right]}}{2 \left[\frac{B_2^2(x)}{Q(x)} - \frac{1}{\gamma^2 P(x)} B_1^2(x) \right]}.$$

Since $K_2 > 0$, then

$$K_2(x) = \frac{A(x) + \sqrt{A^2(x) + C^2(x)S(x) \left[\frac{B_2^2(x)}{Q(x)} - \frac{1}{\gamma^2 P(x)} B_1^2(x) \right]}}{\left[\frac{B_2^2(x)}{Q(x)} - \frac{1}{\gamma^2 P(x)} B_1^2(x) \right]}.$$

Let us take a closer look at a particular case:

$$\dot{x}(t) = x - x^3 + w + u = (1 - x^2)x + w + u,$$

$$y = 2x,$$

$$I = \int_0^\infty [x^2(t) + u^2(t) - \gamma^2 w^2(t)] dt,$$

where $A(x) = (1 - x^2)$, $B_1(x) = 1$, $B_2(x) = 1$, $C(x) = 2$, $Q(x) = 1$, $S(x) = 1$, $P(x) = 1$.

Then (omitting the dependence on x) we get:

$$2AK_2 - K_2^2 \left(1 - \frac{1}{\gamma^2} \right) + C^2 = 0 \rightarrow K_2^2 (1 - \gamma^{-2}) - 2AK_2 - C^2 = 0.$$

Roots of the quadratic equation:

$$K_2 = \frac{A \pm \sqrt{A^2 + C^2(1 - \gamma^{-2})}}{1 - \gamma^{-2}}, \quad \gamma \neq 1, \quad K_2 = -\frac{C^2}{2A}, \quad \gamma = 1.$$

Note that when considering the case $\gamma \neq 1$, it is not yet possible to exclude the extra roots, since $A(x)$ and $(1 - \gamma^{-2})$ can change the sign.

As a result, we obtain the control structures:

$$w^*(x) = \frac{1}{\gamma^2} B_1^T K_2 x = \frac{1}{\gamma^2} K_2 x, \quad u^*(x) = B_2^T K_2 x = -K_2 x.$$

In this case, the equation of the closed system has the form:

$$\dot{x} = [A - (1 - \gamma^{-2})K_2]x = \mp \sqrt{A^2 + C^2(1 - \gamma^{-2})} x.$$

To provide asymptotic stability, we take the minus sign, and in the expression for K_2 – plus. For this example, we get:

1) if $\gamma \neq 1$, then

$$K_2(x) = \frac{A(x) + \sqrt{A^2(x) + C^2(x)(1 - \gamma^{-2})}}{1 - \gamma^{-2}} = \frac{1 - x^2 + \sqrt{(1 - x^2)^2 + 4(1 - \gamma^{-2})}}{1 - \gamma^{-2}} > 0;$$

2) if functions $A(x)$, $C(x)$ are not equal to zero simultaneously, then discriminant $A^2(x) + C^2(x)(1 - \gamma^2)$.

Then,

$$A^2(x) + C^2(x) \geq C^2(x)\gamma^{-2}, \quad \gamma^{-2} \leq \frac{A^2(x) + C^2(x)}{C^2(x)}, \quad \gamma^2 \geq \frac{C^2(x)}{A^2(x) + C^2(x)}, \quad \gamma_{\min}^2(x) = \frac{C^2(x)}{A^2(x) + C^2(x)}.$$

For the example being solved $\gamma_{\min}^2(x) = \frac{C^2(x)}{A^2(x) + C^2(x)} = \frac{4}{(1-x^2)^2 + 4}$, i.e., for each current x , there is its own value $\gamma_{\min}^2(x)$.

For $\gamma = \gamma_{\min}$, $x = 0$, $x(0) = 0$ is satisfied (the condition of asymptotic stability is not satisfied, but $x(t) \equiv 0$ is valid).

For $\gamma = \gamma_{\min}$ we have

$$K_2(x) = \frac{A(x) + \sqrt{A^2(x) + C^2(x)(1 - \gamma^{-2})}}{1 - \gamma^{-2}} = \frac{1 - x^2 + \sqrt{(1 - x^2)^2 + 4(1 - \gamma^{-2})}}{1 - \gamma^{-2}} > 0, \quad \gamma \neq 1.$$

If $\gamma = 1$, then $K_2(x) = -\frac{C^2(x)}{2A(x)} = -\frac{4}{2(1-x^2)}$. To fulfill condition $K_2 > 0$, condition $A(x) = 1 - x^2 < 0$ that defines set

$|x| < 1$ of possible functioning of the system must be fulfilled.

Modeling. For modeling under different initial conditions, finite time interval $T = [0, 20]$ was selected, since all transient processes in a closed system are practically completed.

According to Figures 1–3, the value of the state vector asymptotically tends to zero for different initial conditions, which indicates the stability of the system and the correct selection of parameters, under which the system retains the property of stability subject to any given limited disturbances.

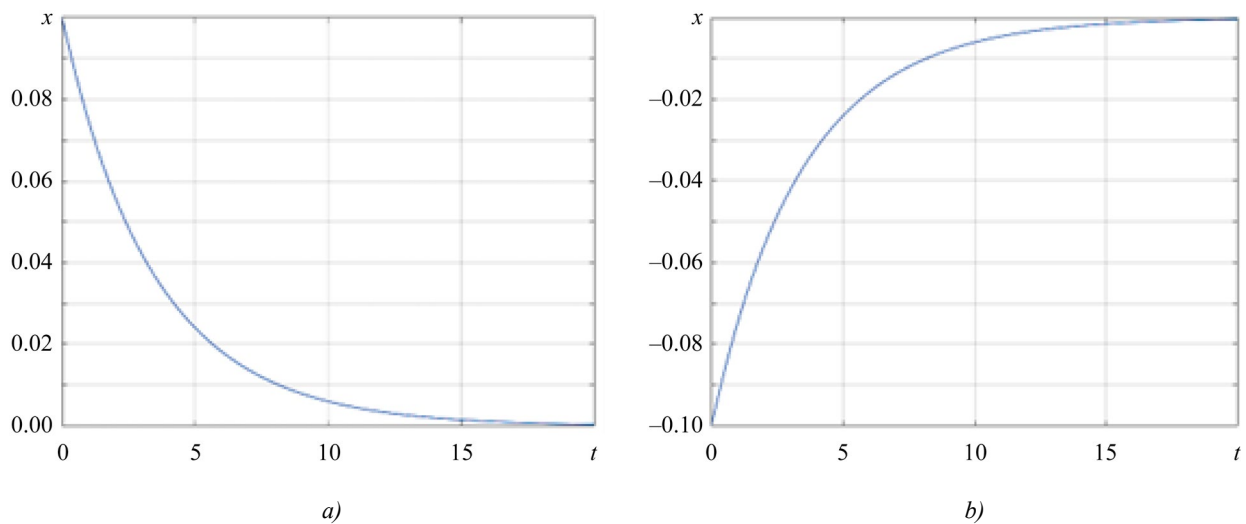


Fig. 1. Change of the state vector:
a — for initial state $x_0 = 0.1$; b — for initial state $x_0 = -0.1$

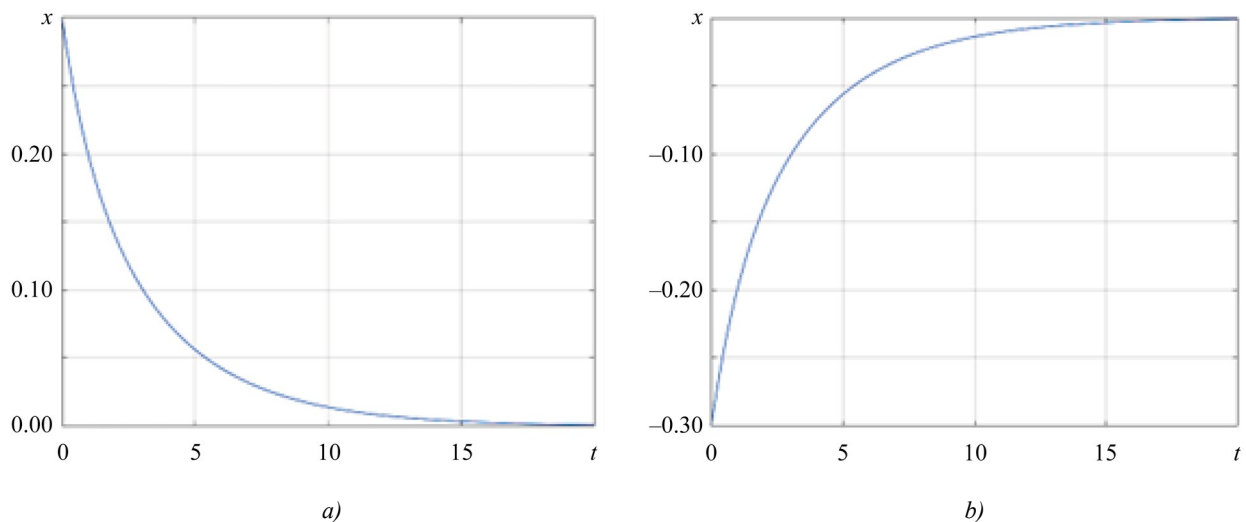


Fig. 2. Change of the state vector:
a — for initial state $x_0 = 0.3$; b — for initial state $x_0 = -0.3$

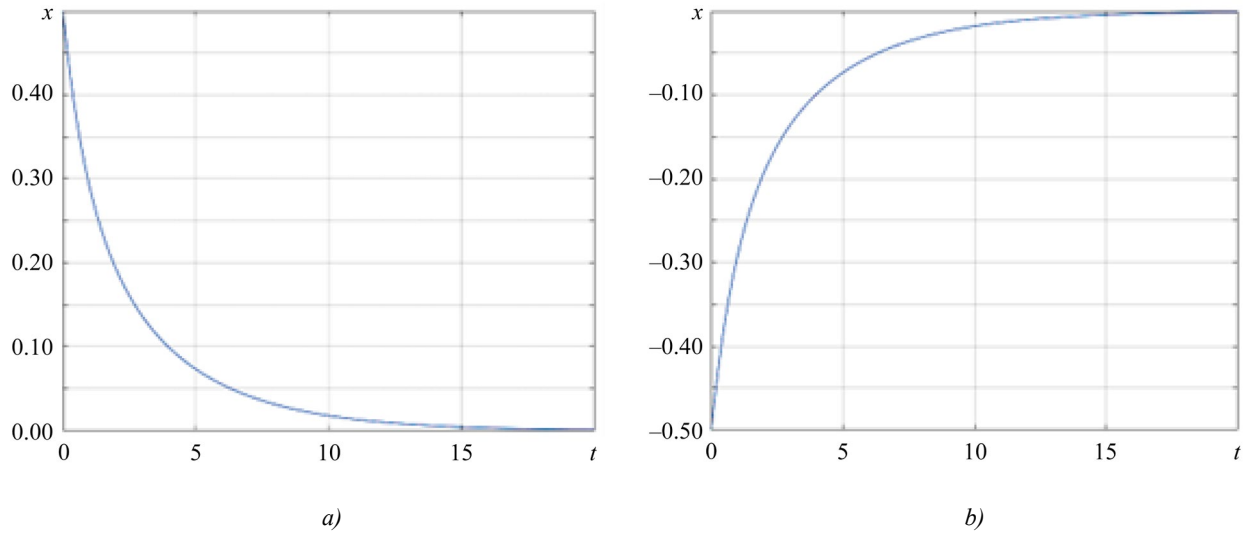


Fig. 3. Change of the state vector:
 a — for initial state $x_0 = 0.5$; b — for initial state $x_0 = -0.5$

Model example No. 2. One of the options of the two-dimensional case is considered, when equations (1), (2) and functional (5) have the form:

$$\dot{x}(t) = \underbrace{\begin{pmatrix} 0 & 1 \\ x_1 & 0 \end{pmatrix}}_{A(x)} x(t) + \underbrace{\begin{pmatrix} 0 \\ 1 \end{pmatrix}}_{B_1(x)} w(t) + \underbrace{\begin{pmatrix} 0 \\ 1 \end{pmatrix}}_{B_2(x)} u(t),$$

$$y(t) = x(t),$$

$$I(u, w) = \int_0^\infty \left[x^T(t) x(t) + u^2(t) - \gamma^2 w^2(t) \right] dt \leq 0,$$

i.e., $C(x) = E_2$, $S(x) = E_2$, $Q(x) = 1$, $P(x) = 1$.

Solution. The control structures of the object and the disturbance follow from (18):

$$u^*(x) = -\begin{pmatrix} 0 & 1 \end{pmatrix} \begin{pmatrix} K_{11}(x) & K_{12}(x) \\ K_{12}(x) & K_{22}(x) \end{pmatrix} \begin{pmatrix} x_1 \\ x_2 \end{pmatrix} = -K_{12}(x)x_1 - K_{22}(x)x_2,$$

$$w^*(x) = \frac{1}{\gamma^2} \begin{pmatrix} 0 & 1 \end{pmatrix} \begin{pmatrix} K_{11}(x) & K_{12}(x) \\ K_{12}(x) & K_{22}(x) \end{pmatrix} \begin{pmatrix} x_1 \\ x_2 \end{pmatrix} = -\frac{1}{\gamma^2} [K_{12}(x)x_1 + K_{22}(x)x_2],$$

and equation (17) has the form:

$$\begin{pmatrix} K_{11}(x) & K_{12}(x) \\ K_{12}(x) & K_{22}(x) \end{pmatrix} \begin{pmatrix} 0 & 1 \\ x_1 & 0 \end{pmatrix} + \begin{pmatrix} 0 & x_1 \\ 1 & 0 \end{pmatrix} \begin{pmatrix} K_{11}(x) & K_{12}(x) \\ K_{12}(x) & K_{22}(x) \end{pmatrix} -$$

$$- \begin{pmatrix} K_{11}(x) & K_{12}(x) \\ K_{12}(x) & K_{22}(x) \end{pmatrix} \left[\begin{pmatrix} 0 \\ 1 \end{pmatrix} \begin{pmatrix} 0 & 1 \end{pmatrix} - \frac{1}{\gamma^2} \begin{pmatrix} 0 \\ 1 \end{pmatrix} \begin{pmatrix} 0 & 1 \end{pmatrix} \right] \begin{pmatrix} K_{11}(x) & K_{12}(x) \\ K_{12}(x) & K_{22}(x) \end{pmatrix} + \begin{pmatrix} 1 & 0 \\ 0 & 1 \end{pmatrix} = \begin{pmatrix} 0 & 0 \\ 0 & 0 \end{pmatrix}.$$

From here,

$$2K_{12}x_1 - \delta K_{12}^2 + 1 = 0,$$

$$K_{11} + K_{22}x_1 - \delta K_{12}K_{22} = 0,$$

$$2K_{12} - \delta K_{22}^2 + 1 = 0,$$

where $\delta = \frac{\gamma^2 - 1}{\gamma^2} = 1 - \gamma^{-2}$.

Solution to the first equation $\delta K_{12}^2 - K_{12}x_1 - 1 = 0$ has the form:

$$K_{12} = \frac{2x_1 \pm \sqrt{4x_1^2 + 4\delta}}{2\delta} = \frac{x_1 \pm \sqrt{x_1^2 + \delta}}{\delta}.$$

Solution to the third equation:

$$K_{22} = \sqrt{\frac{2K_{12} + 1}{\delta}} = \sqrt{\frac{2x_1 + \delta \pm 2\sqrt{x_1^2 + \delta}}{\delta^2}}.$$

Solution to the second equation:

$$K_{11} = K_{22}(\delta K_{12} - x_1) = \sqrt{\frac{2x_1 + \delta \pm 2\sqrt{x_1^2 + \delta}}{\delta^2}} \pm \sqrt{x_1^2 + \delta}.$$

In the obtained solutions, positive signs were selected taking into account condition $K_2 > 0$.

Modeling. To model the system, it is required to select the minimum possible value γ , so that it satisfies (4) and at the same time guarantees the asymptotic stability of the closed system. In example 1, the value of parameter γ was found analytically, but a problem arose with determining the value of the optimal parameter γ^* , therefore value γ , used in the modeling, was selected experimentally. When $\gamma^* = 1.5$, the system remained stable according to expression (19). For modeling, the time interval $T = [0, 10]$ was selected, since transient processes in the closed system decayed fairly quickly. Modeling was performed for various initial conditions.

According to Figures 4–5, it can be concluded that the coordinates of the state vector asymptotically tend to zero. This result is observed for each of the initial conditions considered. This indicates that the system is stable, and its parameters are selected correctly, which allows maintaining the property of stability under any initial conditions and under the worst disturbances.

The initial conditions significantly affect the trajectories of the change in the coordinates of the state vector, but from Figures 4–5, it is clear that the proposed approach allows us not only to compensate for external disturbances, but also to stabilize the trajectory of motion.

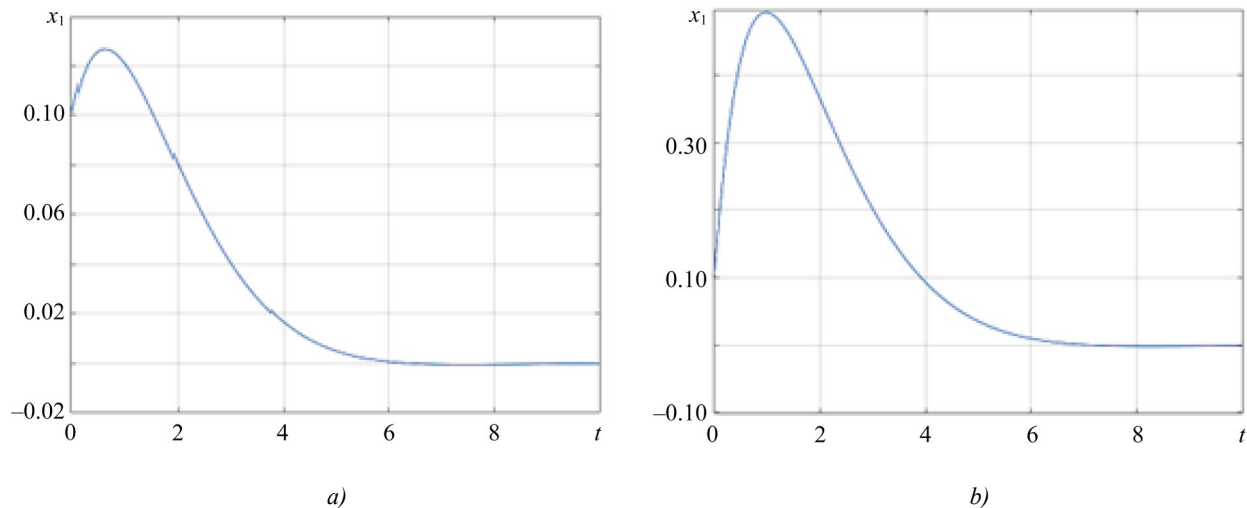


Fig. 4. Change of $x_1(t)$:
a — for initial state $x_0 = (0, 1; 0, 1)^T$; b — for initial state $x_0 = (0, 1; 1)^T$

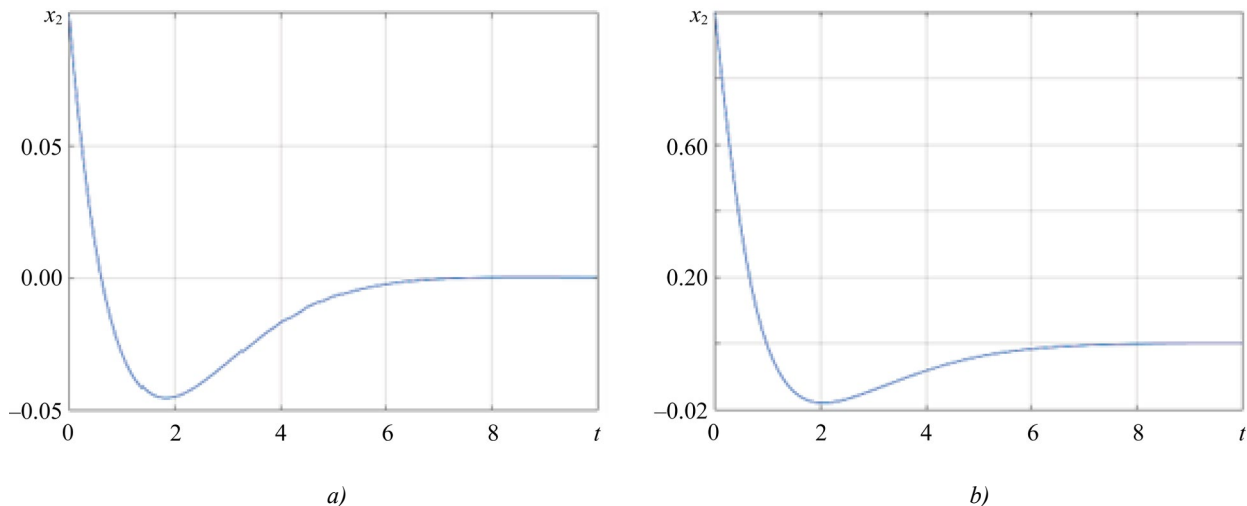


Fig. 5. Change of $x_2(t)$:
a — for initial state $x_0 = (1; 0, 1)^T$; b — for initial state $x_0 = (1; 1)^T$

Discussion of the Results. As a result of the study, sufficient H_∞ – control conditions were formulated and substantiated, an approximate solution method was developed. The method proposed within the framework of the problem was tested on two model examples. The simulation results allow us to conclude that the use of the developed controller synthesis method guarantees the required quality of transient processes and provides asymptotic stability of closed systems.

Conclusion. The results and methods proposed in this paper can be applied to solve control problems of varying complexity — from designing simple autopilots to developing complex automatic navigation systems for manned and unmanned aerial vehicles. This emphasizes the prospects of using the proposed approach and makes it an attractive option for further research.

References

1. Kurdyukov AP, Andrianova OG, Belov AA, Gol'din DA. In between the LQG/H₂- and H_∞ -Control Theories. *Automation and Remote Control*. 2021;(4):8–76. <https://doi.org/10.31857/S0005231021040024>
2. Wanigasekara C, Liruo Zhang, Swain A. H_∞ State-Feedback Consensus of Linear Multi-Agent Systems. In: *Proc. 17th International Conference on Control & Automation*. Piscataway, NJ: IEEE Xplore; 2022. P. 710–715. <https://doi.org/10.1109/ICCA54724.2022.9831897>
3. Banavar RN, Speyer JL. A Linear-Quadratic Game Approach to Estimation and Smoothing. In: *Proc. of the American Control Conference*. New York City: IEEE; 1991. P. 2818–2822. <https://doi.org/10.23919/ACC.1991.4791915>
4. Chodnicki M, Pietruszewski P, Wesołowski M, Stępień S. Finite-Time SDRE Control of F16 Aircraft Dynamics. *Archives of Control Sciences*. 2022;32(3):557–576. <https://doi.org/10.24425/acs.2022.142848>
5. Pantelev A, Yakovleva A. Approximate Methods of H_∞ Control of Nonlinear Dynamic Systems Output. *MATEC Web of Conferences. XXII International Conference on Computational Mechanics and Modern Applied Software Systems (CMMASS 2021)*. 2022;362:012021. <https://doi.org/10.1051/mateconf/202236201021>
6. Hamza A, Mohamed AH, Badawy A. Robust H_∞ Control for a Quadrotor UAV. *AIAA SCITECH 2022 Forum*. Reston, VA: AIAA; 2022. <https://doi.org/10.2514/6.2022-2033>
7. Fei Han, Qianqian He, Yanhua Song, Jinbo Song. Outlier-Resistant Observer-Based H_∞ -Consensus Control for Multi-Rate Multi-Agent Systems. *Journal of the Franklin Institute*. 2021;358(17):8914–8928. <https://doi.org/10.1016/j.jfranklin.2021.08.048>
8. Junfeng Long, Wenye Yu, Quanyi Li, Zirui Wang, Dahua Lin, Jiangmiao Pang. Learning H_∞ Locomotion Control. *arXiv preprint arXiv*. 2024;2404:14405. <https://doi.org/10.48550/arXiv.2404.14405>
9. Fayin Chen, Wei Xue, Yong Tang, Tao Wang. A Comparative Research of Control System Design Based on H_∞ and ALQR for the Liquid Rocket Engine of Variable Thrust. *International Journal of Aerospace Engineering*. 2023;(2):1–12. <https://doi.org/10.1155/2023/2155528>
10. Yazdkhasti S, Sabzevari D, Sasiadek JZ. Adaptive H_∞ Extended Kalman Filtering for a Navigation System in Presence of High Uncertainties. *Transactions of the Institute of Measurement and Control*. 2022;45(8):1430–1442. <https://doi.org/10.1177/01423312221136022>
11. Balandin DV, Biryukov RS, Kogan MM. Multicriteria Optimization of Induced Norms of Linear Operators: Primal and Dual Control and Filtering Problems. *Journal of Computer and Systems Sciences International*. 2022;61(2):176–190. <http://doi.org/10.1134/S1064230722020046>
12. Aalipour A, Khani A. Data-Driven H_∞ Control with a Real-Time and Efficient Reinforcement Learning Algorithm: An Application to Autonomous Mobility-on-Demand Systems. *arXiv:2309.08880*. <https://doi.org/10.48550/ARXIV.2309.08880>
13. Pantelev AV, Yakovleva AA. Sufficient Conditions for H_∞ Control on the Finite Time Interval. *Journal of Physics: Conference Series*. 2021;1925:012024. <https://doi.org/10.1088/1742-6596/1925/1/012024>
14. Pantelev AV, Yakovleva AA. Sufficient Conditions for the Existence of H_∞ -infinity State Observer for Linear Continuous Dynamical Systems. *Modelling and Data Analysis*. 2023;13(2):36–63. <https://doi.org/10.17759/mda.2023130202>
15. Çimen T. State-Dependent Riccati Equation (SDRE) Control: A Survey. *IFAC Proceedings Volumes*. 2008;41(2):3761–3775. <https://doi.org/10.3182/20080706-5-KR-1001.00635>
16. Cloutier JR, D'Souza CN, Mracek CP. Nonlinear Regulation and Nonlinear H_∞ Control via the State-Dependent Riccati Equation Technique: Part 1, Theory. In: *Proc. International Conference on Nonlinear Problems in Aviation and Aerospace*. Daytona Beach, FL: Embry-Riddle Aeronautical University Press; 1996. P. 117–131. URL: <https://clck.ru/3M4kki> (accessed: 04.02.2025).

About the Authors:

Andrei V. Pantelev, Dr.Sci. (Phys.-Math.), Full Professor, Head of the Department of Mathematical Cybernetics, Institute of Information Technology and Applied Mathematics, Moscow Aviation Institute (4, Volokolamskoe Shosse, Moscow, 125993, Russian Federation), [SPIN-code](#), [ScopusID](#), [ORCID](#), avpantelev@inbox.ru

Aleksandra A. Yakovleva, Postgraduate Student of the Department of Mathematical Cybernetics, Institute of Information Technology and Applied Mathematics, Moscow Aviation Institute (4, Volokolamskoe Shosse, Moscow, 125993, Russian Federation), [SPIN-code](#), [ScopusID](#), [ORCID](#), ayakovleva982@gmail.com

Claimed Contributorship:

AV Panteleev: conceptualization, supervision, methodology, writing – review & editing.

AA Yakovleva: methodology, software, writing – original draft preparation, visualization.

Conflict of Interest Statement: the authors declare no conflict of interest.

All authors have read and approved the final manuscript.

Об авторах:

Андрей Владимирович Пантелеев, доктор физико-математических наук, профессор, заведующий, кафедра «Математическая кибернетика» института информационных технологий и прикладной математики, Московского авиационного института (национальный исследовательский университет) (125993, Российская Федерация, г. Москва, Волоколамское шоссе, д. 4), [SPIN-код](#), [ORCID](#), [ScopusID](#), avpanteleev@inbox.ru

Александра Алексеевна Яковлева, аспирант, кафедра «Математическая кибернетика» Московского авиационного института (национальный исследовательский университет), (125993, Российская Федерация, г. Москва, Волоколамское шоссе, д. 4), [SPIN-код](#), [ORCID](#), [ScopusID](#), ayakovleva982@gmail.com

Заявленный вклад авторов:

А.В. Пантелеев: разработка концепции, научное руководство, разработка методологии, написание рукописи.

А.А. Яковлева: разработка методологии и программного обеспечения, написание черновика рукописи, визуализация.

Конфликт интересов: авторы заявляют об отсутствии конфликта интересов.

Все авторы прочитали и одобрили окончательный вариант рукописи.

Received / Поступила в редакцию 30.04.2025

Reviewed / Поступила после рецензирования 24.05.2025

Accepted / Принята к публикации 28.05.2025